

Numerical modeling of compositional two-phase reactive transport in porous media with phase change phenomena including an application in nuclear waste disposal

Dissertation for awarding the academic degree

Doctor of Engineering (Dr.-Ing)

Submitted by

M.S c. Yonghui Huang

06.05.1989 in China

Reviewers: Prof. Dr. -Ing. Olaf Kolditz, Technical University of Dresden.

Junior-Prof. Dr. Marc Walther, Technical University of Dresden.

PD, Dr. Georg Kosakowski, Paul Scherrer Institute.

Date of defense: 31.05.2018

Leipzig, June 2018

Erklärung zur Eröffnung des Promotionsverfahrens:

1. Hiermit versichere ich, dass ich die vorliegende Arbeit ohne unzulässige Hilfe Dritter und ohne Benutzung anderer als der angegebenen Hilfsmittel angefertigt habe; die aus fremden Quellen direkt oder indirekt übernommenen Gedanken sind als diese kenntlich gemacht.
2. Bei der Auswahl und Auswertung des Materials sowie bei der Herstellung des Manuskriptes habe ich Unterstützungsleistungen von folgenden Personen erhalten:

Junior Prof. Dr. Haibing Shao, Dr. Thomas Nagel
.....
3. Weitere Personen waren an der geistigen Herstellung der vorliegenden Arbeit nicht beteiligt. Insbesondere habe ich nicht die Hilfe eines kommerziellen Promotionsberaters in Anspruch genommen. Dritte haben von mir weder unmittelbar noch mittelbar geldwerte Leistungen für Arbeiten erhalten, die im Zusammenhang mit dem Inhalt der vorgelegten Dissertation stehen.
4. Die Arbeit wurde bisher weder im Inland noch im Ausland in gleicher oder ähnlicher Form einer anderen Prüfungsbehörde vorgelegt und ist – sofern es sich nicht um eine kumulative Dissertation handelt – auch noch nicht veröffentlicht worden.
5. Sofern es sich um eine kumulative Dissertation gemäß § 10 Abs. 2 handelt, versichere ich die Einhaltung der dort genannten Bedingungen.
6. Ich bestätige, dass ich die Promotionsordnung der Fakultät Umweltwissenschaften der Technischen Universität Dresden anerkenne.

Leipzig, 18. June. 2018

Ort, Datum

Unterschrift des Doktoranden

ÜBEREINSTIMMUNGSERKLÄRUNG

Die Übereinstimmung dieses Exemplars mit dem Original der Dissertation zum Thema:

'Numerical modeling of compositional two-phase reactive transport in porous media with phase transition phenomena including an application in nuclear waste disposal'

wird hiermit bestätigt.

.....
Ort, Datum

.....
Unterschrift (Vorname Name)

ABSTRACT

Non-isothermal compositional two-phase flow is considered to be one of the fundamental physical processes in the field of water resources research. The strong non-linearity and discontinuity emerging from phase transition phenomena pose a serious challenge for numerical modeling. Recently, Lauser et al.[1] has proposed a numerical scheme, namely the Nonlinear Complementary Problem (NCP), to handle this strong non-linearity. In this work, the NCP is implemented at both local and global levels of a Finite element algorithm. In the former case, the NCP is integrated into the local thermodynamic equilibrium calculation. While in the latter one, it is formulated as one of the governing equations. The two different formulations have been investigated through several well established benchmarks and analyzed for their efficiency and robustness.

In the second part of the thesis, the presented numerical formulations are applied for application and process studies in the context of nuclear waste disposal in Switzerland. Application studies comprehend the coupling between multiphase transport model and complex bio-geo-chemical process to investigate the degradation of concrete material due to two major reactions: carbonation and Aggregate Silica Reaction(ASR). The chemical processes are simplified into a look-up table and cast into the transport model via source and sink term. The efficiency and robustness of the look-up table are further compared with a fully reactive transport model.

ZUSAMMENFASSUNG

Nichtisotherme Mehrkomponenten Zweiphasenprobleme in porösen Medien sind durch äußerst komplex gekoppelte, nichtlineare und oftmals nichtisotherme Prozesse charakterisiert, wobei zwischen den beteiligten Fluidphasen ein Massentransfer von Komponenten stattfinden kann. Ein großes Problem bei der Simulation von Mehrkomponenten Zweiphasenströmungen mit Löslichkeitseffekten tritt auf, wenn Phase verschwindet und auftaucht. Kürzlich haben Lauser et al [1] ein neues numerisches Schema vorgeschlagen, nämlich das nichtlineare Komplementaritätsproblem (NCP). In dieser Arbeit werden zwei Formulierungen mit Komplementaritätsproblemen vorgestellt. Erstens ist die NCP-Bedingung in die lokale thermodynamische Gleichgewichtsberechnung integriert. Zweitens, die NCP-Bedingung des Primärvariablentauschmodells können wir auch direkt in das globale Gleichungssystem einbeziehen. Anhand mehrerer Testprobleme werden diese beiden Formulierungen numerisch untersucht.

Diese Verfahren sind in der OpenGeoSys-Simulationsumgebung implementiert. Die Verpressung von CO_2 in salzhaltigen Wasserschichten numerisch zu simulieren. Es wird eine sehr gute Übereinstimmung zu den Ergebnissen anderer Simulatoren erzielt.

Im zweiten Teil dieser Doktorarbeit richtet sich spezifisch an die Anwendungen für die Atommüllentsorgung. Vor allem an die Mehrphasenströmungsprozesse und chemisch reaktiven Transportkopplung in diesem Bereich. Die chemischen Prozesse werden in eine "look-up table" vereinfacht. Die Methode der Simulation wird für die Schäden an Betonmaterial eingesetzt. Zwei Hauptreaktionenprozesse werden berücksichtigt: Carbonatisierung und Aggregate Silica Reaction (ASR). Die Effizienz und Robustheit der "look-up table" wird weiter mit einem vollreaktiven Transportmodell verglichen.

THESES

This thesis combines model development, validation and application studies for non-isothermal compositional two-phase reactive transport in porous media, including phase transition problem. Most essential achievements are listed comprehensively in the following.

1. Two formulations of non-isothermal compositional two-phase flows incorporating the nonlinear complementarity condition have been shown to lead to equivalent performances of the phase transitions.
2. Several Equation of State (EoS) models are presented for both ideal and non-ideal mixing condition. A special model proposed by Spycher et al.[2] is applied to describe the properties of CO₂ and brine system. While, Peng-Robinson model is applied for a general non-idealize mixing system.
3. A nonsmooth inside-out algorithm proposed by Watson et al.[3] is applied and extended in order to suppress the numerical challenge where the cubic equation of state is involved for the non-ideal properties.
4. The two formulation are implemented in the OpenGeoSys framework. Fully implicit Euler scheme is used for time discretization, while the Standard Galerkin finite element method is applied for space discretization. Standard Newton and semi-smooth Newton are developed for linearization.
5. The presented methods are verified by numerical test simulations of gas transport in nuclear waste repository, as well as the CO₂ injection in saline aquifers. Different test cases demonstrated the capability of the implemented two formulations.
6. A new coupling scheme between multiphase flow and reactive transport is proposed based on a "look up table" approach. The complex chemical processes are simplified into a look-up table and cast into the multiphase transport model via source and sink term.
7. The presented numerical models are applied to investigate the degradation of concrete material subjected to two major chemical reactions: carbonation and Aggregate Silica Reaction(ASR). The numerical results from the presented model agree well with the output of a fully reactive transport model. While in terms of

calculation efficiency, the presented model can achieve 10 times faster compared to the reactive transport model.

THESEN

Diese Arbeit kombiniert Modellentwicklungs-, Validierungs- und Anwendungsstudien für einen nicht-isothermen zweiphasigen reaktiven Transport in porösen Medien, einschließlich Phasenbergangsproblemen. Die wichtigsten Leistungen sind im Folgenden umfassend aufgeführt.

1. Es hat sich gezeigt, dass zwei Formulierungen von nicht-isothermen Mehrkomponenten-Zweiphasenströmungen, die nichtlineare Komplementaritätsbedingung beinhalten, zu äquivalenten Leistungen der Phasenübergänge führen.
2. Mehrere EoS-Modelle werden sowohl für ideale als auch für nicht-ideale Bedingungen vorgestellt.
3. Ein nicht-glatte Inside-Out-Algorithmus, von Watson et al. [3], wird angewendet und erweitert, um die numerische Herausforderung zu unterdrücken, wenn das kubische EoS-Modell für die nicht-idealen Bedingungen verwendet wird.
4. Die zwei Formulierungen sind in der OpenGeoSys Simulationsumgebung implementiert. In der vorliegenden Implementierung, wird die Formulierungen mit einer Finite-Elemente-Methode diskretisiert. In dieser Arbeit wird die Verwendung des Newton-Verfahrens für die globalen und lokalen Probleme vorgestellt.
5. Die Verpressung von CO_2 in salzhaltigen Wasserschichten numerisch zu simulieren. Es wird eine sehr gute Übereinstimmung zu den Ergebnissen anderer Simulator.
6. Ein neues Kopplungsschema zwischen Mehrphasenströmung und reaktivem Transport wird basierend auf einem NachschlagetabellenAnsatz vorgeschlagen. Die komplexen chemischen Prozesse werden in eine Nachschlagetabelle vereinfacht und bei Quell- und Senkzeit in das Mehrphasen-Transportmodell umgewandelt.
7. Die vorgestellten numerischen Modelle werden angewendet, um die Degradation von Betonmaterial. Zwei wichtige chemische Reaktionen werden untersucht: Carbonatisierung und Aggregate Silica Reaction (ASR). Es wird eine gute Übereinstimmung zu den Ergebnissen eines vollständig reaktiven Transportmodells. Das vorgestellte Modell kann 10-mal schneller als das reaktive Transportmodell sein.

ACKNOWLEDGEMENTS

In the last four years, I have conducted my PhD research in the Department of Environmental Informatics, Helmholtz Centre of Environmental Research - UFZ. It has been a wonderful and rewarding journey for me. I feel grateful and indebted to many people who have provided me with their unconditional support. I would like to take the opportunity to express my deep gratitude.

First of all I would like to thank my supervisor, Prof. Olaf Kolditz, for his help and constant encouragement. My second advisor, Junior-Prof. Haibing Shao, has played a key role in both my research career and personal development. I am most grateful of the strong friendship we were able to establish in the last couple of years. I am indebted to Haibing for his help and support on the development of my research presented in this dissertation. Also, I would like to express my gratitude to Dr. Georg Kosakowski, who brings me a deeper understanding of reactive transport modelling and the knowledge about nuclear waste disposal. I appreciate his patience and supports.

This work would not have been finished without the OpenGeoSys platform, so I want to thank all OpenGeoSys developers for their worthwhile suggestion and support.

Furthermore, I would like to deliver my gratefully acknowledgement to the China Scholarship Council. Their financial support allows me to focus on the research work presented in the dissertation.

Most of all, I want to thank my family for their patience, inspiration and support throughout all these years. Special thanks go to my wife, Zhou Yang, for her love and understanding. I only wish I could have had more time to be company with her in the past four years.

CONTENTS

I	BACKGROUND, THEORY AND NUMERICS	1
1	INTRODUCTION	2
1.1	Motivations	2
1.2	Challenges	3
1.3	Current state of research	4
1.4	Scope of this thesis	6
1.5	Outline of this thesis	6
2	MATHEMATICAL FORMULATIONS OF NON-ISOTHERMAL TWO-PHASE MULTI-COMPONENT FLOW	8
2.1	Fundamental Concepts	8
2.2	Conservation of mass	9
2.3	Conservation of energy	9
2.4	Intrinsic constraints and closure relationship	10
2.5	Phase behavior	11
2.5.1	Flash calculation	11
2.5.2	Primary Variable Switching (PVS)	12
3	MODELING PHASE CHANGE WITH NON-LINEAR COMPLEMENTARY CONDITION	13
3.1	Non-smooth model for phase behavior calculation	13
3.1.1	Idealized system	15
3.1.2	Non-ideal system	16
3.2	Comparative phase behaviour calculation	18
4	TWO NON-SMOOTH FORMULATIONS FOR PHASE CHANGE	22
4.1	Formulation based on overall-composition variables	22
4.1.1	Governing equation	22
4.2	Formulation of natural variables	24
4.2.1	Treatment of phase appearance and disappearance	25
4.2.2	Treatment of phase appearance and disappearance	27
4.3	Comparison between different formulations	27
5	EQUATION OF STATE (EOS)	29
5.1	Ideal Mixing system	29
5.2	Equation of State (EoS) for a brine/CO ₂ system	30
5.3	Cubic Equation of State	32
6	NUMERICS	35
6.1	Discretization	35
6.1.1	Linearization strategy	36
6.1.2	Interface continuity requirement	40

7	TWO-PHASE REACTIVE TRANSPORT MODEL WITH A LOOK-UP TABLE	42
7.1	Background	42
7.2	Concrete degradation and creation of look-up table	44
7.2.1	Hydrated mortar	44
7.2.2	Carbonation	44
7.2.3	ASR	46
7.2.4	Chemical and physical changes upon concrete degradation	46
7.3	The coupling strategy	47
8	MODEL APPLICATIONS	49
8.1	Benchmarks for idealize system	50
8.1.1	Benchmark I: Drying by gas injection	50
8.2	Benchmarks for non-ideal system	54
8.2.1	Benchmark II: Injection of CO ₂ into water saturated domain	54
8.2.2	Benchmark III: Cold CO ₂ injection into a saline aquifer	58
8.2.3	Benchmark IV: Co-injection CO ₂ and Impurities in CCS application	63
8.3	Benchmarking the look-up table approach	70
8.3.1	Conceptual of the application	70
8.3.2	Model configuration	70
8.3.3	Model dimensions and discretization	71
8.3.4	Results and discussion	71
8.3.5	Reference	78
II	SUMMARY AND OUTLOOKS	1
1	DISCUSSION AND SUMMARY	2
1.1	Remarks on the non-isothermal compositional two-phase flow model	3
1.1.1	Background	3
1.1.2	Conclusion	4
1.1.3	Reference	4
1.2	Remarks on the two-phase reactive transport model with look-up table	4
1.2.1	Discussion	4
1.2.2	Conclusion	6
1.2.3	Reference	7
1.3	Outlooks	7
1.3.1	Application	7
1.3.2	Model extension	8
III	APPENDIX	9
A	APPENDIX	10
A.1	Paper 1	10
A.2	Paper 2	34

A.3 Code availability 53

NOMENCLATURE

Greek symbols

μ_α	Dynamic viscosity of phase α	[Pa s]
λ_T	Effective heat conductivity tensor	[W (m K) ⁻¹]
ν	The normalized molar fraction of gas phase	[-]
Ω	(sub)domains	
ω	test function	
ϕ	Porosity	[-]
Φ^i	Fugacity coefficient	[-]
ρ	Mass density	[kg m ⁻³]

Operators

\wedge	Logical and
∇	Gradient operator
\perp	Complement operator
div	Divergence operator

Roman symbols

$c_{p\alpha}$	Specific heat capacity of fluid phase α	[J (kg K) ⁻¹]
c_{pS}	Specific heat capacity of soil grain	[J (kg K) ⁻¹]
D_α^i	Diffusivity tensor	[m ² s ⁻¹]
D_a	Apparent diffusion coefficient.	[m ² s ⁻¹]
F^i	Source or sink term of component i	[kg (m ³ s) ⁻¹]
f_α^i	Fugacity of component i in α phase	[Pa]
g	Gravitational acceleration	[m s ⁻²]
H	Henry constant	[mol (Pa m ³) ⁻¹]
h_α	Specific enthalpy of phase α	[J kg ⁻¹]
J_α^i	Diffusive flux of component i in phase α	[mol m ⁻² s ⁻¹]
K	Intrinsic permeability tensor	[m ²]

k	The equilibrium ratio	[-]
$k_{r\alpha}$	Relative permeability of phase α	[-]
M^i	Molar mass of i^{th} component	[kg mol ⁻¹]
N_α	Molar density of phase α	[mol m ⁻³]
N_c	Total number of components existing in the system	
P_α	Pressure in phase α	[Pa]
P_C	Capillary pressure	[Pa]
P_{sat}	Vapor saturation pressure	[Pa]
P_{vap}	Vapor pressure	[Pa]
\mathbf{q}	Darcy velocity	[m s ⁻¹]
Q_T	Heat source or sink	[W m ⁻³]
S	Saturation	[-]
s_{sal}	The salinity of water	[-]
T	Temperature	[K]
u_α	Specific internal energy	[J kg ⁻¹]
U^P	Primary variable set	
U^S	Secondary variable set	
x_α^i	Molar fraction of i^{th} component in phase α	[-]
x^i	Molar fraction of component i in liquid phase	[-]
y^i	Molar fraction of component i in gas phase	[-]
z^i	The overall molar fraction of component i	[-]

ACRONYMS

BC	Boundary condition
CCS	Carbon Capture Storage
DOF	Degree of freedom
EoS	Equation of State
NCP	Nonlinear Complementary Problem
FEM	Finite Element Method
IC	Initial condition
OGS	OpenGeoSys
PVS	Primary Variable Switching
PPC	Pressure-Capillary Pressure formulation
THMC	Thermo-hydro-mechanical-chemical
OpenGeoSys-MP-LT	Opengeosys multiphase model coupled with look-up table approach
OpenGeoSys-GEM	Opengeosys coupled with GEM
ASR	Alkali-Silica-Reaction

Part I

BACKGROUND, THEORY AND NUMERICS

INTRODUCTION

1.1 MOTIVATIONS

Modelling non-isothermal compositional two-phase flows is considered to be one of the most fundamental physics processes in many geo-scientific applications. A traditional yet still active field is in petroleum engineering, where people are trying to predict the flow of oil and gas in deep reservoirs. Numerical reservoir models are often employed to maximize hydrocarbon production rates, and thus to increase the profitability [4]. Another newly emerged topic nowadays is to reduce the atmospheric carbon dioxide (CO_2) concentration by the so-called CO_2 geological sequestration, i.e. CO_2 capture and storage (CCS) in subsurface geological formations. Instead of being released to the atmosphere, gaseous CO_2 is condensed into the super-critical state and pumped into subsurface reservoirs, which have to fulfill special conditions, concerning e.g. minimum depth, temperature and the presence of a well-sealed cap-rock. Other recent applications of non-isothermal compositional two-phase numerical models include the investigation of gas generation and migration in underground nuclear waste repositories. There, the radioactive wastes are stored in sealed containers. Under the influence of (bio)chemical reactions, corrosion and degradation happens along with the radiolysis of water over thousands to millions of years. Over this long period, multiple gas components might be generated both within the containers and migrate through the repository. These processes might lead to pressure build-up within the container, as well as in the repository scale. In the worst case scenario, when the pressure reaches a critical value, the generated gas could lead to cracks in the engineered barrier system and undesired release of radioactive material. In this context, the numerical modelling of compositional two-phase transport serves as a critical tool in the long-term safety design and assessment of the nuclear waste repository.

These above mentioned applications are challenging with respect to the complex chemical and physical processes associated with the two-phase flow and transport, which are represented by different yet coupled partial differential equations. They can hardly be solved by analytical solution, and thus numerical simulation tools are rising as a widely adopted approach to interpret the aforementioned coupled

processes. Due to the complexity of the porous media, the nonlinear behaviour of fluid properties and their interactions, it is crucial to develop accurate and efficient numerical models and computational methodologies of two-phase flow and transport for a better understanding of the aforementioned geo-scientific applications.

1.2 CHALLENGES

Conventionally, an immiscible two-phase flow model, e.g. black-oil reservoir models [5], is utilized to simulate the flow of two immiscible phases in the porous medium. The model normally consists a system of two coupled transient and nonlinear partial differential equations. The drawback of such model formulation is that it does not include solubility, and the phase exchange can not be properly described either. Thus, such model is not suitable for physical scenarios where solubility has important impact.

The mathematical framework that includes solubility and equilibrium phase exchange is called compositional two-phase flow model. In such a framework, the liquid and gas phases are constituted by (more than) two components. In contrast to the immiscible model, each phase is allowed to consist of multiple chemical components, which can be exchanged across the phases. Moreover, the phase behavior is typically represented by the choice of corresponding Equation of State (EoS) within a certain pressure and temperature range.

Non-isothermal compositional simulation is typically much more challenging and complex in comparison with an isothermal model. The main complexities or challenges stem from the thermal effects embedded in the tight coupling between pressure, temperature and phase compositions. Two well-known problems associated with this coupling in a reservoir simulation are the so-called *narrow-boiling point problem* [6] and the *apparent negative compressibility effect* [7]. They impose significant nonlinear convergence difficulties.

One of the most critical challenges in modeling non-isothermal compositional two-phase flow is to determine the phase behavior especially when phase change happens in the model domain. The phase change phenomena is mathematically challenging to simulate due to several reasons. Firstly, the governing equations that describe two-phase zones and single-phase zones are qualitatively different, since the composition of two-phase zones is controlled by thermodynamic equilibrium, while it is not the case in single-phase zone [8]. Moreover, the pore fluid mixture can either be in a single-phase or a two-phase state, depending on the local pressure, temperature and phase composition. Such phase transition creates discontinuities in the primary or secondary variables e.g. phase saturation. In addition to that, phase change induced latent heat effects cause nonlinearities

in the energy balance equation, which can lead to difficulties in numerical convergence.

1.3 CURRENT STATE OF RESEARCH

Over the past decades, several researchers have suggested reliable approaches for handling the aforementioned uncertainties and challenges associated with phase change. One widely used approach is based on a two-stage procedure, combining phase stability analysis and flash calculation. Usually the phase stability test is applied in prior to detect whether a postulated number of equilibrium phases is stable by using the Gibbs tangent plane criterion [9]. This requires the solution of a global optimization problem for each set of trial phase until the set corresponds to a stable mixture. After the phase stability analysis, a flash calculation is applied to determine the phase compositions. Such a guess-and-check routine is considered computationally expensive and prone to slow convergence [10].

Another widely used model is so-called Primary Variable Switching method initially presented by Coats et al. [7] based on a natural variable formulation. In the following decades, many numerical models were further developed based following this approach, i.e. Wu et al. [11] and also Class et al. [12]. In their models, a local criteria based upon saturation pressure test is employed to detect the phase stability. In the two-phase region, phase pressure and saturation are used as primary variables, while in the one-phase region, the saturation is replaced by total concentration or mass/mole fraction. Nevertheless, switching the primary variables is a intrinsically non-differentiable process that can again potentially lead to numerical difficulties [1] of convergence.

More recently, a variety of methods have been proposed to model the gas phase appearance and disappearance in a nuclear waste disposal. Panfilov et al. [13] proposed a negative saturation scheme and extended the saturation definition to artificial negative values and also values higher than 1, which correspond to the unsaturated and over-saturated zones respectively. Bourgeat et al. [14] suggested to use persistent primary variables to handle phase change by regularizing Henry law formulation. Neumann et al. [15] and Amaziane et al. [16] provide different possibilities for the choice of persistent primary variable set. However, limited research have been made regarding a non-ideal condition where Henry law cannot be applied.

Lauser et al. [1] present a novel method that formulate the phase change logic as nonlinear complementary constraints and use semi-smooth Newton to solve the non-smooth equation system. A similar algorithm can be found in [17]. Recent study [18] indicates that conventional natural formulation shows even better performance against the natural formulation with a complimentary constraints under non-

ideal mixing condition. The reason behind that is possibly the ill-conditioned or rank deficient global Jacobian matrix structure [19], or a bad initial input for the semi-smooth Newton iteration at places where phase appears or vanishes [15].

It needs to be mentioned that Watson et al. [3] proposed a non-smooth formulation for simulating the phase appearance and disappearance in chemical processes engineering. In their model, the phase change logic is firstly formulated as a nonlinear complementary condition similar to [1], then these NCPs are rewritten as a non-smooth model. The proposed model leads to a differential algebraic equation system which can be efficiently solved by an improved non-smooth inside-out algorithm [20]. Unlike the previous work mentioned above, this model neither requires the rigorous and costly stability analysis, nor does it introduce discontinuities in the model equations. In addition, the performance of this model is not strongly dependent on good initial guesses, therefore the phase change problems can be handled in a very compact way.

Owing to the similarities shared between chemical processes engineering modeling and fully compositional reservoir model with respect to the thermodynamic equilibrium flash part [21], this novel non-smooth model can be applied to compositional phase behavior model. Finally in this work, a fully EoS-oriented approaches for the flash calculation which are agnostic to the number of phases presents in the system are developed for two-phase compositional flow model. To the author's knowledge, the non-smooth thermodynamic equilibrium model can be implemented in two different ways associated with different primary variable choices.

Local-NCP formulation employs the overall-composition variables [22, 10] as the primary variable set. In this formulation, the NCP is combined with thermodynamic model to construct the local problem for solving all secondary variables such as phase saturation [23]. A nonlinear solver of the semi-smooth Newton type is applied to determine the phase state on the local level, as well as the other secondary variables. Meanwhile, standard Newton iterations are employed to solve the global mass and energy conservation for all global primary degrees of freedoms.

Global-NCP formulation employs natural variables [7] as the primary variable set. In this formulation, the NCP constraints are combined with mass and energy balance equations, along with thermodynamic equilibrium model, to construct the global governing equations. The extended global system can now be solved by an iterative semi-smooth Newton algorithm without requiring nested Newton iterations to identify the local phase state.

To the author's knowledge, there has been rarely a detailed analysis of these two nonsmooth formulations, with respect to their numerical performance and computational efficiency in solving the non-

isothermal compositional two-phase flow problem. In this work, the investigation will be based on the scientific simulator OpenGeoSys [24, 25], which has been extended to have both NCP implementations equipped. The spatial discretization is based on the Galerkin Finite Element method (*GFEM*), while a fully implicit Euler scheme is applied for time integration.

1.4 SCOPE OF THIS THESIS

In this thesis, a non-isothermal two-phase compositional simulation module has been implemented, analyzed, and further extended based on the OpenGeoSys (OGS). It will be demonstrated to handle the challenging phase change problem properly. The newly implemented model was further applied to investigate the gas generation and migration in a nuclear waste repository.

The following key scientific questions have been investigated in this work.

- Which numerical schemes are robust and efficient enough in handling non-isothermal two-phase compositional flow with phase change phenomena?
- How is the numerical performance of the two aforementioned NCP formulations in real case studies with (non)-ideal gas-liquid distribution conditions?
- Are there new physical understandings obtained when applying the newly implemented two-phase model integrated with chemical reactive processes in simulating the degradation of concrete in the context of long-term safety assessment of the nuclear waste repository?

1.5 OUTLINE OF THIS THESIS

This thesis is structured as follows. In Chapter 2, the fundamental theorem of non-isothermal compositional two-phase fluid flow is reviewed and explained. The mathematical formulations for mass and energy conservation are derived, along with the local thermodynamic equilibrium. The non-smooth numerical model for handling phase change is further interpreted in Chapter 3. The details of local and global NCP formulations are introduced in Chapter 4. Following that, Chapter 6 focuses on the technical issues regarding spatial and temporal discretization, as well as linearization and numerical solution strategies. In Chapter 7, the chemical model for concrete degradation and the approximation by the look-up table is explained, moreover, the couple strategy between look-up table and compositional two-phase flow transport model are describe. In Chapter 8, three groups

of benchmarks are dedicated to the model verification and validation. Numerical performance analysis of different numerical schemes are further compared and discussed.

MATHEMATICAL FORMULATIONS OF
NON-ISOTHERMAL TWO-PHASE
MULTI-COMPONENT FLOW

In this chapter, a system of partial differential equations describing non-isothermal two-phase compositional flow in the porous medium is derived. The multiphase flow and transport in the porous medium is described using a continuum approach on a macroscopic scale.

2.1 FUNDAMENTAL CONCEPTS

Different length scales have to be taken into account for modeling flow in porous media. For a continuous model on the macroscopic scale possible heterogeneities and characteristics on the smaller scale have to be taken into account. In this work the averaging procedure by Bear [26] is used, where an average value for each point in the continuum is determined through a representative elementary volume (REV) on the microscopic scale. With the REV concept in mind, the porous media can be mathematically described with the following properties.

- **Porosity.** In a porous medium, the porosity ϕ is defined as the ratio between the volume of the void space over the total volume of a given REV.
- **Saturation.** The saturation S is defined as the ratio between the volume of phase and the total volume of pore space in a given REV.
- **Intrinsic Permeability** Intrinsic Permeability K measures the ability of a fluid to flow through a porous medium. The tensor K solely depends on the porous medium, not the fluid. If the porous medium has a preferred flow direction, K is anisotropic.
- **Relative Permeability** If more than one phase exist in the porous medium, the flow of one phase is inhibited by the presence of the other phase. This is measured by the relative permeability k_{rel} of phase α , which only depends on the saturation of the phase $k_{\text{rel}}(S_\alpha)$.

The fluid is then characterized with the following properties:

- **Viscosity.** Viscosity μ describes the resistance of a fluid to deformation by shear stress. Dynamic viscosity heavily depends on the pressure and temperature, as well as the phase composition.
- **Molar(mass) Density.** Molar(mass) density is defined as the number of moles(mass) per volume in phase α . The density depends on pressure and temperature and also on the composition of the phase.
- **Molar(mass) fraction.** Molar(mass) fraction of component i in phase α is the ratio of the molar(mass) of component i in phase α and the mass of phase α in a REV. In this work, the symbol X and x denote the mass and molar fraction, respectively. For two components, e.g. component i and j , the relationship of molar fraction and mass fraction can be derived by

$$x_{\alpha}^i = \frac{X_{\alpha}^i M^j}{X_{\alpha}^j M^i + (1 - X_{\alpha}^j) M^j} \quad (2.1)$$

where M is the molar mass of component κ . By definition, the molar or mass fractions in one phase sum up to unity.

$$\sum_{i=0}^{N_c} x^i = 1 \quad \sum_{i=0}^{N_c} X^i = 1 \quad (2.2)$$

2.2 CONSERVATION OF MASS

The mass conservation equation system for conventional two-phase isothermal compositional reservoir simulation can be written as

$$\phi \frac{\partial}{\partial t} \left(\sum_{\alpha \in \{G,L\}} N_{\alpha} S_{\alpha} x_{\alpha}^i \right) + \text{div} \left[\sum_{\alpha \in \{G,L\}} N_{\alpha} (x_{\alpha}^i \mathbf{q}_{\alpha} + \mathbf{J}_{\alpha}^i) \right] = F^i. \quad (2.3)$$

Here, x_{α}^i is the molar fraction of component i in phase α , and S_{α} is the saturation of phase α , N_{α} represents the phase molar density. For a particular phase α , its velocity \mathbf{q}_{α} is given by the generalized Darcy's law:

$$\mathbf{q}_{\alpha} = -\frac{\mathbf{K}k_{r\alpha}(S)}{\mu_{\alpha}} (\nabla P_{\alpha} - \rho_{\alpha} \mathbf{g}), \quad (2.4)$$

with ρ_{α} indicating the mass density of phase α , and the diffusive flux \mathbf{J}_{α}^i governed by Fick's law

$$\mathbf{J}_{\alpha}^i = -\phi S_{\alpha} \mathbf{D}_{\alpha}^i \nabla x_{\alpha}^i. \quad (2.5)$$

2.3 CONSERVATION OF ENERGY

When thermal effects need to be considered, the energy balance equation is then augmented along with the above mass balance formulations

$$\begin{aligned} & \phi \frac{\partial}{\partial t} [(1 - S_G) \rho_L u_L + S_G \rho_G u_G] \\ & + (1 - \phi) \frac{\partial}{\partial t} (\rho_S c_{pS} T) + \operatorname{div} [\rho_G h_G \mathbf{q}_G] + \operatorname{div} [\rho_L h_L \mathbf{q}_L] - \operatorname{div} (\lambda_T \nabla T) = Q_T \end{aligned} \quad (2.6)$$

where ρ_G , ρ_L , ρ_S represent the mass density of the gas, liquid and solid phase, respectively. c_{pS} denotes its specific heat capacity. The specific internal energy u_L and u_G define the total energy of the molecules of liquid and gas phase per unit mass (kg), respectively. The specific enthalpy h_α in phase α can be computed as

$$h_\alpha = \int_{T_0}^T c_{p\alpha} dT. \quad (2.7)$$

Note that the enthalpy of gas phase is higher than that of the liquid, and the difference between them equals to the latent heat of vaporization at given pressure and temperature, which guarantees that the phase transition from liquid to gas.

The relationship between specific internal energy u_α and the specific enthalpy h_α is related to the pressure volume work. Since the liquid phase is assumed to be incompressible in this work, i.e. the volume change in the liquid phase is neglected. Then its enthalpy is quantitatively the same as its internal energy ($u_L = h_L$). For the compressible gas phase, however, its specific enthalpy is regulated by

$$h_G = u_G + \frac{P_G}{\rho_G} \quad (2.8)$$

To sum up, the equations (2.3) to (2.6) provide a general mathematical framework for non-isothermal componential two-phase flow.

2.4 INTRINSIC CONSTRAINTS AND CLOSURE RELATIONSHIP

A saturation constraint holds on phase saturation given by

$$\sum_{\alpha \in \{G,L\}} S_\alpha = 1 \quad (2.9)$$

The capillary pressure is a monotonic and continuous function of phase saturation. By its definition, it can be written as:

$$P_c(S) = P_G - P_L \quad (2.10)$$

where P_G is the gas phase pressure, and P_L is the liquid phase pressure.

2.5 PHASE BEHAVIOR

Instantaneous thermodynamic equilibrium is the most general assumption for the non-isothermal two-phase compositional model and it can be expressed as equality of fugacity in the gas and liquid phase, i.e.

$$f_G^\kappa(P, T, x_G^\kappa) = f_L^\kappa(P, T, x_L^\kappa) \quad (2.11)$$

holds for any component κ in gas (G) and liquid (L) phases. Here, f_G^κ and f_L^κ represents the fugacity of component κ , usually it can be expressed as a function of reference pressure, temperature, molar fraction of component κ in gas/liquid phase.

$$f_\alpha^\kappa := \Phi_\alpha^\kappa P_\alpha x_\alpha^\kappa, \quad \alpha \in \{G, L\} \quad (2.12)$$

where Φ_α^κ indicates the fugacity coefficient of component κ . It can be further determined by using the equation of state. For ideal mixture, $\Phi_G^\kappa = 1$ holds for the ideal gas phase, while in the liquid phase, Henry law and Raoult law are applied to calculate the fugacity coefficient of solute components and solvent components, respectively. For non-ideal mixture, cubic equation of state (e.g. Peng-Robinson Equations[27]) are usually utilized.

In two-phase compositional simulation, a mixture z at a given pressure (P) and temperature (T) condition, can either be in a single phase, or two-phase state. The phase behavior calculation differs depending on the current phase status of the system, since the composition of single phase is no longer controlled by the thermodynamics.

Conventionally, there are two widely used approaches to handle the difficulties associated with phase change:

2.5.1 Flash calculation

The flash calculation refers to the thermodynamic equilibrium calculation which splits the overall molar fraction of components into the component molar fraction in each phase. This method generally include a two-stage calculation, namely phase stability analysis and flash calculation. For this method, an overall molar fraction of components is usually chosen as primary variable. The solution routine of this method can be summarized as follows:

- For any element in which a single phase is present, the phase stability analysis is performed to check whether the current phase status is stable or switch to a two-phase states. Usually, a tangent plane distance analysis [9] is used to determine the phase stability and obtain the number of stable phases.
- The flash calculation are then performed on each element to compute the phase compositions at equilibrium. A scheme com-

binning successive substitution iteration and Newton iteration is performed for the solution of the flash calculation.

2.5.2 *Primary Variable Switching (PVS)*

In this method, different primary variable set are applied according to the number of existing phases for each element. In the two-phase region, a phase pressure and saturation are used as primary variables, while in the single phase region, the saturation is replaced by the concentration or mass/mole fraction for the present phase. The phase appearance and disappearance can be detected as follows:

- After each global Newton iteration, if the saturation is detected to be negative, the saturation is set to zero and molar fraction is used as primary variable.
- After each global Newton iteration, if saturation is detected to be zero, then a saturation pressure is calculated for this single phase element. If the saturation pressure is larger than the phase pressure, then saturation is used as primary variable again.

Both of two approaches have demonstrated the capability to model phase transition, yet some specific restrictions remain. For example, in the PVS scheme, numerical oscillation might be introduced within Newton iterations due to frequent switching of primary variables, which often leads to irregular convergence behavior, whereas for the flash calculation approach, the global minimization of Gibbs free energy required by phase stability analysis usually leads to a time consuming computation.

3

MODELING PHASE CHANGE WITH NON-LINEAR COMPLEMENTARY CONDITION

In this chapter, a novel non-smooth inside-out algorithm [3] is presented and extended aiming at handling both idealize and nonidealize thermodynamic flash calculation which includes the associated phase change phenomena.

3.1 NON-SMOOTH MODEL FOR PHASE BEHAVIOR CALCULATION

Let z be the overall molar fraction. For a two-phase system with n_c components, the over all molar fraction z can be represented as a linear combination of liquid phase molar compositions x and gas phase molar composition y :

$$z^i = (1 - \nu)x^i + \nu y^i \quad (3.1)$$

with x^i , y^i correspond the molar fraction of component i in liquid and gas phase, respectively. ν is the normalized molar fraction of gas phase. In a single gas phase, $\nu = 1$, and in a single liquid phase, $\nu = 0$, while in a two-phase zone, $0 < \nu < 1$.

The relation between the phase molar fraction and saturation is given by:

$$\nu = \frac{S_G N_G}{S_G N_G + (1 - S_G) N_L} \quad (3.2)$$

In Masson et al. [28], it is proven that the sign of phase molar fraction provides equivalent criteria for phase change to the phase saturation. The equilibrium ratio k for a component i between phases is given by:

$$k^i = y^i / x^i \quad (3.3)$$

It represents the distribution of component i in gas and liquid phase (also recalled k-value), which is generally a function of temperature, pressure and phase composition. By rearrange the above equations, the liquid phase molar compositions x and gas phase molar composition y can be reformulated as follows:

$$x^i = \frac{z^i}{1 + \nu(k^i - 1)} \quad (3.4)$$

$$y^i = \frac{z^i k^i}{1 + \nu(k^i - 1)} \quad (3.5)$$

Thermodynamic equilibrium and the constitutive equation is assumed to hold:

$$\sum_{i=1}^{n_c} y^i - \sum_{j=1}^{n_c} x^j = 0 \quad (3.6)$$

Substituting Eq (3.4) and Eq (3.5) into Eq (3.6), the well known Rachford-Rice equation [29] can be obtained and replace the Eq (3.6):

$$\sum_{i=1}^{n_c} \frac{z^i (k^i - 1)}{1 + \nu(k^i - 1)} = 0 \quad (3.7)$$

the Rachford-Rice equation is more preferred due to its desirable convergence and good numerical properties [30]. The function is monotonically decreasing, which indicates that the solution of this function contains no false roots, i.e. nonphysical roots.

Watson and Barton [3] proposed a new method to allow this function to convergence to a single-phase zone. By using the following non-smooth equation to replace the Eq (3.7), the phase transition can be detected in a more natural way without a trial and guess procedure or solving a non-convex optimization problem.

$$\text{mid} \left(\nu, - \sum_{i=1}^{n_c} \frac{z^i (k^i - 1)}{1 + \nu(k^i - 1)}, \nu - 1 \right) = 0 \quad (3.8)$$

where the function $\text{mid}: \mathbb{R}^3 \rightarrow \mathbb{R}$ maps to the median value of its three arguments and is a piecewise-continuously differentiable function, meaning that in a neighborhood of every point it is described by a member of a finite collection of continuously differentiable functions. A detailed description of the mid function can be referred to appendix.

As discussed in [3], the three arguments in the mid function in Eq (3.8) correspond to the solutions for a single liquid phase, a two-phase, and a single gas phase, respectively. The equation behaves as follows:

- when only single liquid phase exist,
 $\nu = 0$ and the Rachford-Rice residual [31] is negative, while the third term is equal to -1, therefore the mid function choose the first term and evaluates to zero, satisfying Eq (3.8)
- when only single gas phase exist,
the only gas phase case is analogous, $\nu = 1$ and the Rachford-Rice residual is positive [31], and the third term is equal to 0, therefore the mid function choose the third term and evaluates to zero, which satisfies Eq (3.8).

- when two phases co-exist in the system, we have $0 < \nu < 1$ and the Rachford-Rice residual must be zero, therefore in Eq (3.8) the first term is positive. The second term is zero and the third term is negative, thus the mid function chooses the second term and evaluates to zero.

Noted that, as indicate in Sahlodin et al. [32], this formulation was proven to follow from local minimization of total molar Gibbs free energy of a mixture.

3.1.1 Idealized system

For an idealized system, the K-values (k^i) are considered to be independent of phase composition. Henry law and Raoult law are applied to denote the K-values for different components:

$$k^j = \frac{H^j(T)}{P_G} \quad (3.9)$$

$$k^v = \frac{P_{sat}}{P_G} \quad (3.10)$$

superscript (\cdot^v) denotes the water vapor component, while j denotes the multiple gas component except water vapor. $H^j(T)$ refers to the Henry constant for component j which is a function only depends on temperature. While P_{sat} is the saturated vapor pressure and is given by ClausiusClapeyron equation:

$$P_{sat}(T) = P_0 \exp \left[\left(\frac{1}{T_0} - \frac{1}{T} \right) \frac{h_{\Delta e} M^w}{R} \right] \quad (3.11)$$

where $T_0 = 373K$, $P_0 = 10^5 Pa$, R is the universal constant, $h_{\Delta e}$ is enthalpy of vaporization, M^w is molar mass of water. When the capillary pressure is high enough, the vapor pressure lowering due to the capillary effects, should be regularized by Kelvin equation.

$$P_{sat}^* = \exp \left(\frac{RT}{M^w \rho_L} \right) \quad (3.12)$$

It is evident from the Eq (3.9) and (3.10) the K-value calculation requires no iterations. Thus, the phase behavior calculation for idealize system can be summarized as:

$$\begin{cases} f_G^i(P_G, T, x_G^i) - f_L^i(P_L, T, x_L^i) = 0 \\ \text{mid} \left(\nu, - \sum_{i=1}^{n_c} \frac{z^i (k^i - 1)}{1 + \nu(k^i - 1)}, \nu - 1 \right) = 0 \end{cases} \quad (3.13)$$

By solving Eq (3.13), we can obtain the ν , x^i and y^i . Then using ideal gas law to compute the gas phase molar density N_G , while the water

density is described by IAPWS equations ([33]). Finally the phase saturation S_G is given by

$$S_G = \frac{v/N_G}{v/N_G + (1-v)/N_L} \quad (3.14)$$

3.1.2 Non-ideal system

In a non-ideal system, the equilibrium ratio k^i is highly dependent on the phase composition, which leads to a strong nonlinear equation system. Furthermore, the existence of complementary condition leads the formulation of phase behavior model to being non-smooth and makes it difficult and computationally expensive to solve. Besides, a good initial guess is usually required when Newton-type iteration method is utilized to handle the nonlinearities, which can be potentially challenging to generate without a prior information about the phase status. Especially when phase change happens, the initial guess might differ with the solution in different phase status, which consequently results in slow convergence, or even failure.

To this end, Watson et al. [34] proposed a non-smooth inside-out algorithm, by extending the conventional Boston-Britt inside-out algorithm [20] to cover the phase change problem. In this work, we extend the algorithm of Watson et al. to two-phase compositional P-T flash calculation scenario. Two distinguished modifications are made:

- Fugacity equality is applied instead of the enthalpy balance.
- Newton-type iteration is applied to accelerate the convergence.

The inside-out algorithm is an iterative two-loop nested procedure, with the two loops referred to the inner loop and outer loop. In the outer loop, the phase equilibrium and fugacity equality model are applied to generate parameters for the inner loop, e.g. the phase equilibrium ratios K^i are provided. Then in the inner loop, the flash calculations are converged to get the the phase fraction. The nested loop repeated until the error of outer loop drops in a pre-setting ranges.

Next, a detailed inside-out algorithm for a typical P-T flash calculation is discussed. Following Boston and Britt's idea [20], an iterative volatility parameter'' u is introduced for the outer loop iteration, and it is defined as:

$$u^i = \ln(k^i/k^b) \quad (3.15)$$

where k^b is a reference equilibrium ratio.

While another iterative variable R is introduced in the inner loop in order to relax the phase equilibrium constraints for the single phase zone, and it is given by the following identity

$$R = \frac{k^b v}{k^b v + k_0^b(1-v)}, \quad (3.16)$$

where k_0^b is a constant used to avoid numerical trouble when k^b is very large or small. In this work, k_0^b is set to 1. Next we can set up a variant of complementarity function Eq. 3.17 by replacing ν with R , and it is given as

$$\text{mid} \left(R, - \sum_{i=1}^{n_c} \frac{z^i (k^i - 1)}{1 + R(k^i - 1)}, R - 1 \right) = 0. \quad (3.17)$$

An extra vector \mathbf{p} which is associated with each component is introduced and defined as follow:

$$p^i \equiv \frac{x^i(1 - \nu)}{1 - R} = \frac{z^i}{1 - R + k_0^b R k^b / k^b} \quad (3.18)$$

The definition of \mathbf{p} allows the k^b can be reformulated in terms of \mathbf{p} and \mathbf{u} :

$$k^b = \frac{\sum_{i=1}^{n_c} p^i}{\sum_{i=1}^{n_c} e^{u_i} p^i} \quad (3.19)$$

Therefore, the gas/liquid phase composition can be calculate as follows.

$$x^i = \frac{p^i}{\sum_{i=1}^{n_c} p^i} \quad (3.20)$$

$$y^i = e^{u_i} \frac{p^i}{\sum_{i=1}^{n_c} p^i} \quad (3.21)$$

In summary, the outer loop and inner loop residual functions for the P-T flash calculation are given as follows:

$$\Omega_{PT} = \|\hat{\mathbf{u}} - \mathbf{u}\|_{\infty} \quad (3.22)$$

$$\Psi_{PT} = \text{mid} \left(R, \sum_{i=1}^{n_c} p^i - k^b \sum_{i=1}^{n_c} e^{u_i} p^i, R - 1 \right) \quad (3.23)$$

where Ω_{PT} , Ψ_{PT} correspond to the residual function of the outer and inner loop, $\hat{\mathbf{u}}$ is the vector of calculated iteration variables during each iteration update, while vector \mathbf{u} is the starting points.

It is evident that the outer loop variables u^i is carefully designed to be independent of each other and not strongly relying on the physical quantities, e.g. temperature, pressure and phase composition. On the other hand, the inside loop variables R serves as proxies for the temperature, pressure, vapor/liquid composition and vapor fraction of the system. Owing to the introduction of these largely independent variables, the performance of this algorithm is quite insensitive to the quality of the initial guess, which is considered to be a significant advantage over the conventional methods. However, there is a substantial amount of initialization that must take place to begin calculations. The initial K-value (k^i) can be obtained by Wilson equation:

$$k^i = \frac{P_{\text{crit}}^i}{P} \left(5.37(1 + \omega^i) \left(1 - \frac{T_{\text{crit}}^i}{T} \right) \right) \quad (3.24)$$

Here, P_{crit}^i and T_{crit}^i are the critical pressure and temperature for component i , and ω^i is the acentric factor.

Alternatively, a better initial guess can also come from a previous time step calculation.

The full implementation of the inside-out calculation is given in Algorithm 1. The inside loop can be solved by semi-smooth Newton Linearization method, while the outer loop convergence can be achieved by a combination of Successive Substitution Iteration and Newton-type of iteration.

Algorithm 1 The proposed non-smooth inside-out algorithm for a PT-flash

```

1: Guess  $\nu=0.5$ 
2: Guess initial  $k^i$  using Wilson equation.
3: Set  $k^b \leftarrow 1, k_0^b \leftarrow 1$ .
4: Calculate initial  $u$  from Eq 3.15
5: Set tolerance  $\epsilon_{\text{out}}$  and  $\epsilon_{\text{in}}$  for outside and inside loop.
6: while  $\|\Omega_{\text{PT}}\| > \epsilon_{\text{out}}$  do ▷ The outside loop
7:   Solve  $\nu$  from Rachford-Rice equation.
8:   Calculate  $R$  from Eq 3.16.
9:   while  $\|\Psi_{\text{PT}}\| > \epsilon_{\text{in}}$  do ▷ The inside loop
10:    Solve  $p$  for Eq 3.18.
11:    Using semi-smooth Newton to solve  $\|\Psi_{\text{PT}}\|$  from Eq 3.23.
12:    Update new value of  $R$ 
13:   end while▷ At this point, we have converged  $R$  for the model
14:   Calculate  $k^b$  from Eq 3.19
15:   Calculate  $x$  and  $y$  from Eq 3.20 and Eq 3.21.
16:   Calculate fugacity coefficient  $\Phi_G$  and  $\Phi_L$  from cubic EoS.
17:   Calculate  $k^i$  from
           
$$\ln k^i = \ln(\Phi_L) - \ln(\Phi_G)$$

18:   Calculate  $\hat{u}$  from Eq 3.15.
19:   Calculate  $\|\Omega_{\text{PT}}\|$  from Eq 3.22.
20:   Set  $u \leftarrow \hat{u}$ .
21:   Update a new initial guess of  $\nu$  for Rachford-Rice equation.
22: end while

```

3.2 COMPARATIVE STUDY FOR PHASE BEHAVIOUR CALCULATION WITH PHASE CHANGE

In this section, a few benchmarks have been selected to show that the proposed algorithm allows the phase behaviour model to handle the phase change problem. In all the benchmarks, the following tolerance and parameters are used: $\epsilon_{\text{in}} = 10^{-9}$, $\epsilon_{\text{out}} = 10^{-8}$.

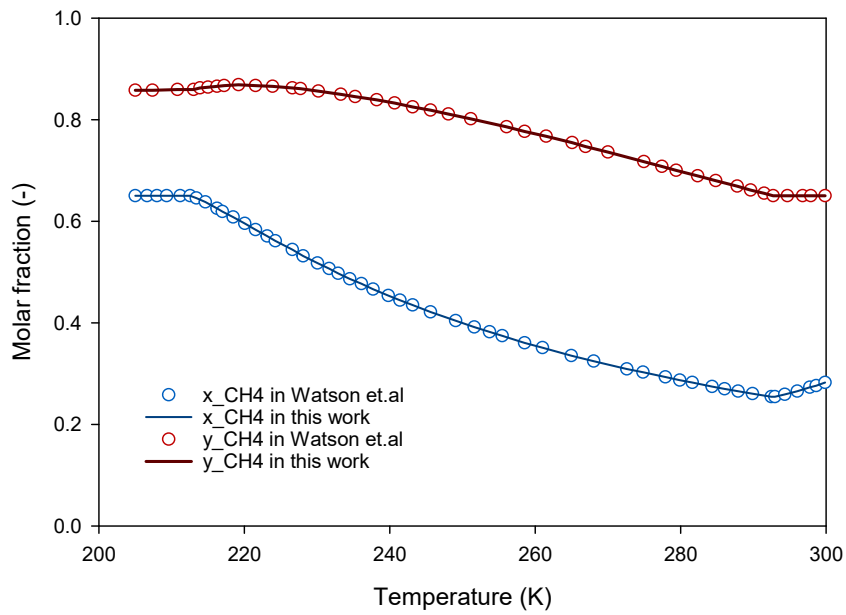


Figure 1.: Results for varying pressure in the hydrocarbon mixture problem described in Example 1, compared against the results proposed in Watson et al. (circle symbols)

The first benchmark involves a P-T flash of 5 components hydrocarbon system, which is originally proposed in Kamath et al. [35]. It was further extended by Watson et al. [34] using Peng-Robinson EoS. The gas and liquid mixture is composed of 2.5 % nitrogen, 65 % methane, 15 % ethane, 15 % propane and 2.5 % butane, with an initial pressure at 5.5 MPa and temperature varies in the range from 205 K to 300 K with 0.1 K increments. Peng-Robinson EoS [27] is used to describe the gas and liquid phase properties and the non-smooth phase behaviour model is calculated based on the proposed inside-out algorithm. The simulation results are shown in Figure (1) with respect to the molar fraction of methane in gas and liquid phase, respectively. And the results are compared against the result proposed in Watson et al. [34].

The second benchmark is performed in the same hydrocarbon mixture, while the temperature is fix to be constant. The pressure is varied ranging from 0.1 MPa to 12 MPa with an increments of 0.01 MPa. The other input parameters are kept the same as the previous test. The simulation results are shown in Figure (2) with respect to the molar fraction of methane in gas and liquid phase.

It can be observed from both figures, that good agreements exist between our simulation results and results reported in Watson et al., which indicates our implementation can reproduce the phase composition split calculation in a wide range of pressure and temperature

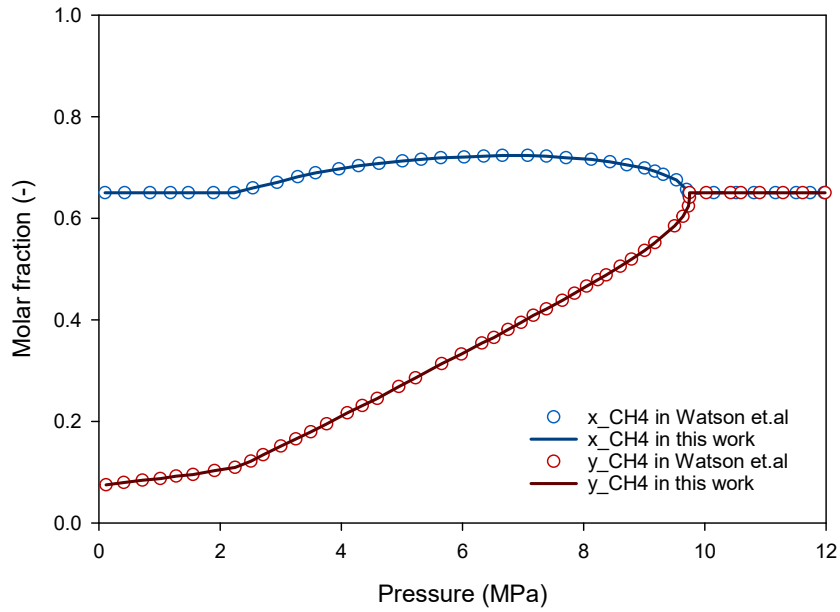
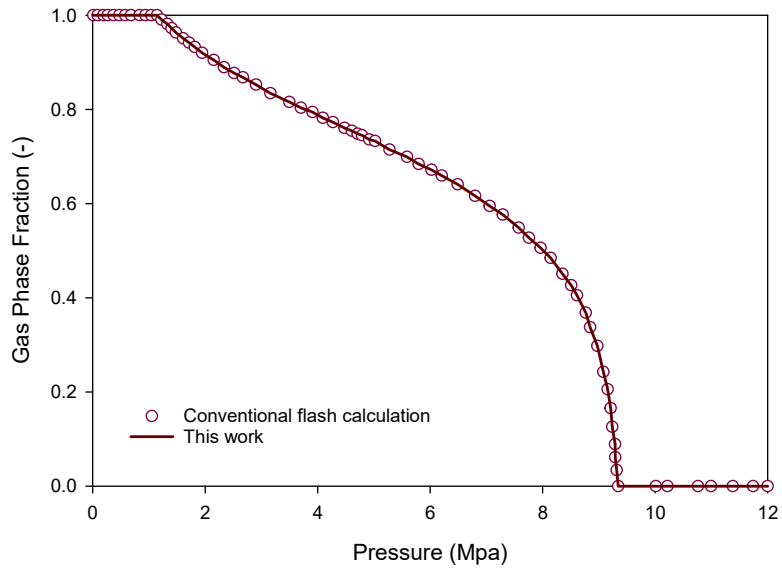


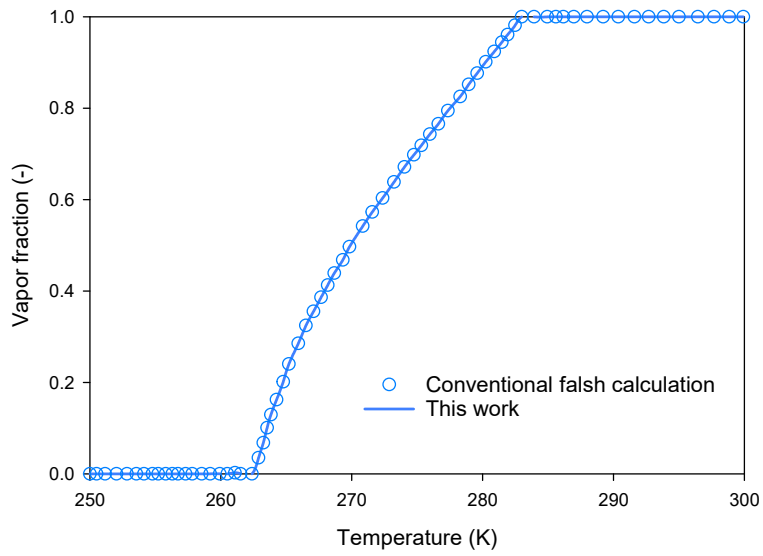
Figure 2.: Results for varying pressure in the hydrocarbon mixture problem described in benchmark 2, compared against the results proposed in Watson et al. paper (circle symbols)

within considerable good accuracy. A further investigation is performed in terms of the gas phase fraction ν for the scenario when phase change is taken into account. Two configurations are considered. In the first one, we fix the temperature to be 260 K and gradually increase the pressure from 0.01 MPa to 12 MPa, while in the second one, the pressure is fixed to be 9.5 MPa while the temperature varies from 250 K to 300 K. A comparison is made against the conventional two-stage flash calculation method, where the phase stability analysis is based on the Gibbs tangent plane method [9].

It can be observed that under these configurations the phase status for the mixture system undergoes from one-phase to two-phase and back to one-phase again. In the first test, along with the increasing of pressure, the liquid phase begin to formulate after pressure exceeds the dew point, while the gas phase will completely vanish after pressure exceeds the bubble point. Similar performance can be observed from the second experiment. The gas bubble is formulated once the temperature exceeds the bubble point, while the liquid phase will completely vanish after the temperature exceeds the dew point. Furthermore, it can be observed that a good match exists between the results obtained by this work and the results of the conventional method. The correctness of the implementation are verified.



(a)



(b)

Figure 3.: Comparison of gas phase fraction between simulation results in this work and reference results generated by conventional flash calculation method which are reported in Watson et al. for the hydrocarbon mixture

4

TWO NON-SMOOTH FORMULATIONS FOR PHASE CHANGE

The thermodynamic models are usually cast into two-phase compositional simulator by using one of two strategies [36]:

- Treat the thermodynamic equilibrium equations as model constraints, and they are solved together with the mass and energy conservation equations. (cf. Eq 2.3).
- Solve the thermodynamic equilibrium equations separately and couple them with the mass and energy conservation equations in a two-step approach.

Based on these two strategies, two non-smooth formulations of non-isothermal two-phase compositional flow in porous medium are derived along with the corresponding governing equations in this chapter.

4.1 FORMULATION BASED ON OVERALL-COMPOSITION VARIABLES

This formulation was first proposed by Young and Stephenson [22], and later extended by Collins et al. [37], Marchand et al. [38], in which the primary variables are chosen to be a *overall-composition variables* set [10]. It includes

- the reference phase pressure P ,
- overall molar fraction z^i , $i \in [1, \dots, n_c - 1]$, with $(n_c - 1)$ degrees of freedom,
- and the local temperature T .

4.1.1 Governing equation

In this formulation, the phases are quantified in terms of the overall molar fraction z^i for each component i

$$z^i = \frac{\sum_{\alpha \in \{G,L\}} N_\alpha S_\alpha \chi_\alpha^i}{\sum_{\alpha \in \{G,L\}} N_\alpha S_\alpha} \quad (4.1)$$

where N_α is the molar density of the phase α , and x_α^i is the molar fraction of component i in phase α . If we denote N to be the total molar density, then

$$N = \sum_{\alpha \in \{G,L\}} N_\alpha S_\alpha \quad (4.2)$$

and the mass conservation in terms of each component can be written based on the overall composition

$$\phi \frac{\partial}{\partial t} (z^i N) + \text{div} \left[\sum_{\alpha \in \{G,L\}} N_\alpha (x_\alpha^i \mathbf{q}_\alpha + \mathbf{J}_\alpha^i) \right] = F^i \quad (4.3)$$

where the nomenclature follows those introduced in Chapter 2. Once the primary variable set is fixed, the remaining unknowns are treated as secondary variables, which include the phase saturation and component molar fraction in each phase. Then, the thermodynamic equilibrium equations are constructed as stand-alone calculation procedure and serve as local problem in each global Newton iteration loop. Thereby all secondary variables are solved based on integration points of each element. To summarize, For a given set of primary variables P, z^i ($i \in [1, \dots, n_c - 1]$) and T , the local problem reads,

$$\begin{cases} f_G^i(P_G, T, x_G^i) - f_L^i(P_L, T, x_L^i) = 0 \\ z^i = (1 - \nu)x_L^i + \nu x_G^i \\ k^i = x_G^i / x_L^i \\ \text{mid}(\nu, -\sum_{i=1}^{n_c} \frac{z^i(k^i - 1)}{1 + \nu(k^i - 1)}, \nu - 1) = 0 \end{cases} \quad (4.4)$$

In total, there are $2n_c + 2$ equations, along with $2n_c + 2$ secondary variables, including $\nu, x_\alpha^i, \alpha \in \{G, L\}, i \in [1, \dots, n_c]$. The solution procedure of this local problem with respect to ideal and non-ideal cases utilize the algorithms discussed in Section 3.1.1 and 3.1.2.

Here we are in a position to discuss the complete solution procedure of the overall-composition formulation. In a FEM fully coupled fully implicit scheme, the solution is computed in each time step as follows: Within each global Newton iteration, the global governing equation system (coupling mass and energy conservation equations) is solved for updated primary variable values. Subsequently, the local problem Eq (4.4) is resolved on each Gauss integration point to update the secondary variables, while the primary variables are known prior. In return, the updated secondary variables are delivered to the next round of global Newton iteration in order to solve for primary variables again.

Note that, the thermodynamic equilibrium is solved as local problem, in which case the appearance or disappearance of a phase is thus shifted to the local level. In such configuration, the local problem is considered to be semi-smooth, due to the presence of the NCP constraints and the introducing of the "mid" function. A semi-smooth

Newton type method is used for linearizing and solving the system of equations, which enable a quadratically convergence in a neighborhood of the solution. On the other hand, the global governing equation system is smooth over the domain and can be directly solved by standard Newton method. For the sake of simplicity, this formulation is named as local Nonlinear Complementary Problem (NCP) formulation in the rest of the thesis.

4.2 FORMULATION OF NATURAL VARIABLES

An alternative to the local NCP formulation was proposed by Lauser et al. [1], in which the *natural variable* set (cf. Coats et al.[7]) is chosen as primary variables. They are

- the reference phase pressure P ,
- the gas phase saturation S_G ,
- the phase composition x_G^i, x_L^i $i \in [1, \dots, n_c]$, with $(2n_c)$ degrees of freedom,
- and system temperature T .

In this formulation, the system of governing equations (mass and energy conservation) and the algebraic system of equations associated with the thermodynamic equilibrium model are solved in a monolithic way.

While in order to address the phase change problem with respect to the natural variable set, the non-smooth model Eq (3.8) can be replaced by

$$\text{mid} \left(\nu, \sum_{i=1}^{n_c} x_G^i - \sum_{i=1}^{n_c} x_L^i, \nu - 1 \right) = 0 \quad (4.5)$$

or equivalently:

$$\left\{ \begin{array}{l} \min \left(S_G, \left(1 - \sum_{i=1}^{n_c} x_G^i \right) \right) = 0. \\ \min \left(S_L, \left(1 - \sum_{i=1}^{n_c} x_L^i \right) \right) = 0. \end{array} \right. \quad (4.6a)$$

$$(4.6b)$$

In Watson et al.[3], it is evident that Eq 4.5 is equivalent to Eq 3.8. To summarize, let $\mathcal{H}(U)$ represents the mass and energy balance equations (2.3)-(2.6), the global governing equation system reads

$$\left\{ \begin{array}{l} \mathcal{H}(U) = 0 \\ f_G^i(P_G, T, x_G^i) - f_L^i(P_L, T, x_L^i) = 0 \\ \min \left(S_G, \left(1 - \sum_{i=1}^{n_c} x_G^i\right) \right) = 0. \\ \min \left(S_L, \left(1 - \sum_{i=1}^{n_c} x_L^i\right) \right) = 0. \end{array} \right. \quad \begin{array}{l} (4.7a) \\ (4.7b) \\ (4.7c) \\ (4.7d) \end{array}$$

With U represents the primary variable set: $U = [P, S_G, x_G^i, x_L^i, T]^T \in \mathbb{R}^{(n_c+3)}$.

The fugacity equality (Eq 2.11) and phase transition constraint are resolved along with mass and energy conservation equations within the same global Newton loop. Meanwhile, the pressure P , temperature T , phase saturation S_α , and phase composition x_α^i are obtained simultaneously through the global Newton iterations.

4.2.1 Treatment of phase appearance and disappearance

The treatment of phase transition is similar to the overall-composition formulation, since the complementary condition (Eq (4.7b)) have to be full-filled.

- if $S_G - (1 - \sum_{i=1}^{n_c} x_G^i) \leq 0$, it implies $S_G = 0$, and only liquid phase is present in the system. In this case, the component molar fraction in the gas phase in virtual equilibrium with the component molar fraction in the liquid phase can be defined as:

$$\tilde{x}_G^i = \frac{1}{k^i(P, T, x_L^i)} x_L^i, \quad i \in [1, \dots, n_c]. \quad (4.8)$$

- if $S_L - (1 - \sum_{i=1}^{n_c} x_L^i) \leq 0$, it implies $S_L = 0$, and only gas phase presents in the system, the component molar fraction in the liquid phase in equilibrium with the component molar fraction in the gas phase can be defined as:

$$\tilde{x}_L^i = k^i(P, T, x_G^i) x_G^i, \quad i \in [1, \dots, n_c]. \quad (4.9)$$

Preconditioning strategy At the end of each global Newton iteration, we find the nodes which are located in single phase zone. Then we make negative flash calculation (cf. Whitson et al.[29]) on these nodes. We assume the overall molar fraction of component i is equal to the component molar fraction in this single phase. Then pressure, overall molar fraction, temperature are treated as input for the negative flash

to calculate the phase molar fraction ν . If $0 < \nu < 1$, it indicates that the mixture is unstable and the gas and liquid phases will co-exist on this node during the next Newton iteration loop. Therefore, before the initialization in the next round of Newton iteration, we first modify the phase saturation(S_G) by the calculated phase molar fraction ν , according to the equation 3.14.

This formulation was firstly proposed by Lauser et al. [1], in which fugacity is selected as the primary variable. However, in this work, the phase composition are preferred in order to avoid a further calibration of phase composition and their derivatives in terms of the fugacity. For this type of formulation, phase state identification no longer requires additional local Newton iterations on each element or integration point. This means less computational resources are required on the local level, at the price that the global linear equation system is larger. Nevertheless, due to its simple structure and piece-wise linearity of the min-function, a Schur complement reduction strategy can be further applied on the Jacobian matrix to minimize the size of global linear system. More details regarding this procedure will be discussed in section 6.1.1. For the sake of simplicity, we call this formulation as global NCP formulation in the rest of the thesis.

FORMULATION OF PRESSURE-CAPILLARY PRESSURE MODEL

If the saturation can be uniquely obtained with the help of the inverse of the monotone saturation-capillary pressure function by means of

$$S_w = P_c^{-1}(p_c) \quad (4.10)$$

capillary pressure can be selected as the primary variable by replacing saturation. Neumann et al. [15] extend the scope of the gas phase pressure and the capillary pressure and use them as primary unknowns in a two-phase two- component model taking into account the dissolution of gas components. The appearance and disappearance of gas phase are also addressed. Here we propose a further extension of this formulation to non-isothermal compositional two phase flow allowing the appearance and disappearance of both phase.

By considering multi-components($n_c \geq 3$), the following primary variable set can be selected.

- the reference phase pressure P ,
- the capillary pressure \tilde{P}_c ,
- the gas phase composition x_G^i , $i \in [1, \dots, n_c - 1]$, with (n_c) degrees of freedom,
- and system temperature T .

To deal with the phase appearance and disappearance of both phases, one strategy is to extend the saturation-capillary pressure function by its monotone graph, i.e. by $S_w = 1$, $P_c \in [P_c(1), -\infty)$ to deal with the single liquid phase - two-phase transition, and by $S_w = 0$, $P_c \in [P_c(0), +\infty)$ to handle the single gas phase - two phase transition. Therefore, we will denote by \tilde{P}_c the extended saturation-capillary pressure function and its inverse function by \tilde{P}_c^{-1} .

4.2.2 Treatment of phase appearance and disappearance

The entry pressure P_{entry} is the critical capillary pressure that must be applied so that the nonwetting phase appears. One has to distinguish two cases:

1. $P_c \leq P_{entry}$ where $S_G = 0$ and only the wetting phase exists.
2. $P_c > P_{entry}$ where $S_G > 0$ and both liquid and gas phases exist.

4.3 COMPARISON BETWEEN DIFFERENT FORMULATIONS

The local and global NCP formulations have the following common features.

- For both local and global NCP formulations, a fixed governing equation and fixed set of primary variable are applied. No primary variable switching is required if a phase status changes, which indicates that the same primary variables can be used for all elements or integration points.
- By formulating the phase change logic as nonlinear complementary constraints, the rigorous and computationally expensive phase stability analysis can be avoided. The method will converge directly to either single-phase or two-phase solutions that corresponds to a solution of the KKT conditions of the mixture Gibbs free energy minimization problem.

While at the same time, the two formulations have the following differences.

- A distinguished difference is associated with the primary variable choice. In the global NCP formulation, due to the choice of natural-variables as primary variable set, the Jacobian matrix of the mass and energy conservation equations can be computed with regards to these primary variables quite efficiently, since the equations can be explicitly expressed in them. While for local NCP formulation, the mass and energy conservation equations are implicitly expressed by the overall-composition variables, which inevitably leads to the usage of chain rule to calculate the derivatives in order to fill the Jacobian matrix. More

specifically, the chain rule is required to calculate derivatives of phase saturation, component molar fraction in each phase with respect to overall component mole fractions, and it will further increase the computational resources.

- Another difference lies in the way to handle the phase change problem. In the local NCP formulation, the saturation serves as secondary variable and is solved on the local level by a nested Newton iteration. While in the global NCP formulation, the saturation is treated as primary variable and solved simultaneously along with the governing equations, which indicates the phase change is detected and handled on the global level and no additional local Newton iteration is required for phase status identification.

 EQUATION OF STATE (EOS)

In this chapter, different Equation of State (EoS) with respect to several physical scenarios quantities are presented.

5.1 IDEAL MIXING SYSTEM

The ideal gas law can be considered as the simplest form of equation of state.

$$N_G = \frac{P_G}{RT} \quad (5.1)$$

If the following assumptions are made that only limited amount of gas can dissolve in the liquid phase, the Henry's law can be applied to obtain the dissolved gas composition in liquid phase. The mathematical formulation of Henry's law can be written as:

$$x_L^i = \frac{H}{N_L P_G^i} \quad (5.2)$$

Here H is the Henry constant which depends on the temperature, and i represents the gas component except the water component. It can be observed that the correlation in Henry's law assumes a linear relationship between the dissolved gas composition and partial gas pressure. While, on the other hand, Raoult's law can be applied to obtain the solubility of solvent in the gas phase. The mathematical formulation of Raoult's law can be written as:

$$x_G^w = \frac{P_{sat}(T)}{P_G^w} \quad (5.3)$$

Furthermore, if the presence of capillary pressure cannot be negligible, Kelvin's equation is applied to regularize the Eq. (5.3), which is given as

$$x_G^w = \frac{P_{sat}(T)}{P_G^w} \exp\{-M^w P_c / (RT\rho_L)\} \quad (5.4)$$

Here $P_{sat}(T)$ represents water saturation pressure depending only on temperature T . It can be observed that the correlation in Raoult's law also assumes a linear relationship the mole fractions and the vapor pressures of the pure water vapor.

5.2 EQUATION OF STATE (EOS) FOR A BRINE/CO₂ SYSTEM

As mentioned before, Henry's law and Raoult's law are only valid for a very low solute solubility and in relatively low pressure and temperature condition. For a CO₂-brine system in deep geological reservoirs, both pressure and temperature values are very high, and the mutual solubility of CO₂ and water can also be high. Therefore, Henry's law and Raoult's law are not suitable for the EoS of CO₂-brine system.

During the recent decades, enormous research have been made in order to provide accurate Equation of State for brine/CO₂ system. Among them, the EoS of Duan and Sun [39] provides good estimation for the solubility of CO₂ in water. Spycher et al. [2] proposed a more complicated correlation which takes into account the solubility of water in CO₂. In this work, the Spycher and Pruess EoS is preferred due to the mutual solubility model it provided.

The complete EoS of Spycher and Pruess is described in detail in [40]. First the Redlich Kwong cubic equation of state is solved to determine the molar volume of the compressible gas phase. Subsequently the mutual solubility can be computed via a combination of polynomials and exponential functions. In a general formulation, the solubility of the components in a CO₂-brine system is influenced by the pressure P , the temperature T of the system and the salinity of water s_{sal} :

$$x_L^i = x_L^i(P, T, s_{sal}) \quad x_G^a = x_G^a(P, T, s_{sal}) \quad (5.5)$$

Figure 4 shows that the solubility of CO₂ in the water phase increases fast with rising gas phase pressure up to the saturation pressure, above which it rises with a smaller rate. For temperatures below the critical temperature $T_{crit} = 304.15K$, the state of the CO₂ changes from gaseous (below saturation pressure) to liquid. This phase transition results in a not continuously differentiable sharp break at the transition point.

In Figure 5, the solubility of brine in the gas phase is plotted. It decreases sharply with rising gas phase pressure up to the saturation pressure. When the pressure is getting close to the saturation pressure, the solubility undergoes a smaller decreasing rate. Once pressure is above the saturation pressure, the solubility begin to increase sharply and then enters a slowly increasing stage.

To calculate the density of CO₂ phase, model from Duan et al.[41] was applied. The density of CO₂ phase strongly depends on the CO₂ phase pressure. The general format can be written:

$$\rho_L(x_L^i, T), \rho_G(P_G, T) \quad (5.6)$$

Figure 6 shows the density of CO₂ with respect to different temperature. The viscosity of the water phase is computed using a function by Atkins [42], while for viscosity of the CO₂ phase, the approach of

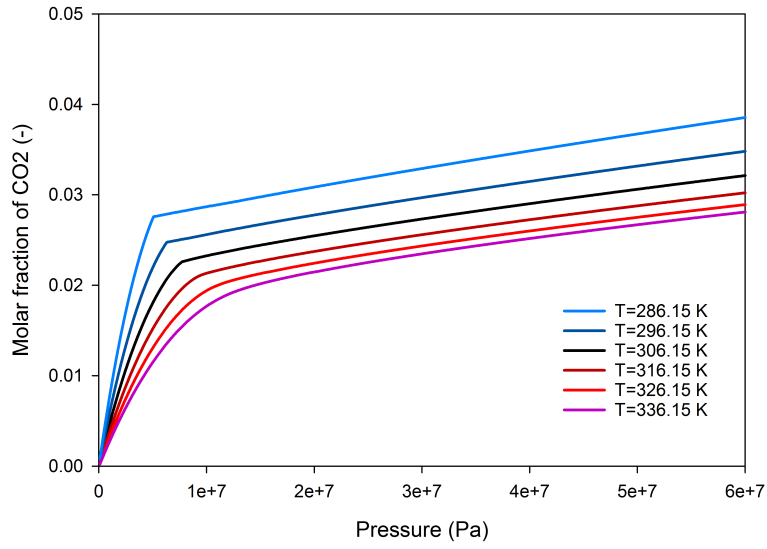


Figure 4.: The solubility of CO₂ in water phase at different temperature.

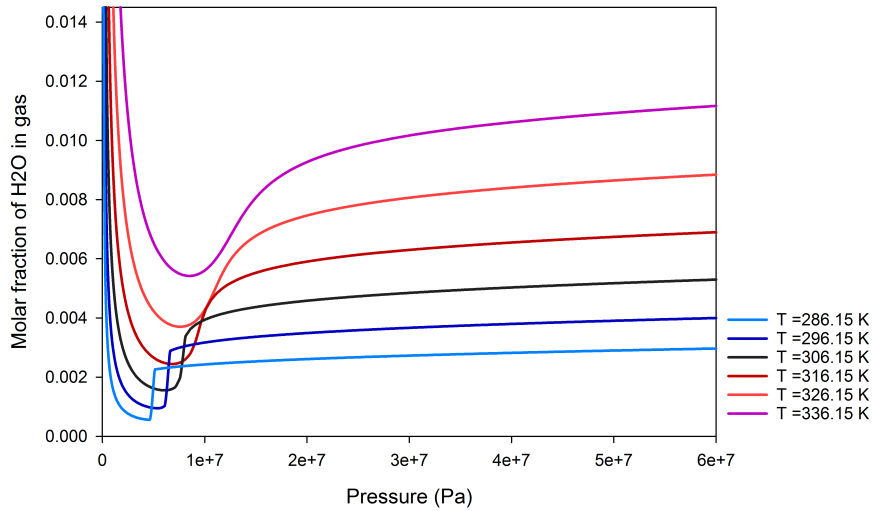


Figure 5.: The solubility of brine in the gas phase at different temperature

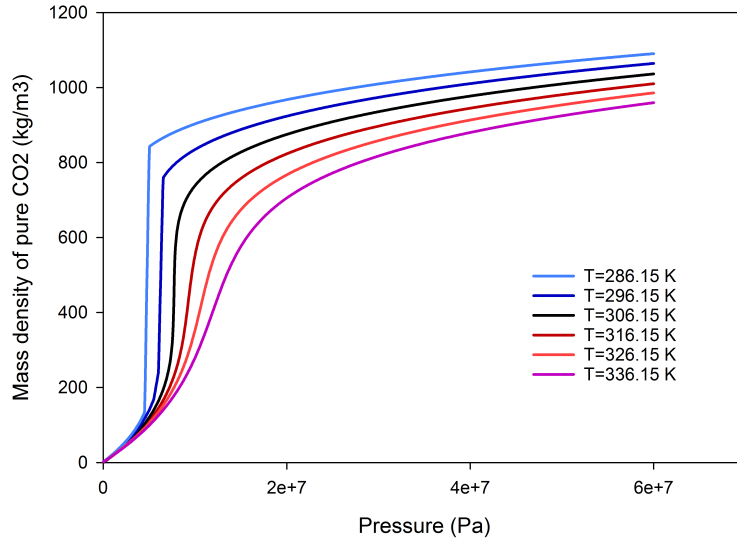


Figure 6.: The mass density of pure CO₂ at different temperature

Fenghour and Vesovic [43] is employed. Figure.7 show the viscosity of CO₂ phase at different temperature. It can be observed that the CO₂ phase viscosity also highly depends on the phase pressure and temperature.

5.3 CUBIC EQUATION OF STATE

More general complex equations of state models were developed for higher temperatures and pressures and more complex phase composition system, notably the cubic equation of state which can offer an accurate description of both liquid and gas phases over a wide range of pressure and temperature. Among them, Peng-Robinson EoS is widely used. The standard Peng-Robinson model (PR78) (cf. Peng and Robinson [27]) for a pure component i takes the following form:

$$P = \frac{RT}{v - b^i} - \frac{a^i(T)}{v(v + b^i) + b^i(v - b^i)} \quad (5.7)$$

where the attraction parameter $a(T)$ and co-volume parameter b in Eq.(5.7) are calculated from the criterion of criticality:

$$a(T) = 0.45724\alpha \frac{R^2 T^2}{P_{\text{crit}}} \quad (5.8)$$

and

$$b = 0.0778 \frac{RT_{\text{crit}}}{P_{\text{crit}}} \quad (5.9)$$

with the α -function can be expressed as

$$\alpha = (1 + m(1 - \sqrt{T/T_{\text{crit}}}))^2 \quad (5.10)$$

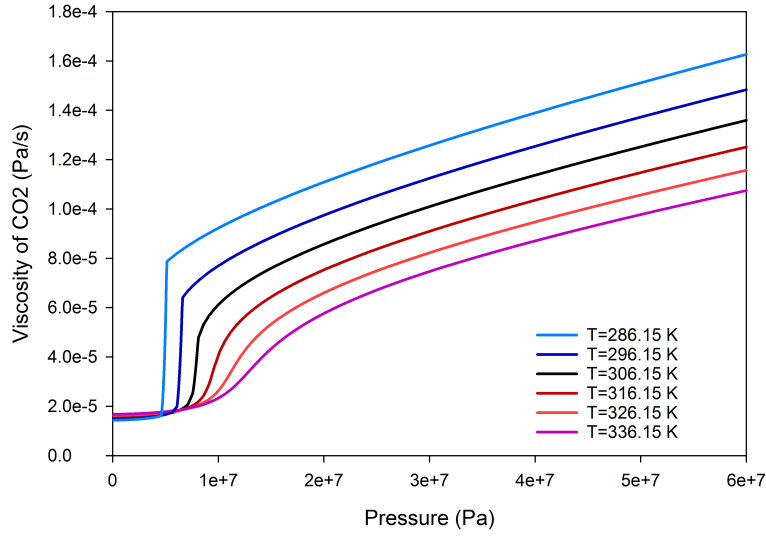


Figure 7.: The viscosity of CO₂ phase at different temperature

$$m^i = \begin{cases} 0.37464 + 1.54226\omega^i - 0.26992(\omega^i)^2 \\ 0.3796 + 1.485\omega^i - 0.1644(\omega^i)^2 + 0.01667(\omega^i)^3 \end{cases}$$

with ω^i denotes the acentric factor.

In this work, the Peng-Robinson EoS in terms of reduced parameters properties is applied, where the reduced properties of a fluid are a set of dimensionless state variables normalized by the fluid's state properties at its critical point.

$$P_r = P/P_{\text{crit}}, \quad T_r = T/T_{\text{crit}} \quad (5.11)$$

thus the parameters can be further expressed as:

$$A = 0.45724\alpha \frac{P_r}{T_r^2} \quad (5.12)$$

$$B = 0.0778P_r/T_r \quad (5.13)$$

In a multi-component mixture system, the mixing rules for the parameters in EoS can be extended as

$$A_{\text{mix}} = \sum_{i,j} x^i x^j A^{i,j} \quad (5.14)$$

where $A^{i,j} = \sqrt{A^i A^j} (1 - k^{i,j})$ and $k^{i,j}$ is the binary interaction parameter with respect to component i and j .

$$B_{\text{mix}} = \sum_i x^i B^i \quad (5.15)$$

Then we consider the polynomial form of the Peng-Robinson EoS in terms of compressibility $Z = \frac{PV}{RT}$:

$$\begin{aligned} Z^3 - (1 - B_{\text{mix}})Z^2 + (A_{\text{mix}} - 2B_{\text{mix}} - 3B_{\text{mix}}^3)Z \\ - (A_{\text{mix}}B_{\text{mix}} - B_{\text{mix}}^2 - B_{\text{mix}}^3) = 0 \end{aligned} \quad (5.16)$$

Eq (5.16) can be solved analytically by the cubic formula. If multiple real roots exist, the one giving the lowest Gibbs energy is selected.

The fugacity coefficient can be calculated for component i in phase α as following:

$$\ln(\Phi_\alpha^i) = \frac{B_\alpha^k}{B_{mix}}(Z_\alpha - 1) - \ln(Z_\alpha - B_{mix,\alpha}) - \frac{A_{mix,\alpha}}{2\sqrt{2}B_\alpha^i} \left(\frac{2A_{mix2}}{A_{mix}} - \frac{B_\alpha^i}{B_{mix,\alpha}} \right) \ln \frac{Z_\alpha + (1 + \sqrt{2})B_{mix,\alpha}}{Z_\alpha + (1 - \sqrt{2})B_{mix,\alpha}} \quad (5.17)$$

where

$$A_{mix2,j} = \sum_i A^{i,j} x^i \quad (5.18)$$

Furthermore, the phase densities can thereby be obtained in the following relationship:

$$N_L = N_L^{std} [C_w(P + P_c - P_0)] \quad (5.19)$$

$$N_G = \frac{P}{Z_\alpha RT} \quad (5.20)$$

where N_L^{std} is the molar density of water at standard condition. P_0 corresponds to the atmospheric pressure.

 NUMERICS

6.1 DISCRETIZATION

In this work, the standard Galerkin finite element method is employed for spacial discretization, with a backward Euler fully implicit scheme for the time integration. On each (sub)domain Ω , the weighted residual method is used to derive the weak form of mass and energy balance equations Eq.2.3-2.5.

It reads

$$\begin{aligned} & \frac{\phi}{\Delta t} \sum_{\alpha \in \{G,L\}} \int_{\Omega} \left[\left(N_{\alpha} S_{\alpha} x_{\alpha}^i \right)^{k+1} - \left(N_{\alpha} S_{\alpha} x_{\alpha}^i \right)^k \right] \omega d\Omega \\ & + \sum_{\alpha \in \{G,L\}} \int_{\Omega} \operatorname{div} \left[N_{\alpha} x_{\alpha}^i \left(\mathbf{q}_{\alpha} + \mathbf{J}_{\alpha}^i \right) \right]^{k+1} \omega d\Omega - \int_{\Omega} (F^i)^{k+1} \omega d\Omega = 0 \quad (6.1) \end{aligned}$$

for component based mass balance, and

$$\begin{aligned} & \frac{\phi}{\Delta t} \sum_{\alpha \in \{G,L\}} \int_{\Omega} \left[\left(\rho_{\alpha} S_{\alpha} u_{\alpha} \right)^{k+1} - \left(\rho_{\alpha} S_{\alpha} u_{\alpha} \right)^k \right] \omega d\Omega \\ & + \frac{(1-\phi)\rho_{SCpS}}{t} \Delta t \sum_{\alpha \in \{G,L\}} \int_{\Omega} \left[T^{k+1} - T^k \right] \omega d\Omega - \int_{\Omega} \operatorname{div} (\lambda \nabla T^{k+1}) \omega d\Omega \\ & + \sum_{\alpha \in \{G,L\}} \int_{\Omega} \operatorname{div} \left(\rho_{\alpha} h_{\alpha} \mathbf{q}_{\alpha} \right)^{k+1} \omega d\Omega = \int_{\Omega} (Q_T)^{k+1} \omega d\Omega \quad (6.2) \end{aligned}$$

for the energy balance. Here $\omega \in H_0^1$ represents the test function. The superscripts \cdot^k and \cdot^{k+1} are employed here to represent the previous (t^k) and current time step t^{k+1} , and Δt denotes the actual time step size ($\Delta t = t^{k+1} - t^k$).

The Laplacian-related terms in the above formulations have the general form of $\int_{\alpha} \operatorname{div} \mathbf{V} \omega d\Omega$, and they yield second order differentials in Euclidean space of the respective primary variables. The reduction of the differentiation order of the Laplacian-related terms can be realised via integration by parts and Green-Gauss theorem as follows:

$$\int_{\Omega} \operatorname{div} \mathbf{V} \omega d\Omega = \int_{\Gamma} \mathbf{V} \cdot \mathbf{n}_{\Gamma} \omega d\Gamma - \int_{\Omega} \mathbf{V} \cdot \nabla \omega d\Omega \quad (6.3)$$

where Γ represents the domain boundary $\partial\Omega$, \mathbf{n}_{Γ} is the unit outward normal at the boundary surface.

In this work, a special attention is paid to the discretization of complementary problem (Eq (4.6)). In global NCP formulation, the NCP are cast as governing equations coupled with mass and energy balance equations. Here the nodal discretized version for NCP is given as follows:

$$\mathbf{C} \left((\mathbf{u}^P)^{k+1} \right) := \begin{bmatrix} C_G((\mathbf{u}^P)^{k+1}) \\ C_L((\mathbf{u}^P)^{k+1}) \end{bmatrix} = \mathbf{0} \quad (6.4)$$

with

$$C_\alpha = \min \left\{ (S_\alpha)^{k+1}, 1 - \sum_{i=1}^{N_c} \left(x_\alpha^i \right)^{k+1} \right\}, \quad \alpha \in \{G, L\}. \quad (6.5)$$

6.1.1 Linearization strategy

6.1.1.1 Semi-smooth Newton scheme

In non-isothermal compositional two-phase flow problems, nonlinearities can emerge from the conservation equations (2.3)-(2.6), from the thermodynamic equilibrium equations (2.11)-(2.12), as well as from the NCP equation (Eq 3.8 and 4.6). Mathematically, these nonlinearities can be categorized into smooth or non-smooth types. In the conservation equations and thermodynamic equilibrium formulations, the function itself, as well its first order derivatives, are continuous with respect to the primary unknowns. Therefore the nonlinearities originated from them are considered to be smooth. On the contrary, the mid function (Eq 3.8) and the minimum functions (Eq 4.6), are considered to be semi-smooth, as discussed in Section 3.1. For the two types of nonlinearities, the corresponding linearization strategies are also different. Smooth nonlinearities can be directly handled by standard Newton scheme, while a semi-smooth Newton scheme (cf. Krutle et al.[44]) must be employed to handle the complementary constraints. This algorithm is proven to achieve local convergence while keeping the quadratic convergence rate.

In the local NCP formulation, the local problem (Eq (3.13)) is of semi-smooth type. Therefore in each time step, semi-smooth Newton scheme is performed on each integration point, while the standard Newton method is used to solve the global mass and energy conservation (Eq (2.3) - (2.6)). In contrast, for the global NCP implementation, equation system (Eq (4.6)) requires a semi-smooth Newton scheme on the global level.

Firstly, let us demonstrate how to use semi-smooth Newton scheme to solve the mid-function of Eq (3.7). First, the notation $f(v)$ is introduced

$$f(v) := \text{mid}(v, g(v), v - 1) \quad (6.6)$$

where

$$g(v) = - \sum_{i=1}^{n_c} \frac{z^i (k^i - 1)}{1 + v(k^i - 1)} \quad (6.7)$$

the k -th step of the semi-smooth Newton iteration can be defined as

$$\mathbf{J}^k \Delta v^k = -f(v^k) \quad (6.8)$$

where \mathbf{J}^k is a generalized derivative of f at v^k , and it represents an element of B-subdifferential of f :

$$\mathbf{J}^k := \frac{\partial f(v^k)}{\partial v^k} \quad (6.9)$$

Algorithm 2 depicts the way to construct the generalized Jacobian matrix \mathbf{J}^k . Assuming an element $j^k \in \mathbf{J}^k$ is selected, and its i -th line is defined as j_i^k :

Algorithm 2 Construct generalized Jacobian matrix for the mid function in local NCP

```

1: if  $v < v - 1$  then
2:   if  $v < g(v) < v - 1$  then
       $j_i^k = \frac{\partial g_i(v^k)}{\partial v^k}$ 
3:   else
       $j_i^k = 1$ 
4:   end if
5: else
6:   if  $v - 1 < g(v) < v$  then
       $j_i^k = \frac{\partial g_i(v^k)}{\partial v^k}$ 
7:   else
       $j_i^k = 1$ 
8:   end if
9: end if

```

where $\frac{\partial g(v^k)}{\partial v^k}$ is defined as the Jacobian matrix of the Rachford-Rice equation.

Next, we also define the semi-smooth Newton routine for the global NCP formulation. In global NCP formulation, the nonlinear complementarity min-functions are solved along with mass and energy conservation equations and thermodynamic equilibrium model, below we introduce some notations for simplicity:

- \mathbf{u} : the vector of primary unknowns for $\mathbf{u} = [P, S_G, x_G^i, x_L^i, T]^T \in \mathbb{R}^{(2N_c+3)}$.
- $\mathcal{H}(\mathbf{u})$: the mass and energy conservation equations.
- $\mathcal{F}(\mathbf{u})$: the fugacity equality model.

$$\mathcal{F}(\mathbf{u}) := f_G^i(P_G, T, x_G^i) - f_L^i(P_L, T, x_L^i) \quad (6.10)$$

- NCP function for gas and liquid phase \mathcal{N}

$$\mathcal{N}_\alpha = \min(\phi_\alpha(\mathbf{u}), \psi_\alpha(\mathbf{u})) \quad (6.11)$$

$$\text{with } \phi_\alpha(\mathbf{u}) = S_\alpha \text{ and } \psi_\alpha(\mathbf{u}) = 1 - \sum_{i=1}^{N_c} x_\alpha^i, \alpha \in \{G, L\}$$

In summary, the governing equation system of global NCP formulation can be denoted as:

$$\mathbf{F}(\mathbf{u}) := \begin{pmatrix} \mathcal{H}(\mathbf{u}) \\ \mathcal{F}(\mathbf{u}) \\ \mathcal{N}_\alpha(\mathbf{u}) \end{pmatrix} \quad (6.12)$$

In the rest part of the , $\partial\mathcal{N}_\alpha(\mathbf{u})$ to denote the generalized Jacobian matrix of \mathcal{N}_α at a point U , and finally the statement of the semi-smooth Newton algorithm can be described in Algorithm 3

Algorithm 3 Semi-smooth Newton algorithm for global NCP formulation

- 1: Define the complementary index sets A_α^k and I_α^k by

$$A_\alpha^k := \{\phi_\alpha(\mathbf{u}^k) < \psi_\alpha(\mathbf{u}^k)\} \quad I_\alpha^k := \{\phi_\alpha(\mathbf{u}^k) \geq \psi_\alpha(\mathbf{u}^k)\}$$

- 2: Select \mathcal{J}_u^k denotes an element of the B-subdifferential of $\partial\mathcal{N}_\alpha(\mathbf{u})$ such that its i -th component is equal to

$$\mathcal{J}_u^k := \left\{ \begin{array}{ll} \partial\phi_\alpha(\mathbf{u}^k) & \text{if } i \in I_\alpha^k \\ \partial\psi_\alpha(\mathbf{u}^k) & \text{if } i \in A_\alpha^k \end{array} \right\}$$

- 3: The k -th step of the semi-smooth Newton iteration is solved as:

$$\begin{cases} \partial\mathcal{H}(\mathbf{u}^k)\Delta\mathbf{u}^k = -\mathcal{H}(\mathbf{u}^k) \\ \partial\mathcal{F}(\mathbf{u}^k)\Delta\mathbf{u}^k = -\mathcal{F}(\mathbf{u}^k) \\ \mathcal{J}_u^k\Delta\mathbf{u}^k = -\mathcal{N}(\mathbf{u}) \end{cases}$$

- 4: The primary variable for the $k + 1$ -th iteration can be updated as:

$$\mathbf{u}^{k+1} = \mathbf{u}^k + \Delta\mathbf{u}^k$$

With $\partial\mathcal{H}(\mathbf{u})$, $\partial\mathcal{F}(\mathbf{u})$ represent the standard Jacobian matrix of $\mathcal{H}(\mathbf{u})$ and $\mathcal{F}(\mathbf{u})$. Note that, only one linear system has to be solved at each Newton iteration.

6.1.1.2 Construction of global Jacobian matrix

To construct the global Jacobian matrix, the derivatives of governing equation system with respect to the primary variables are required. In the global NCP formulation, the derivatives are straightforward to calculate. Whereas in the local NCP, the derivatives calculation is very complicated, due to a nested thermodynamic model. In this

work, the partial derivatives of the secondary variable set \mathbf{u}^S , with respect to the primary variable set \mathbf{u}^P can be obtained by:

$$\frac{\partial \mathbf{u}^S}{\partial \mathbf{u}^P} = \left(\frac{\partial F}{\partial \mathbf{u}^S} \right)^{-1} \frac{\partial F}{\partial \mathbf{u}^P} \quad (6.13)$$

where function F represents the equation system (3.13), and the square matrix $\frac{\partial F}{\partial \mathbf{u}^S}$ is the local Jacobian matrix for equation system (3.13).

6.1.1.3 Jacobian matrix reduction

As already mentioned in Section 4.2, in the global NCP formulation, the Schur complement strategy can be applied on the global Jacobian matrix, such that the size of global linear system can be minimized. Special attention has to be paid to the minimum function. Within a Newton iteration l , the Newton equation for NCP (6.5) can be easily obtained:

$$C_G : \begin{cases} (\delta S_G)^l = -(S_G)^l & \text{if } S_G \leq 1 - \sum_{i=1}^{N_c} (x_G^i) \\ \sum_{i=1}^{N_c} (\delta x_G^i) = 1 - \sum_{i=1}^{N_c} (x_G^i)^l & \text{if } S_G > 1 - \sum_{i=1}^{N_c} (x_G^i) \end{cases} \quad (6.14)$$

$$C_L : \begin{cases} (\delta S_G)^l = 1 - (S_G)^l, & \text{if } 1 - S_G \leq 1 - \sum_{i=1}^{N_c} (x_L^i) \\ x_G^i \frac{\partial k^i}{\partial P} (\delta P)^l + x_G^i \frac{\partial k^i}{\partial T} (\delta T)^l + \sum_{i=1}^{N_c} \left(\frac{\partial}{\partial x_G^i} (k^i x_G^i) \right) (\delta x_G^i)^l = 1 - \sum_{i=1}^{N_c} (k^i x_G^i)^l & \text{if } 1 - S_G > 1 - \sum_{i=1}^{N_c} (x_L^i) \end{cases} \quad (6.15)$$

Here $\delta \cdot$ indicates the change of primary variable in each Newton iteration. Function k is defined in Eq (4.8) or (4.9). Substituting Eq (6.14) and Eq (6.15) into the global Jacobian matrix leads to a linear system with $(N_c + 1)$ primary unknowns, while the secondary unknowns can be computed in the local post-processing procedure, which are summarized as follows

- In the single phase zone, the following linear system needs to be solved

$$\begin{bmatrix} \frac{\partial \mathcal{H}}{\partial P} & \frac{\partial \mathcal{H}}{\partial x_G^i} & \frac{\partial \mathcal{H}}{\partial T} \end{bmatrix} \begin{bmatrix} \delta P \\ \delta x_G^i \\ \delta T \end{bmatrix} = -\mathcal{H} - \delta S_G \frac{\partial \mathcal{H}}{\partial S_G} - \delta x_G^{N_c} \frac{\partial \mathcal{H}}{\partial x_G^{N_c}}, \quad (6.16)$$

$$i \in [1, \dots, N_c - 1].$$

- While in the two-phase zone, the linear equation is given as

$$\begin{bmatrix} \frac{\partial \mathcal{H}}{\partial P} & \frac{\partial \mathcal{H}}{\partial S_G} & \frac{\partial \mathcal{H}}{\partial x_G^i} & \frac{\partial \mathcal{H}}{\partial T} \end{bmatrix} \begin{bmatrix} \delta P \\ \delta S_G \\ \delta x_G^i \\ \delta T \end{bmatrix} = -\mathcal{H} - \delta x_G^{N_c-1} \frac{\partial \mathcal{H}}{\partial x_G^{N_c-1}} - \delta x_G^{N_c} \frac{\partial \mathcal{H}}{\partial x_G^{N_c}}, \quad (6.17)$$

$i \in [1, \dots, N_c - 2].$

Therefore, by conducting the Schur complement procedure in global NCP formulation, the reduced linear system holds the same size as local NCP formulation, i.e. $(N_c + 1)$. After the linearization of the global governing equations, a sparse and asymmetric linear system is assembled and needs to be solved. The BiCGStab solver from the LIS library [45] is employed with an ILU preconditioner to obtain the solution.

6.1.2 Interface continuity requirement

When the model domain is heterogeneous, the neighbouring materials can have highly contrasted physical properties, such as the capillary pressure and relative permeability. Therefore, an accurate treatment of the interface condition should be addressed in the model in order to account for the saturation jump at the material interface.

Let $\Omega^{(1)}$ and $\Omega^{(2)}$ be the two neighbouring materials characterised by two different Brooks-Corey type capillary pressure relationships $P_c^{(1)}$ and $P_c^{(2)}$. The corresponding entry pressures $P_e^{(j)}$ ($j \in \{1, 2\}$) are assumed with: $P_e^{(1)} < P_e^{(2)}$, i.e. $\Omega^{(1)}$ holds a smaller entry pressure. With the requirement of cell-wise continuity, the capillary pressure at the interface can be reformulated with the known entry pressure value, following [46].

$$\begin{cases} P_c^{(2)} = P_c^{(1)} & \text{if } P_c^{(1)} \geq P_e^{(2)} \\ P_c^{(2)} = P_e^{(2)} & \text{if } P_c^{(1)} \leq P_e^{(2)} \end{cases}$$

In the case of global NCP formulation, the saturation is treated as primary variable which thereby requires the capillary pressure to be prescribed at each node. Then in order to account for the saturation discontinuity, the saturation at the interface should be regulated as the following form:

$$S_G^{(2)} = (P_c^{(2)})^{-1} \left[P_c^{(1)}(S_G^{(1)}) \right] \quad (6.18)$$

where $(P_c^{(2)})^{-1}$ indicates the inverse function of the capillary pressure relationship at sub-material domain $\Omega^{(2)}$. While for the local NCP formulation, the overall molar fraction (X^i) is chosen as the primary

variable. A similar strategy is applied to formulate the interface condition for X^i :

$$X^{i,(2)} = \frac{N_L^{(2)} x_L^{i,(2)} (1 - S_G^{(2)}) + N_G^{(2)} x_G^{i,(2)} S_G^{(2)}}{N_L^{(2)} (1 - S_G^{(2)}) + N_G^{(2)} S_G^{(2)}} \quad (6.19)$$

While $S_G^{(2)}$ is defined following equation(6.18). Besides, due to the fact that saturation is selected as a secondary variable, it is calculated in local problem by the primary variable P, X^i, T .

$$\begin{cases} S_G^{(2)} = (P_c^{(2)})^{-1} [P_c^{(1)}(S_G^{(1)})] \\ S_G^{(1)} = S_G^{(1)}(P^{(1)}, X^{i,(1)}, T^{(1)}) \end{cases}$$

For the local NCP formulation, the interface conditions have already been incorporated into the local problem and solved on each integration point, and these conditions are further guaranteed at each node throughout the global Newton iterations.

TWO-PHASE REACTIVE TRANSPORT MODEL WITH A LOOK-UP TABLE

In this chapter, the efforts aims at extending the aforescribed compositional two-phase flow model into a coupled two-phase reactive transport framework based on a look-up table approach. A special concern is dedicated to the dynamic concrete degradation in the nuclear waste disposal.

This chapter was mainly adopted from the publication[47]:

7.1 BACKGROUND

In Switzerland it is planned to store low and intermediate level radioactive waste (L/ILW) in a deep geological repository using a clay rock formation as host rock. Such a repository contains large amounts of cement based materials (concrete, mortars) for waste conditioning, tunnel support (shotcrete) and backfill of cavities. The use of cement-based materials shall provide a stable mechanical and a high pH chemical environment throughout the repository for a very long period. Highly alkaline conditions are favorable for conditioning the waste, as the sorption of radionuclides is enhanced on cement phases in these conditions, and further corrosion of metals and microbial degradation of organic wastes is decelerated. The long-term chemical stability of cement materials is further of great importance, as in the course of concrete degradation cement phases are successively dissolved which reduces the pH buffering capacity of cement paste and results in a continuous drop in pH with time. Therefore, characterizing the long-term evolution of such materials is a topic of great interest, and thus receives continuous attention by the scientific community.

The spatial and temporal evolution of cementitious materials in a deep geological repository is influenced by several external and internal processes involving chemical reactions and water/humidity transport, which are usually tightly coupled with each other. According to Kosakowski et al.[48] the most important processes controlling concrete degradation in a cement-based repository are the ingress of host rock pore water, concrete carbonation due to the production of CO₂ by (bio-)chemical degradation of organic wastes, internal degradation

of concrete due to the use of reactive silicate aggregates, and interactions between waste materials and cement paste. Note that the latter processes involve water consuming reactions. All these processes must be assessed in the context of a repository system to ensure the long-term safety of nuclear waste storage.

Among these, carbonation is of major concern in cement-based repositories. The carbonation of concrete is a well investigated phenomena in civil engineering. Current research (c.f. [49]) shows that the process is mainly controlled by the transport of gaseous CO_2 , the atmospheric humidity/water saturation of the concrete, and the cement composition. Therefore, the carbonation of concrete in a unsaturated cement repository is normally not limited by the diffusive transport of CO_2 , but instead it largely depends on CO_2 generation.

Furthermore, internal degradation of concrete due to the presence of aggregates has a potentially detrimental effect on the cement-based materials. One of the main type of internal degradation of concrete due to the reaction of cement phases with aggregates is known as the alkali-silica reaction (ASR). The kinetics of the dissolution of silicate aggregates is the main factor that controls the progress of ASR.

Due to the complex interaction of different chemical and physical processes in the nuclear repository, the numerical model is arising as a powerful tool to investigate the intricate feedback system on multi-scales, from single waste package up to a repository level. In this work, the efforts are dedicated to investigating the concrete degradation due to two reactive substances: SiO_2 and CO_2 .

Coupling the multiphase flow and reactive transport has already been investigated over the last decade. Several numerical simulators have been proposed and performed in both reservoir simulation area or hydrogeochemical modeling area. Among them, GEM-GHG (Nghiem et al., [50]), GPRS (Fan et al., [51]) extended the original compositional flow simulators to couple the chemical reactive transport by solving the coupled system in a fully implicit way. On the contrary, several reactive transport simulators: PFLOTRAN (Lu and Lichtner, [52]), STOMP (White and Oostrom, [53]), TOUGHREACT (Xu and Pruess, [54]), integrated the multiphase flow model based on an operator-splitting approach, in which the computations for one time step are split into a flow problem and a reactive transport problem, respectively.

To the author's knowledge, there is rare reactive transport code available that allows to calculate full coupling between chemical reactions and transport for the complex thermodynamic setup for the concrete material we are investigating. Codes like TOUGHREACT [54] can certainly handle the feedback between chemistry and transport, but are unable to calculate the thermodynamic setup that includes several solid-solutions.

Our calculations utilize the afore proposed compositional two-phase transport module in the OpenGeoSys software system. Couplings between transport and chemical processes are achieved via source/sink terms for gases and water calculated by rate laws for internal degradation of concrete. The complex chemical degradation of concrete is simplified into a look-up table which provides pH and allows estimating changes in rate law parameters in dependence of local carbonation degree and internal degradation.

This simplified approach for coupling chemical and transport processes allows including spatially heterogeneous chemical conditions in compositional two-phase transport calculations without the need to include computationally expensive chemical calculations.

7.2 CONCRETE DEGRADATION AND CREATION OF LOOK-UP TABLE

We approximate the complex carbonation and ASR into a fast-to-calculate look-up table. The look-up table presented in this work is based on the thermodynamic model of a sulphate-resisting Ordinary Portland Cement (OPC), similar as the one described by Lothenbach and Wieland [55]. The exact recipe and the thermodynamic setup of the utilized concrete is given in [56]. Therefore, only the most important information is explained in this work.

The normative composition of the concrete is given in Table 1. The setup represents a typical mortar used for backfilling void space in waste packages. All calculations were conducted with the GEM-Selektor V3 chemical modelling package [57, 58] based on the PSI/Nagra thermodynamic database.

7.2.1 *Hydrated mortar*

We first calculate the equilibrium composition for the fully hydrated mortar. The equilibrated mortar is the starting composition for the concrete degradation calculations serving as the basis of the look-up table. Only two degradation reactions have been considered for this work: the Alkali-Silica-Reaction (ASR) and the carbonation. Both reactions successively dissolve calcium bearing cement phases to form carbonates in case of carbonation or C-S-H with low C/S ration, resp. silica gel, in case of ASR. The progress of both processes was calculated with help of the sequential batch module of the GEM-Selektor V3 software.

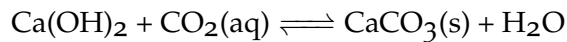
7.2.2 *Carbonation*

The cement carbonation is simulated by adding the increasing amounts of CO₂ to the chemical systems. After each step the system was equi-

Table 1.: Setup and properties of generic mortar[47]

Phase/Material	amount [g]	Remark
Water (H ₂ O)	169.25	
CEM I 52.5 N HTS ₁	300	Corresponding composition is given in the Appendix A.
NaCl	0.1	Represents small amount of salts in the water
Aggregate (SiO ₂ /quartz)	1830	for the initial equilibration, aggregate is assumed to be not reactive
total mass	2299.35 g	
W/C ratio (adjusted to give a porosity of 0.076)	0.564	Wieland et al. [56] considered an additional gas phase, here fully saturated conditions are assumed

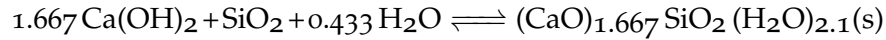
librated and the result of the GEM-Selektor calculation was saved. Initially all solid phase volumes and the fluid phase volume add up to 1. With the addition of CO₂, portlandite is first dissolved and transformed into calcite according to the following reaction:



While water is released through the reaction. After portlandite is consumed, C-S-H phases with a high C/S ratio are transformed into C-S-H with low C/S. This transformation also frees water. Once all calcium has been leached from the C-S-H phases as a consequence of reduction of the C/S ratio, successively hydrogarnet, ettringite, hydrotalcite and C-S-H with the lowest possible C/S ratio are dissolved. The leached calcium is used to form calcite. The dissolution of the AFm and AFt phases also releases aluminium which serves as the basis to form zeolites. Ettringite dissolution leads to the formation of sulfates, in this case gypsum, and magnesium is used up due to the transformation of C-S-H into M-S-H. Excessive silica resulting from the C-S-H dissolution gives rise to the precipitation of SiO₂, which is shown in the model as the formation of amorphous silica or quartz. The final, completely carbonated system is composed of largely unaffected quartz aggregates, considerable amounts of carbonates and minor amounts of clay minerals.

7.2.3 ASR

In our thermodynamic setup the ASR is mainly driven by the dissolution of the quartz aggregates. The released silica reacts with calcium leached from the cement phase to form C-S-H solid solutions.



As a consequence of progressing silica release, silica is continuously bound by C-S-H and therefore, the C/S ratio of the C-S-H phase decreases until a tobermorite composition is formed. The general sequence of dissolving cement minerals and precipitated secondary phase is very similar to the carbonation reaction, except for the two main differences: Firstly, during carbonation, C-S-H is dissolved and carbonates are formed, whereas for ASR carbonates do not participate in any reactions and C-S-H is the main reaction product. Secondly, for the ASR, zeolites will be transformed to clay phases in the very last degradation stage. Such transformation is not present in the carbonation reactions.

7.2.4 *Chemical and physical changes upon concrete degradation*

The combined effects of carbonation and ASR on the chemical and physical changes of the degradation of concrete are further analyzed. For each pair of CO_2 and SiO_2 the, we extract the results from the GEM-Selektor model in terms of pH in pore water, on porosity, water volume and quartz dissolution rate. The look-up table is further visualized as 3-D surface plots as shown in Figure.8:

The pH in the system decreases during concrete degradation, for both carbonation and ASR. In the initial hydrated concrete, the pH is 12.9 whereas the pH of degraded concrete only reaches 10.1. At the final degradation stage by carbonation, the pH drops further to 8.3 as a consequence of the presence of clay phases.

The quartz dissolution rate was calculated as described by Wieland et al.[56]. The dissolution kinetics of siliceous sand (aggregate) can be expressed in terms of a (simplified) pH-dependent rate in accordance with [48] which holds in neutral and alkaline conditions.

After reaction of the corresponding moles of SiO_2 and CO_2 , the volume of the liquid phase was calculated which was used as the source/sink terms for liquid in the governing equation of multi-phase transport process. The difference in fluid volume before and after adding CO_2 and SiO_2 revealed the amount of mass added into or subtracted from the liquid volume. The source/sink terms of water are in principle the directional derivatives of the look-up table. Numerical differentiation can be obtained e.g. by finite difference schemes.

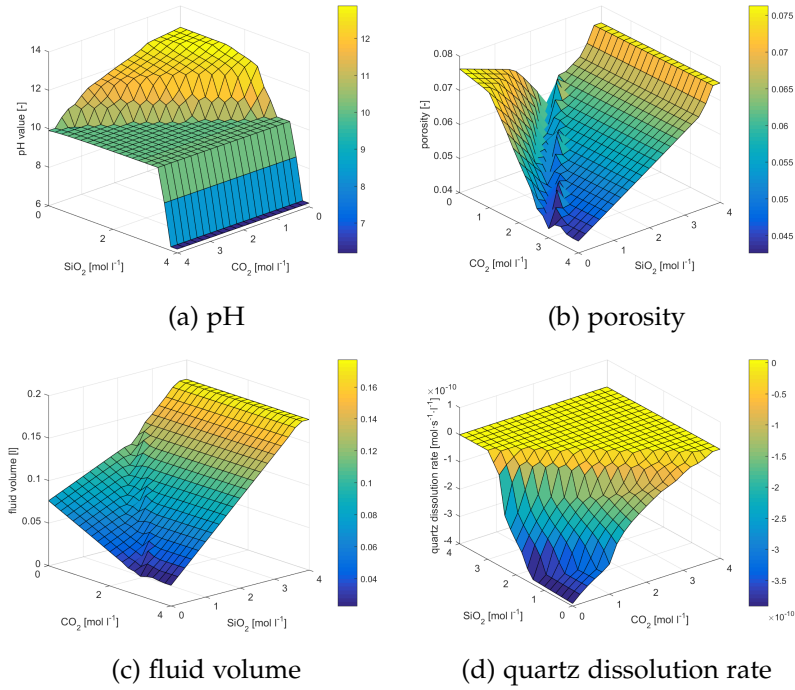


Figure 8.: 3D surface plots for the combined effects of CO_2 addition (carbonation) and SiO_2 addition (ASR) on pH (a), porosity (b), fluid volume (c) and quartz dissolution rate (d).[47]

The porosity was calculated based on the changes of cumulative solid phase volume fractions with respect to the initial volume. The position and extension of the porosity changes are uncertain and strongly depend on the mineral phases included and the adopted thermodynamic data.

7.3 THE COUPLING STRATEGY

The coupling strategy for the look-up table of the complex carbonation and ASR with the two-phase multi-component transport model is depicted in Fig. 9. The table provides pH, porosity, water consumption/release and kinetic rates for dissolution of (quartz) aggregate on dependence of CO_2 and SiO_2 reacted in a unit volume. Carbonation was calculated based on the accumulated amount of CO_2 that reaches on a node/volume by transport, while ASR was calculated based on the dissolution of SiO_2 with the kinetic rates provided by the look-up table.

Our approach for incorporating the look-up table into the two-phase multi-component transport model was accomplished via source and sinks term and updates of porosity values. The source/sink term represents the production/consumption rate of one particular component due to chemical reactions. For each Newton iteration a call was

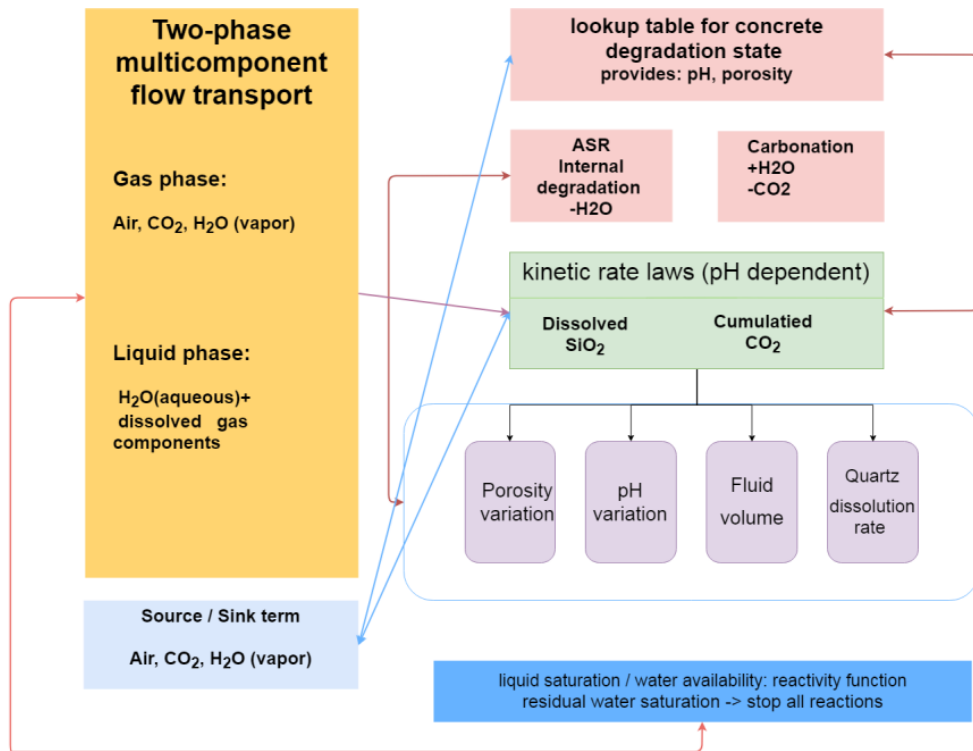


Figure 9.: Schematic illustration of the coupling strategy between two-phase multi-component transport and chemical processes via the look-up table approach[47]

made to the look-up table to define the desired values. The total cumulatively consumed CO₂ and dissolved SiO₂ concentrations are given as input values from the look-up table, while a bi-linear interpolation method is employed to output the chemical system information based on the look-up table.

The detailed coupling procedure is explained in [47].

MODEL APPLICATIONS

After briefly sketching the numerical algorithms in the previous chapters, we will now compare the physical accuracy and the computational efficiency of the presented numerical models for fluid flow in porous media. In this chapter, the verification of the nonisothermal compositional two-phase flow model is performed by simulating problems with literature results; in addition, a benchmark exercise for the two-phase flow and reactive transport modeling of the concrete degradation is proposed to verify and validate the look-up table coupling methods.

In the first part, in order to analyze the accuracy and computational performance of the aforementioned numerical formulations, two groups of benchmarks have been adopted. The first group is dedicated to simulate an idealized system. The first benchmark reproduces the drying process of a porous media saturated with water by subjecting to a dry gas phase, where gas phase appearance and liquid disappearance are involved (section 8.1.1). In the second group, the non-ideal mixture system is taken into account under high pressure and temperature condition. A major interest is focused on the complex phase behavior. Three different cases are presented in the context of CO₂ storage. First, a 2-D CO₂ injection process are investigated (section 8.2.1). The second benchmark goes further by considering a non-isothermal radial symmetric CO₂ injection problem in an anisotropic and heterogeneous saline aquifer (section 8.2.2). While the last benchmark is dedicated to simulating a multicomponent transport problem associated with the injection of CO₂ and multiple impure gas components (section 8.2.3).

In the second part, a 1-D reactive transport benchmark is proposed by considering the two main chemical reactions which control the concrete degradation: ASR and carbonation. We contrast three different configurations of the benchmark to explore the pattern of competition between ASR and carbonation in the long-term degradation of concrete. The numerical model derived from the look-up table approach is compared against a full reactive transport code to validate its accuracy and efficiency.

IMPLEMENTATION

All numerical experiments are conducted with the OpenGeoSys software (cf. Kolditz et al. [24], Huang et al. [25]). Both fixed and adaptive time stepping features are employed. With the later case, the successive time step size is doubled when the number of Newton iterations in the previous time step is less than 7, and it will be cut into half if more than 15 iterations are required. Meanwhile, the nonlinear solver convergence criteria for the L_2 -norm of the residual vectors are set to 10^{-14} for the local problem and 10^{-7} for the global one. Note that local tolerance must be lower because solution accuracy of the local problem is crucial for the convergence on global level. All benchmarks are performed on a computer equipped with 8 GB of memory and an Intel(R) Core(TM) I5-3230 processor @2.6 GHz. It is noted although the OpenGeoSys software has the capability of running parallel simulations (cf. Wang et al. [59]), only single-CPU core serial computation is performed here, so that the time spent in different parts of the simulation can be more directly analyzed.

8.1 BENCHMARKS FOR IDEALIZE SYSTEM

8.1.1 *Benchmark I: Drying by gas injection*

In order to investigate the performance of the two formulations regarding phase change problem, we consider a benchmark including gas appearance and wetting phase disappearance by injection of dry gas. This benchmark is proposed by Masson et al. [28] in the context of simulating the drying process of a geological nuclear waste repository.

The porous media is represented by a horizontal 1D domain with a length of 1000 m. The temperature is fixed to $T = 360$ K. The vapor pressure is defined by the following relationship ([28]):

$$P_{\text{sat}}(T) = P_0 \exp\{13.7 - 5120/T\} \quad (8.1)$$

with P_0 corresponds to the atmospheric pressure (101325 Pa). The relative permeability and the capillary pressure are again given by the Van Genuchten model. Note that in order to account for the liquid phase disappearance, the capillary pressure is extended linearly to $S_w = 0$ between $(S_{w,0}, P_{c,0}) = (P_c^{-1}(P_{c,0}), P_{c,0})$ and $(S_{w,1}, P_{c,1}) = (0, 2P_{c,0})$ with $P_{c,0} = 4Pr$ ($Pr = 1 \times 10^5$ Pa). Figure 10 gives the regularized van Genuchten curve for the relation of saturation and capillary pressure. The liquid and gas phases are represented as mixtures of water(w) and air(air) components. The Henry law is applied to describe the solubility of air in the water with the Henry constant fixed to $H^{air} = 10^8$ Pa, and the Fick diffusion can be neglected due to the dominant Darcy convection.

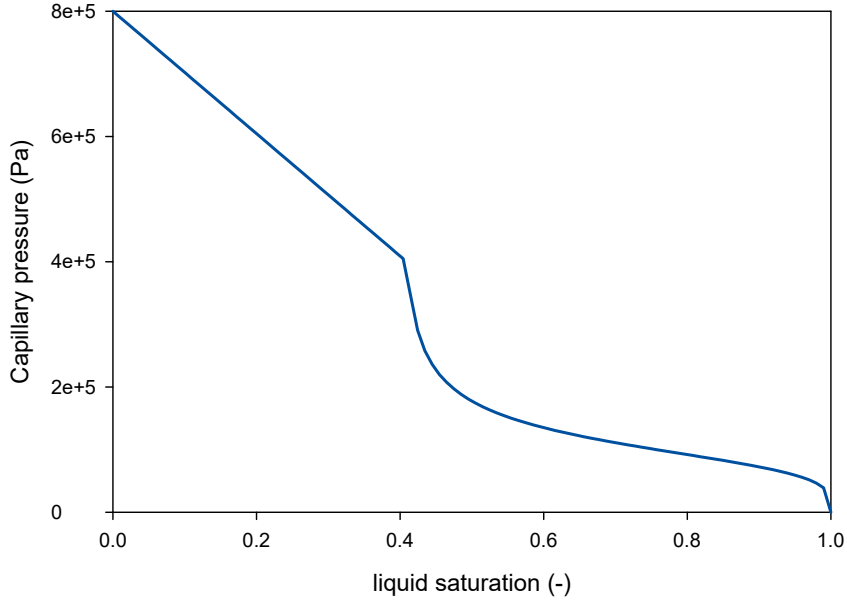


Figure 10.: The regularized van Genuchten curve for the relationship of liquid saturation and capillary pressure.

Initial condition

The initial conditions are defined by a pure water liquid phase:

Gas phase pressure: $P_G = 40 \times 10^5$ Pa

Liquid phase pressure: $P_L = 40 \times 10^5$ Pa

Capillary pressure: $P_c = 0$ Pa

Molar fraction of air in liquid phase: $x_L^{air} = 0$

Molar fraction of water in liquid phase: $x_L^w = 1$

Boundary condition

At the left end, the Dirichlet boundary conditions are applied with the same as the initial conditions:

Gas phase pressure: $P_G = 40 \times 10^5$ Pa

The capillary pressure: $P_c = 0$ Pa

The molar fraction for both components read:

$$x_L^{air} = 0 \quad x_L^w = 1$$

At the right part, the gas phase ($S_G = 1$) is injected with a mixture of air and water vapor which includes 0.5 % water vapor, which corresponds to a capillary pressure ($P_c \approx 6 \times 10^8$ Pa)

Gas phase pressure: $P_G = 50 \times 10^5$ Pa

The capillary pressure: $P_c = 6 \times 10^8$ Pa

The composition of the gas phase is composed of:

$$x_G^{air} = 0.9995 \quad x_G^w = 5 \times 10^{-4}$$

Table 2.: The parameters used for the benchmark case of drying by gas injection

Parameter	Symbol	Value	Unit
Water density	ρ^w	1×10^3	kg m^{-3}
Molar mass of water	M^w	18×10^{-3}	kg mol^{-1}
Molar mass of air	M^{air}	29×10^{-3}	kg mol^{-1}
Henry constant	H	1×10^8	Pa
Viscosity of gas	μ_G	1.8×10^{-5}	$\text{Pa} \cdot \text{s}$
Viscosity of water	μ_L	1×10^{-3}	$\text{Pa} \cdot \text{s}$
Diffusion coefficient	D_L^h	3×10^{-9}	$\text{m}^2 \text{s}^{-1}$
Porosity	ϕ	0.15	–
Intrinsic permeability	K	10^{-12}	m^2
Temperature	T	360	K
van Genuchten parameter	n	4	–
van Genuchten parameter	P_r	1×10^5	Pa
Residual saturation	$S_{L,\text{res}}$	0.4	–

8.1.1.1 Benchmark configuration

The geometry is uniformly discretized into 100 elements, and the simulation is run over the time span of 40 years. Adaptive time stepping is applied for the simulation with an initial time step of 1×10^3 seconds, a maximum time step of 1×10^5 seconds until the gas reaches the left end ($t=1$ year), and a maximum time step of 1×10^7 seconds in the remaining of the simulation.

The parameters used for this benchmark case are listed in Table 2

8.1.1.2 Results

Figure.11 exhibits the gas saturation front at different times obtained with the local NCP formulation. The simulated results are also compared against reference data from Masson et al. [28]. Our simulation results fit quite well with the reference data. It can be observed that the gas hydrodynamic front propagates from right to left at the beginning of the simulation due to the gradient of the pressure, and after around 1 year it reaches the left end of the domain. Next, at the vicinity of the injection boundary, the liquid saturation decreases to around 0.4 which corresponds to the residual saturation. That can be explained by the immobility of the liquid phase. The liquid saturation keeps decreasing due to the vaporization of the water and injection of the dry gas. However, that process is observed to be much slower. After around 5 years, the liquid phase begins to disappear from the vicinity of the injection boundary. At the end of simulation (40 years), half of the domain is composed of single gas phase.

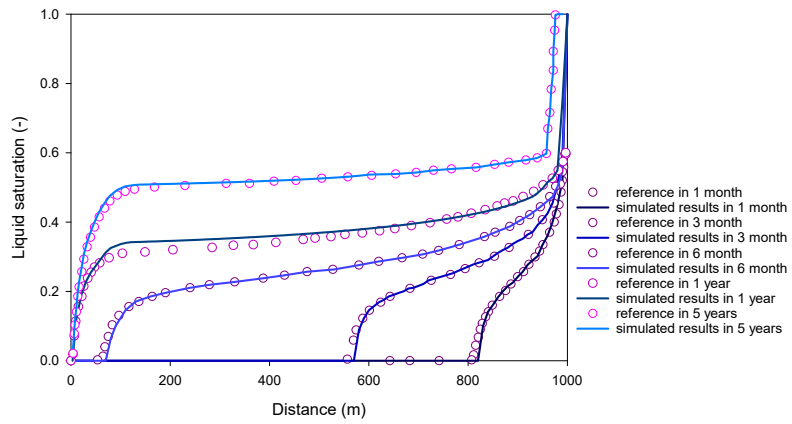
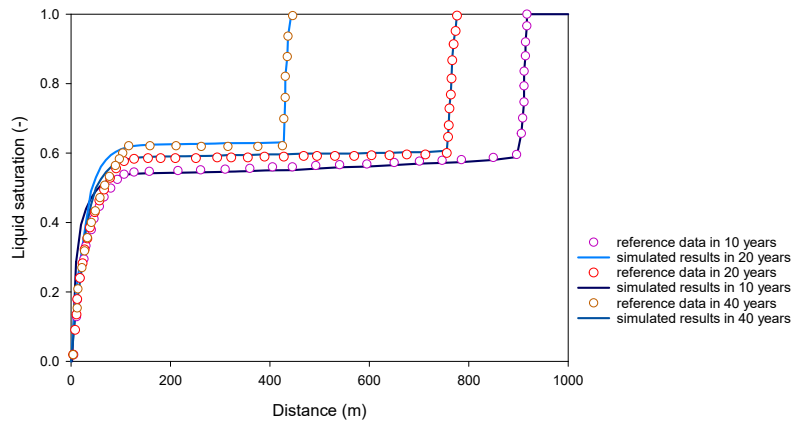
(a) Liquid saturation profile at times $t = 0.1, 0.25, 0.5, 1, 5$ years(b) Liquid saturation profile at times $t = 10, 20, 40$ years

Figure 11.: Liquid phase saturation profile at different time obtained by local NCP formulation, compared against reference data reported in [28]

Table 3.: Comparison of the performance between both NCP formulation and PVS scheme. Here, n corresponds to the number of time steps required to reach steady state, t_{CPU} is the total CPU time required to reach simulation end and n_{Newton} is the overall Newton iterations, while $\text{avg}_{\text{Newton}}$ represents the average Newton iterations required for each time steps.

	Global NCP	Local NCP	PVS[28]
t_{CPU} [s]	679.56	792.99	-
n [-]	223	216	172
n_{Newton} [-]	969	919	1477
$\text{avg}_{\text{Newton}}$ [-]	4.345	4.25	8.587

8.1.1.3 Numerical comparison

We compare as in the previous benchmark case the numerical performance with respect to different formulations. In Table 3, a detailed comparison is presented with respect to the total number of time steps, overall Newton iterations, and the CPU time which both numerical formulations required to reach the simulation time end on a mesh with 160 elements. For reference, the numerical behaviors of PVS scheme are also summarized in Table 3.

It can be observed from Table 3 that both the NCP formulations behave roughly the same efficiency in terms of Newton convergence with a slightly better performance of local NCP formulation. However, local NCP formulation is 10 % slower in terms of total CPU time compared with the global one. Both NCP formulations demonstrate better behavior than PVS scheme in terms of the Newton convergence, since less overall/average Newton iterations are required by NCP formulations.

8.2 BENCHMARKS FOR NON-IDEAL SYSTEM

The previous benchmark is focused on the idealize system, now we increase the complexity by taking the non-ideal mixture into account. This is numerically more difficult than the idealize system due to the fact that all fluid properties and coefficient functions are tight coupled and highly nonlinear. It is of great interest to investigate the numerical performance of both formulations for the complex phase behavior.

8.2.1 Benchmark II: Injection of CO_2 into water saturated domain

In this section, we consider a benchmark case related to the injection of CO_2 into a deep aquifer initially saturated with pure water for the purpose of permanent CO_2 geological sequestration. This benchmark

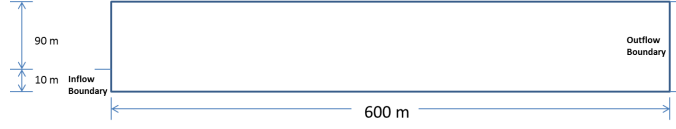


Figure 12.: The spatial domain of the radially symmetric CO_2 injection problem.

is firstly proposed by Neumann et al. [15], an extensive literatures also reported the simulation results for this case, here we refer to [60, 61, 62]. In this work, the same settings and parameters reported in [60] are applied.

Typically, CO_2 is injected in its super-critical state where its properties fall between a gas and a liquid. More precisely, its viscosity is lower than a gas and the density is higher than a liquid [60]. Consequently, the ideal gas law is no longer applicable for this case. On the other hand, regarding the solubility of CO_2 , the high pressure and temperature condition of the reservoir leads the Henry law invalid as well. Therefore, the equation of state discussed in section 5.2 are applied.

The aquifer is located under 800 m depth, which assures the super-critical condition of the injected CO_2 . The geometry can be represented by a 2D rectangle domain with 600 m length and 100 m height, as Figure 12 shown. The CO_2 is injected from the left bottom corner while a hydrostatic pressure distribution boundary is imposed on the right part. For the simplicity, in the below, we use (\cdot^{CO_2}) and (\cdot^{w}) to denotes the component of CO_2 and water, respectively

Initial and boundary conditions

At the beginning of the simulation, the domain is fully water-saturated with no CO_2 in the liquid phase. The initial conditions read: The gas phase pressure is assumed to be equal to the liquid pressure which holds a hydrostatic pressure conditions in the domain:

$$P_{G,\text{ini}} = 101325 + (900 - z)\rho^{\text{w}}g \text{ Pa} \quad (8.2)$$

with z is the z -axis coordinate.

The molar fraction for each component reads:

$$x_{G,\text{ini}}^{\text{CO}_2} = 0 \quad x_{L,\text{ini}}^{\text{CO}_2} = 0 \quad (8.3)$$

A constant injection flux is imposed on the inflow boundary part:

$$q_{in}^{\text{CO}_2} = 0.04 \text{ kg m}^{-2} \text{ s}^{-1} \quad (8.4)$$

Pure water and hydrostatic pressure distribution on the outflow boundary

$$x_{L,\text{out}}^{\text{CO}_2} = 0, \quad P_{G,\text{out}} = P_{G,\text{ini}} \quad (8.5)$$

Table 4.: The parameters used for the 2-D CO₂ injection problem.

Parameter	Symbol	Value	Unit
Molar mass of water	M^w	18×10^{-3}	kg mol^{-1}
Molar mass of CO ₂	M^{CO_2}	44×10^{-3}	kg mol^{-1}
Diffusion coefficient	$D_L^{\text{CO}_2}$	2×10^{-9}	$\text{m}^2 \text{s}^{-1}$
Porosity	ϕ	0.2	—
Intrinsic permeability	K	10^{-12}	m^2
Temperature	T	313.15	K
Brooks-Corey parameter	λ	2	—
Brooks-Corey parameter	P_{entry}	1×10^3	Pa
Residual saturation	$S_{L,\text{res}}$	0.0	—
Residual saturation	$S_{G,\text{res}}$	0.0	—

8.2.1.1 Model configuration

The simulation domain is uniformly discretized into 9600 (240×40) quad elements. The simulation is run over a time span of 100 days. An adaptive time stepping control is applied for the whole simulation, with an initial time step size (Δt) of 500 seconds.

All the parameters used for this benchmark are listed in Table 4.

8.2.1.2 Simulation results

The simulation results of this benchmark case are plotted in Figure 13, which are obtained by local NCP formulation. Each figure depicts the CO₂ phase saturation distribution after 7, 20, 65 days. In comparison with the results reported in [60], a very good agreement can be observed.

Shortly after the injection of CO₂ (after 500 seconds), a free gas phase starts to appear (correspond to a gas saturation of 0.05). The CO₂ propagates upwards until it reaches the top of the domain driven by the gravitational force. Then the CO₂ keeps accumulating below the top of the domain and starts to migrate to the outflow boundary driven by the advective forces. After around 15 days, it is observed that the gas saturation at the vicinity of the injection boundary becomes 1 which indicates a complete dry out of liquid water and the disappearance of the liquid phase. However, such phenomena are not observed in [60]. The difference might come from the different choice of primary variables, or different capillary pressure regularization scheme adopted for Brooks-Corey model when gas saturation approaches 1.

8.2.1.3 Formulation Comparison

Differ with other reference simulations, in this work, the model is run in single core without parallel. A special attention is paid to the

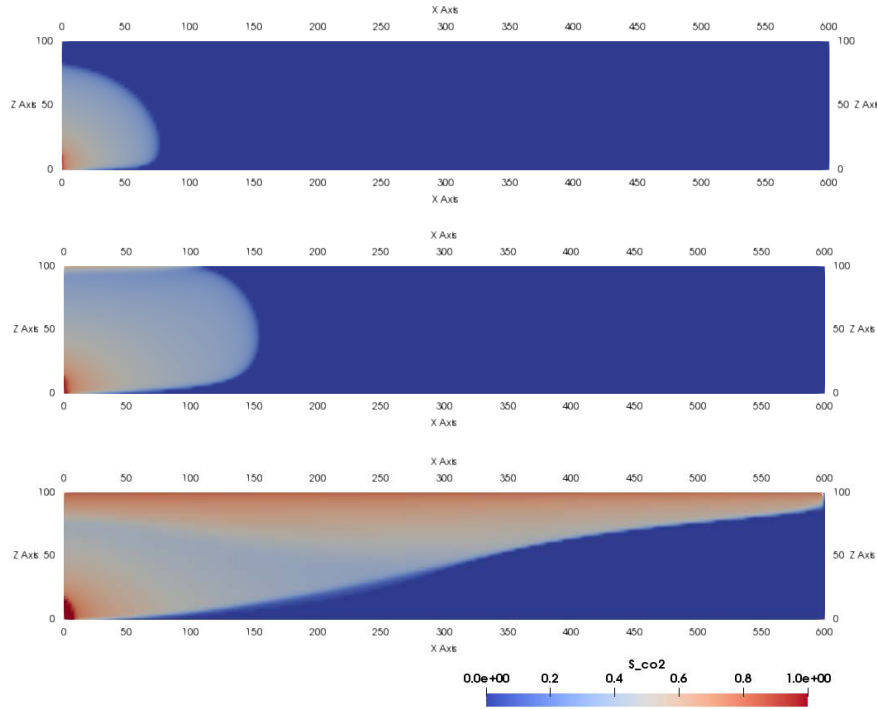


Figure 13.: Gas phase saturation profile after the CO_2 injection of 7, 20, and 65 days

numerical performance between local and global NCP formulations, since the results obtained by both formulations are very similar to each other. The PPC formulation adopted in [15, 60] are also compared as a reference. The detailed comparison are listed in Table 5.

It can be observed that, the PPC formulation consumes the least CPU time compared with the both NCP formulation, that can be explained by the fact that, in PPC formulation, saturation is only dependent on capillary pressure, which relaxes the nonlinearity significantly, and save computational time thereby. However, it requires the most average Newton iteration per time step, which indicates a worst converge behavior.

While with respect to the comparison between the global and local NCP formulation, it can be observed from Table 5 that global NCP formulation consumes approximately 20 % less CPU time. However, local NCP formulation delivers a slightly better numerical performance compared to the global one. Since it requires the least averaged Newton iteration per time step, and a larger averaged time step size is allowed in the local NCP formulation.

Table 5.: Comparison of numerical behavior between two NCP formulations and PPC [60, 62] approach for the simulation of 2-D CO₂ injection benchmark over a 9600-element mesh. $\text{avg}_{\Delta t}$ indicates the averaged time step size.

	Global NCP	Local NCP	PPC
t_{CPU} [s]	15195	18169	13975
$\text{avg}_{\Delta t}$ [s]	4027.97	4056.3	3841.7
n_{Timestep} [-]	2145	2130	2249
n_{Newton} [-]	7400	7200	8872
$\text{avg}_{\text{Newton}}$ [-]	3.45	3.38	3.9

8.2.2 Benchmark III: Cold CO₂ injection into a saline aquifer

In CO₂ geological storage, thermal effect is a very important factor, due to the temperature dependence of the fluid density, viscosity and mutual solubility relationships. These properties are crucial to determine the flow and transport processes. From modeling point of view, such functions are highly nonlinear which impose numerical challenge for the simulation. Therefore, in this section, a special interest has been focused on a non-isothermal radially symmetric CO₂ injection problem by considering a benchmark proposed in Zhao et al. [63].

In this benchmark, the simulated geometry is a heterogeneous anisotropic sandstone aquifer with a thickness of 100 m, which is located 1300 m depth under the surface. A 2-D axisymmetric mesh is adopted to simulate the full 3-D radial symmetric problem.

Supercritical CO₂ is injected into the aquifer at 20 m distance from the bottom of the aquifer. The injection temperature is 32 °C and the injection rate is 15.85 kg/s. The injection period is 10 years.

The porosity and intrinsic permeability are defined following the original benchmark setting:

$$\phi = 0.4e^{-0.5z} + 0.05 \quad (8.6)$$

$$k_x = 10^{22.58\phi - 18.15}; \quad k_z = k_x/4 \quad (8.7)$$

where ϕ is porosity, z is depth (km), k_x and k_z is the intrinsic permeability in the horizontal and vertical directions, respectively.

The fluid properties and porous media parameters used for the simulation are listed in Table 6.

8.2.2.1 Model Configuration

The geometry domain is uniformly discretized into 1×10^4 quad elements. In the horizontal direction, a total of 500 grid elements are

Table 6.: Parameters applied in the cold CO₂ injection problem

Parameters Name	Symbol	Value	Unit
Thermal conductivity of porous medium	λ_{pm}	2.51	W (m K) ⁻¹
Heat capacity of the soil grains	c_s	920	J (kg K) ⁻¹
Density of the soil grain	ρ^s	2600	kg m ⁻³
Residual saturation non-wetting	$S_{res,n}$	0.05	–
Residual saturation wetting	$S_{res,w}$	0.3	–
van Genuchten parameter	P_r	1.961×10^4	Pa
van Genuchten parameter	n	1.84162	–
van Genuchten parameter	m	0.457	–

used, including the injection well with a radius of 0.3 m. While in the vertical direction, the domain is divided into 20 layers.

The simulation is run over a time span of 10 years. Adaptive time stepping control is applied for the simulation with a initial time step size of 500 seconds.

The initial and boundary conditions for this simulation are summarized as follow:

Initial condition

At the beginning of the simulation, the aquifer is fully saturation with brine:

$$S_{L,ini} = 1, \quad x_{L,ini}^{CO_2} = 0 \quad (8.8)$$

The initial temperature for the aquifer is set to be constant distribution:

$$T_{ini} = 334.45 \text{ K} \quad (8.9)$$

The initial pressure for the aquifer domain is following the hydrostatic distribution:

$$P_{L,ini} = 101325 + (1400 - z)\rho^w \cdot g \text{ Pa} \quad (8.10)$$

with z is the z -axis coordinates.

Boundary condition

Neumann boundary condition is imposed on the injection well:

$$q_{inj}^{CO_2} = 15.85 \text{ kg s}^{-1} \quad (8.11)$$

The temperature of injected CO₂ is:

$$T_{inj}^{CO_2} = 305.15 \text{ K} \quad (8.12)$$

On the right hand side, a hydrostatic distribution is imposed for the liquid phase pressure, while the gas phase saturation and dissolved CO₂ molar fraction keep the same as initial condition

$$P_{out} = 101325 + (1400 - z)\rho^w \cdot g \text{ Pa}, \quad S_{L,out} = 1, \quad x_{out}^{CO_2} = 0.0 \quad (8.13)$$

8.2.2.2 Results

CO₂ migration

The injected CO₂ initially spreads laterally away from the injection well, and buoyancy forces simultaneously lead CO₂ to moving upward until it arrives at the top of the aquifer. Then CO₂ accumulates there and is forced to migrate laterally, as the Figure 14a. Some CO₂ dissolves in the formation water during CO₂ migration. More CO₂ dissolves in the vicinity of the injection well because amounts of cold CO₂ govern the temperature distribution there, as the Figure 14b. The heterogeneity of the aquifer results in the convective mixing occurring after the injection stops, which will be detailed discussed in the latter part.

Temperature evolution

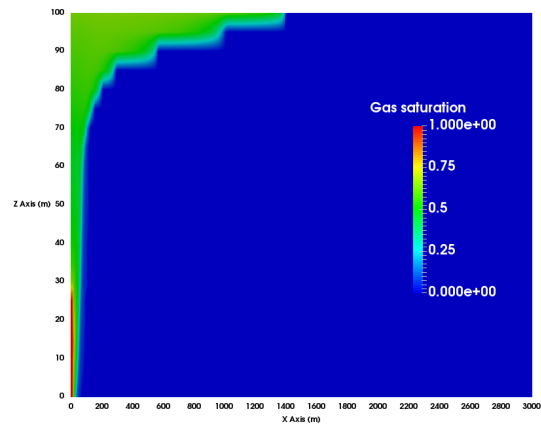
CO₂ migration in the aquifer is accompanied by heat transport processes. These thermal processes control the temperature distribution in the aquifer. Here we focus on studying the characteristics of temperature distribution after the cold CO₂ injection.

The temperature drops below the CO₂ injection temperature around the injection well (from 0.3 m to 70 m) and the maximum value of the temperature drop reaches 0.7 K at 10 years as Figure 14c shown. This is mainly due to the Joule-Thomson cooling effects[64] and endothermic water vaporization. Then heat conduction which is due to the temperature gradient leads the gradual increase of temperature away from the injection well (from 70 m to 250 m). In the region with larger radius, the temperature rises to exceed the initial value. The maximum value of the temperature increase reaches approximately 1 K at 10 years. The reason is that exothermic CO₂ dissolution occurs near the CO₂ plume front. Furthermore, heat conduction increases the temperature of the surrounding zone, where there is no CO₂ dissolved. Based on the evolution of temperature during the CO₂ injection, the aquifer can be divided into three distinguished zones: temperature drop zone ($T < 305.15$ k), temperature transition zone (from $T=305.15$ K to $T=333.45$ K), and temperature rise zone ($T > 333.45$ K). These three zones vary spatially and temporally as the migration of CO₂.

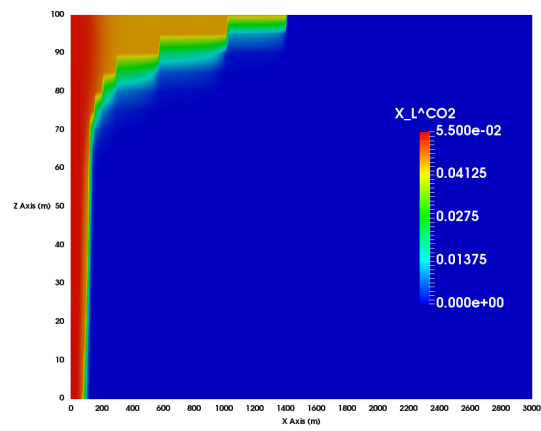
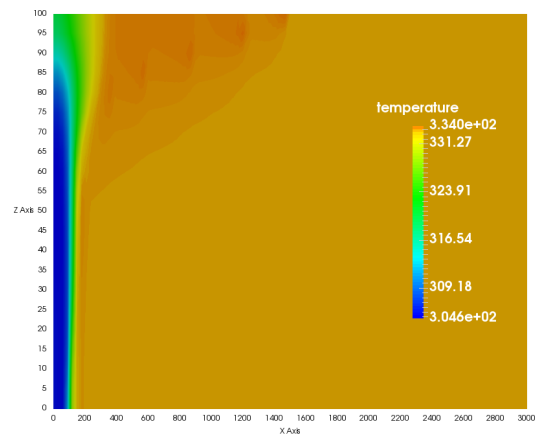
Observation points

We further pick up three observation points(A,B,C) which are located on the top of the aquifer and in the direction away the injection well with the distance of 50 m, 100 m, 500 m, respectively. We plot the temporal evolution of temperature and saturation on these observation points in Figure 15 and compared against the results reported in Zhao et al.[63] which is generated by software TOUGH[65]. A good agreement can be observed between each other.

When CO₂ plume arrives at observation point A ($r = 50$ m) at about 90 days, phase change happens and gas saturation starts to increase dramatically. Meanwhile, the temperature increases slightly. The



(a) Gas saturation distribution

(b) Dissolved CO₂ molar fraction in liquid phase

(c) Temperature

Figure 14.: Results of the Synthetic cold CO₂ Injection Problem after around 10 years

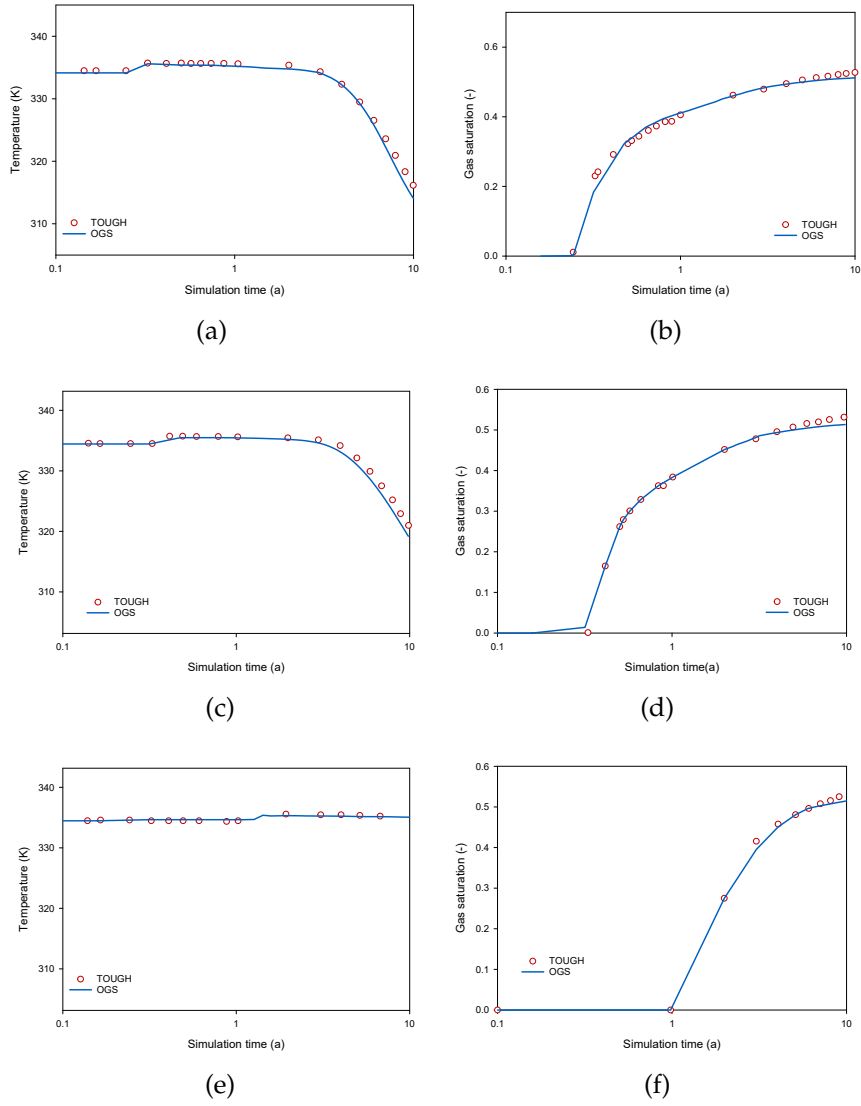


Figure 15.: Evolution of temperature, CO₂ saturation at different observation points

maximum value of the temperature increasing reaches 1.2 K (cf. Figure 15a). From 90 days to around 600 days, the temperature remains stable with only a slightly drop, while saturation keeps increasing. After 600 days, the temperature undergoes a dramatic drops with $T = 316.15$ K at 10 years.

It can be also observed that the temperature and saturation evolution at observation point B ($r = 100$ m) is similar to the trend of observation point A. While for observation point C ($r = 500$ m) which is a bit far away from injection well, a different pattern has been exhibited. After the CO₂ plume arrives (at around 1 year), the gas phase emerges and the gas saturation starts to increase as the previous observation points. However, the temperature only increase slightly, the maximum increase of temperature is around 1 K. Furthermore, at the end of CO₂ injection (10 years), the temperature doesn't drop below the initial temperature of the aquifer, which is owing to the fact that the CO₂ has already been heated during the long distance migration.

Convective mixing

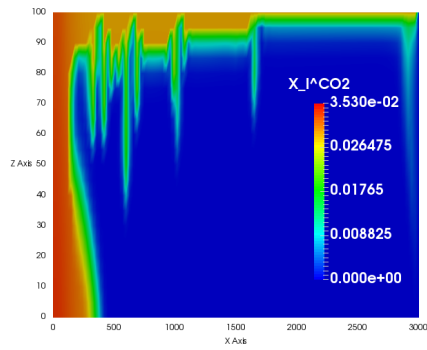
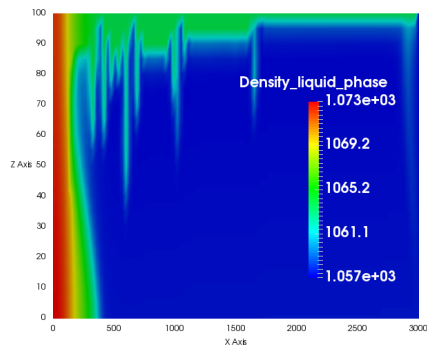
Convective mixing is a common phenomena and plays an important role in CO₂ sequestration. There is convective mixing that occurs because the density of brine saturated with CO₂ is approximately 1 % more than the unsaturated brine.

During the injection period, the convective mixing can hardly been seen due to the fact that the CO₂ displacement is the dominant mechanism. However, within the post-injection period, the CO₂ diffusion and convective mixing become more and more important, especially for a long-term CO₂ migration and storage. The convective mixing becomes the primary mechanism with more CO₂ dissolved in the brine. Moreover, the heterogeneity and anisotropy of the saline aquifer further enhance the convective mixing occurring after the injection stops.

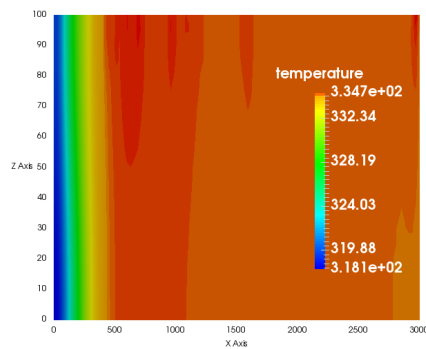
After around 40 years, a distinguished convective mixing phenomena can be observed from the dissolved CO₂ molar fraction distribution, which indicates that in the long term CO₂ migration and storage, the dominant mechanism for dissolution of CO₂ is convective mixing rather than the pure diffusion. Figure.16 depicts the the distribution of dissolved CO₂ molar fraction, liquid phase density and temperature at 300 years. It is shown that the convective mixing has significant effect on the local temperature distribution in the aquifer formation.

8.2.3 Benchmark IV: Co-injection CO₂ and Impurities in CCS application

A remarkable aspect of the subsurface storage of CO₂ is the purity of CO₂. In a realistic scenario, a CO₂ product gas contains contaminant gas such as N₂, O₂ H₂S, SO₂. which might lead to unexpected influence during the operation of storage.

(a) Distribution of dissolved CO₂ molar fraction after 300 years

(b) Distribution of density of liquid phase after 300 years



(c) Temperature distribution after 300 years

Figure 16.: Results of the Synthetic cold CO₂ Injection Problem after 300 years

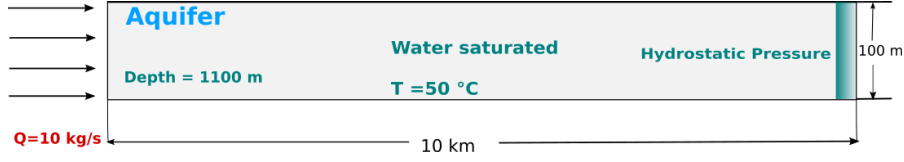


Figure 17.: The geometry for 2-D problem

In this section, we increase the complexity by simulating a benchmark of CO_2 injection associated with the presence of multiple impure gas components. The benchmark was proposed in Sin et al.[61] in the context of the carbon capture sequestration. It highlights an accurate calculation of thermodynamic properties of the involved mixture required by the model to capture the strong interaction between different components under a high pressure and temperature condition.

The geometry is represented by a 100×10000 m rectangle domain which is located at 1100 m depth under the surface, as Figure 17 shown. CO_2 is injected at a constant rate of $10 \text{ kg} \cdot \text{s}^{-1}$ through the left boundary, together with multiple impurity gas components (N_2 and O_2). At the beginning, the aquifer is fully saturated with pure water. We assume a constant temperature at $50 \text{ }^\circ\text{C}$. For the Dirichlet boundary on the right hand side, hydrostatic pressure for the water phase and zero pressure for the CO_2 phase is applied. While the top and bottom of the domain have no-flux boundary conditions. The initial and boundary conditions are summarized as follows:

Initial condition

At the beginning of the simulation, the aquifer is fully saturation with water:

$$S_{L,\text{ini}} = 1, \quad x_{L,\text{ini}}^{\text{CO}_2} = 0, \quad x_{L,\text{ini}}^{\text{N}_2} = 0, \quad x_{L,\text{ini}}^{\text{O}_2} = 0 \quad (8.14)$$

The initial temperature for the aquifer is set to be constant distribution:

$$T_{\text{ini}} = 323.15 \text{ K} \quad (8.15)$$

The initial liquid phase pressure for the aquifer domain is following the hydrostatic distribution:

$$P_{L,\text{ini}} = 101325 + (1100 - z)\rho^w \cdot g \text{ Pa}$$

Boundary condition

The CO_2 is injected from the left hand side with a constant injection rate of 10 kg s^{-1} .

$$q_{\text{inj}}^{\text{CO}_2} = 10 \text{ kg s}^{-1} \quad (8.16)$$

A Dirichlet boundary condition is applied on the left hand side boundary for the overall molar fraction of each gas component:

$$z^{\text{CO}_2} = 0.95, \quad z^{\text{N}_2} = 0.04, \quad z^{\text{O}_2} = 0.01$$

While on the right hand side, a Dirichlet boundary condition is imposed for liquid phase pressure, saturation and overall molar fraction which are the same as the initial condition.

Table 7.: Parameters used for 2-D problem of co-injection CO₂ and impurities.

Parameter	Symbol	Value	Unit
Water density	ρ^w	1×10^3	kg m ⁻³
Molar mass of water	M^w	18×10^{-3}	kg mol ⁻¹
Molar mass of CO ₂	M^{CO_2}	44×10^{-3}	kg mol ⁻¹
Molar mass of N ₂	M^{N_2}	28×10^{-3}	kg mol ⁻¹
Molar mass of O ₂	M^{O_2}	32×10^{-3}	kg mol ⁻¹
Viscosity of gas	μ_G	2.84×10^{-5}	Pa·s
Viscosity of water	μ_L	5.49×10^{-5}	Pa·s
Diffusion coefficient	D_L	3.36×10^{-9}	m ² s ⁻¹
Diffusion coefficient	D_G	1.95×10^{-7}	m ² s ⁻¹
Porosity	ϕ	0.2	—
Intrinsic permeability	K	10^{-12}	m ²
Temperature	T	323.15	K
Brooks-Corey parameter	λ	2	—
Brooks-Corey parameter	P_b	1×10^5	Pa
Gas residual saturation	$S_{G,\text{res}}$	0.05	—
Liquid residual saturation	$S_{L,\text{res}}$	0.15	—

The thermodynamic properties of CO₂ and impurity mixtures are simulated based on the Peng-Robinson EoS discussed in Chapter 5. Because H.Li [66] suggest PR-EoS can provide accurate approximation for the vapor liquid equilibrium properties of binary CO₂-mixtures (e.g CO₂ N₂ or O₂). The calibration routine adopts the algorithm proposed in Chapter 3. Note that the water phase density is given by IAWPS [33].

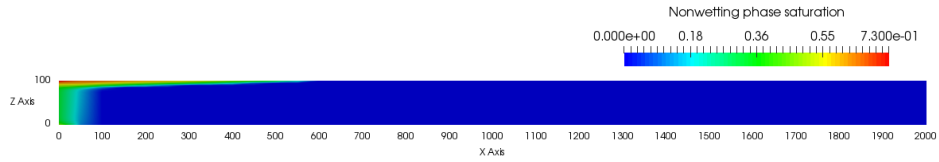
8.2.3.1 Model configuration

The domain is uniformly discretized into 3×10^4 quad elements. The simulation is run over a time span of 10 years. An adaptive time stepping control is applied for the whole simulation, with an initial time step size (Δt) of 250 seconds. The parameters used for this benchmark is listed in Table 7.

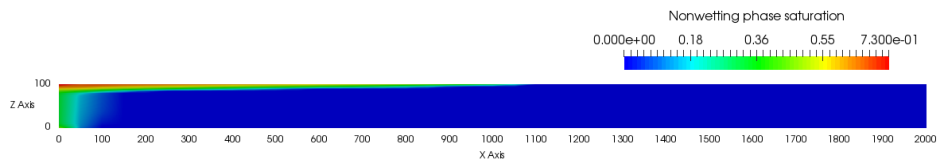
8.2.3.2 Simulation results

It can be observed from Figure.18, at the beginning of the simulation, the injected CO₂ and impure gas components rise up due to the density difference and buoyancy force. Then the impure CO₂ plume spread along the top of the aquifer.

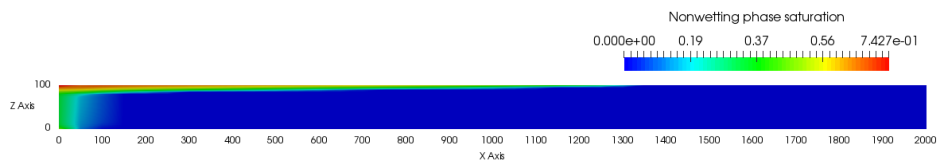
Figure.19 depicts the temporal evolution of molar fraction profile with respect to different components at 2, 6 and 10 years. It can be observed that, N₂ and O₂ dominates the leading edge of the plume while CO₂ follows in the rear. While the molar fraction of N₂ and O₂



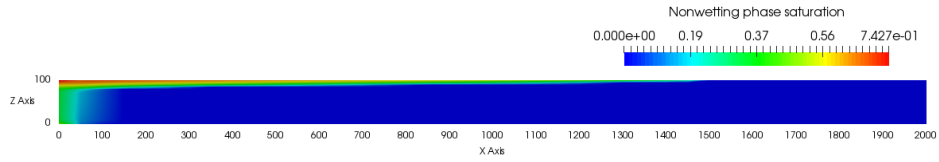
(a) Nonwetting phase saturation distribution at t=2 year



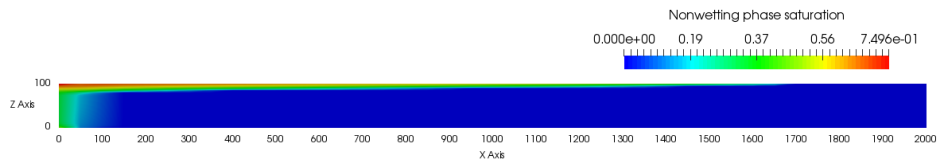
(b) Nonwetting phase saturation distribution at t=4 year



(c) Nonwetting phase saturation distribution at t=6 year



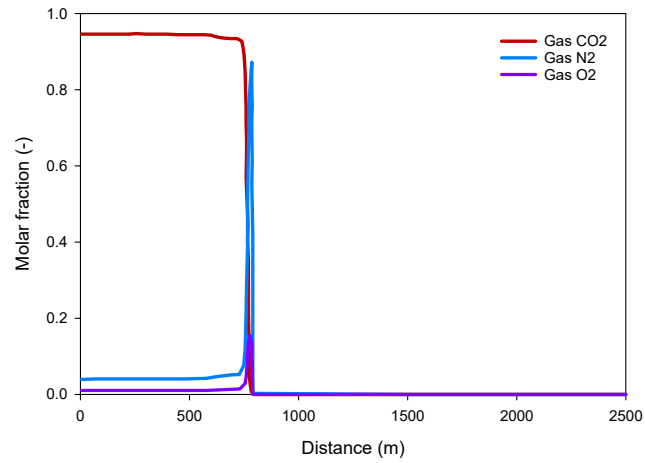
(d) Nonwetting phase saturation distribution at t=8 year



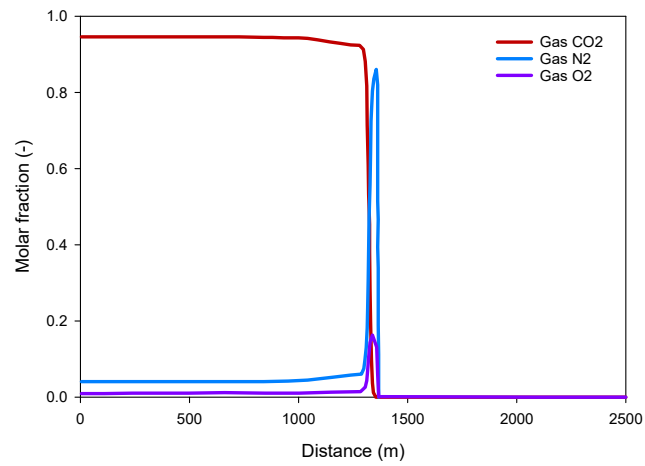
(e) Nonwetting phase saturation distribution at t=10 year

Figure 18.: Nonwetting phase saturation distribution evolution at different time.

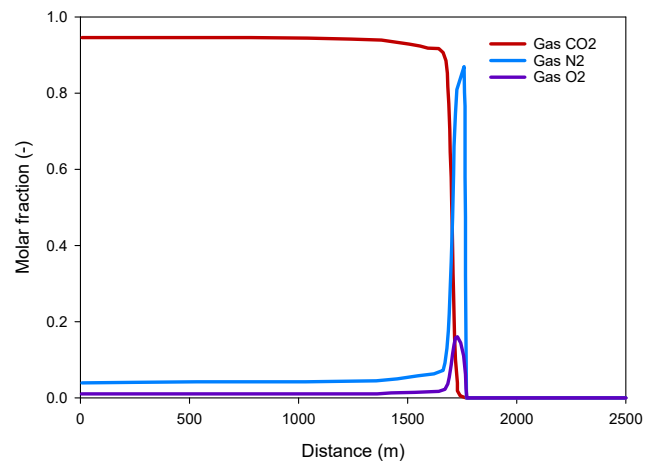
in the leading edge is much higher than the compositions of the injected mixture, with $x_G^{N_2}$ and $x_G^{O_2}$ equal to 0.87 and 0.15, respectively. This is mainly because of the larger dissolution of CO_2 compared with that of N_2 and O_2 . More CO_2 would dissolve in the water at the leading edge of the plume, resulting in higher N_2 and O_2 molar fraction in the gas phase. While the preferential solubility of O_2 compared to N_2 further explains that the peak of N_2 plume is a little bit ahead of that of O_2 plume. The distribution range of N_2 plume is increasing as time. This is mainly due to the lower viscosity of the N_2 . Similar phenomena can be observed for the O_2 plume.



(a)



(b)



(c)

Figure 19.: Molar fraction profile of multiple gas components at t=2, 6, 10 years

8.3 BENCHMARKING THE LOOK-UP TABLE APPROACH

This section presents a reactive transport benchmarking exercise which aims at specifically targeting the pivotal question: how good and under which (transport) conditions the look-up table approach resembles the simulation results of a full coupled two-phase reactive transport model. The exercise is based on a description of the long term degradation of the concrete. We compared the newly proposed look-up table based model OpenGeoSys-MP-LT with the well-established reactive transport code OpenGeoSys-GEM (Kosakowski and Watanabe, [67]).

This part are mainly adopted from [47]

8.3.1 *Conceptual of the application*

Atmospheric degradation of concrete under an unsaturated condition is a complex process that involves intricate couplings between transport of both liquid and vapour water, CO₂ and air(N₂, O₂) in gas and liquid phases, chemical reactions involving cement hydrates with the dissolution of CO₂ in the water phase. Porosity change is also associated with the concrete evolution. In this work, we dedicate to investigating an accelerate atmospheric degradation of concrete. While, two dominated and competing chemical reaction processes: carbonation and ASR, are taken into account. A look-up table is set up for the concrete degradation by only considering two reactants: SiO₂ and CO₂.

8.3.2 *Model configuration*

As Figure.20 shows, the geometry of the benchmarks is represented by a 1D concrete structure. We assume a in-diffusion boundary for the concrete structure a strongly CO₂ dominated gas phase with a concentration of 39.43 mol m⁻³ (0.889e-3 kg m⁻³), which corresponds a much faster carbonation than under atmospheric conditions (i.e. accelerated carbonation). The concrete structure is initially subjected to an atmospheric pressure and under an unsaturated condition with water saturation equals to 0.5. For comparison, the fully reactive transport model OpenGeoSys-GEM are also applied with similar settings.

A sub-set of features was tested in the following benchmark which was limited to consider three cases, where case 3 was further split into of two sub-cases:

- Case 1: Only ASR process is taken into account, no transport of CO₂ (or interaction of CO₂ with concrete) is considered. For



Figure 20.: The geometry for the concrete degradation application

simplicity reasons the default mesh is used in OpenGeoSys-MP-LT. In OpenGeoSys-GEM for minimization of calculation times only a small mesh with 3 nodes and 2 elements is used.

- Case 2: CO₂ diffusive transport in the default geometry. Only carbonation is taken into account.
- Case 3a: CO₂ diffusion dominates, i.e. the progress of carbonation is much faster than the typical time scales for ASR. A 1D setup of a 1 m long concrete domain was applied here for the simulation.
- Case 3b: CO₂ diffusion and ASR compete, i.e. part of the domain is highly affected by ASR before the carbonation front arrives. This case was implemented by enlarging the simulation domain by a factor of 10. In this setup the carbonation front needed 100 times longer time until it reaches the end of the simulation domain.

8.3.3 Model dimensions and discretization

The default setup represents an 1D concrete structure (length = 1m) discretized by a regular mesh of 100 elements with node distances of 1 cm.

Automatic time step sizing was used for all simulations. In addition, the time step size was limited as listed in Table.8

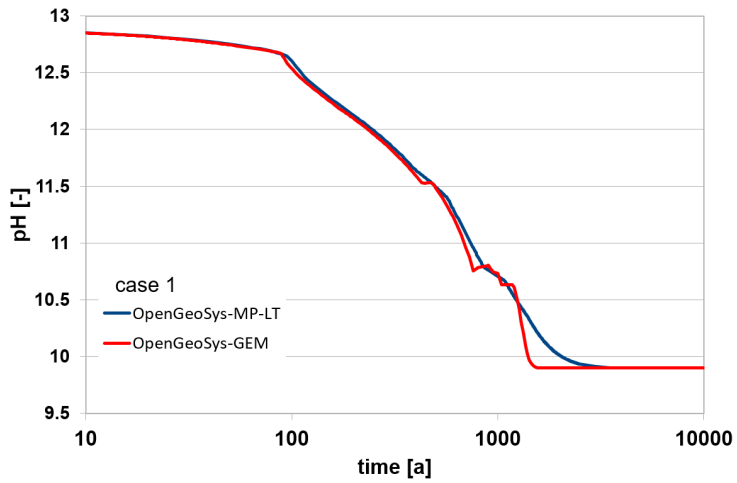
8.3.4 Results and discussion

Case 1

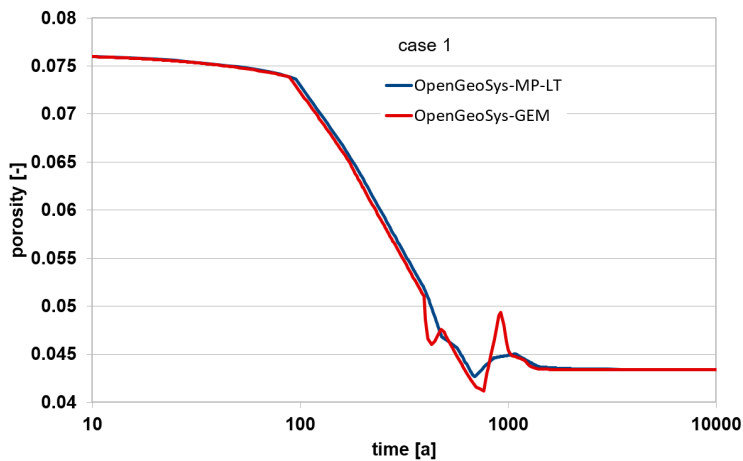
We select the first FE node at the left hand side boundary and plot the temporal evolution of pH value and porosity with respect to the simulation time in Figure.21. The blue lines represent results generated by OpenGeoSys-MP-LT, while the red curves denote the OpenGeoSys-

Table 8.: Maximum time step sizes for simulation cases in OpenGeoSys-GEM and fixed time step sizes in OpenGeoSys-MP-LT.

	OpenGeoSys-GEM: Maximum time step size [s]	OpenGeoSys-MP-LT: Time step size [s]
Case 1	1e3 ($\sim 3.169e-5$ years)	0-2500 yrs: 157,784.63 (0.005 yrs) — >2500 yrs: 15, 778, 463.0 (0.5 yrs)
Case 2	1e5 ($\sim 3.169e-3$ years)	31,556.926 (0.001 yrs)
Case 3a	1e3 ($\sim 3.169e-5$ years)	31,556.926 (0.001 yrs)
Case 3b	1e5 ($\sim 3.169e-3$ years)	157,784.63 (0.005 yrs)



(a) pH evolution



(b) porosity evolution

Figure 21.: The temporal evolution of pH value(a) and porosity(b)

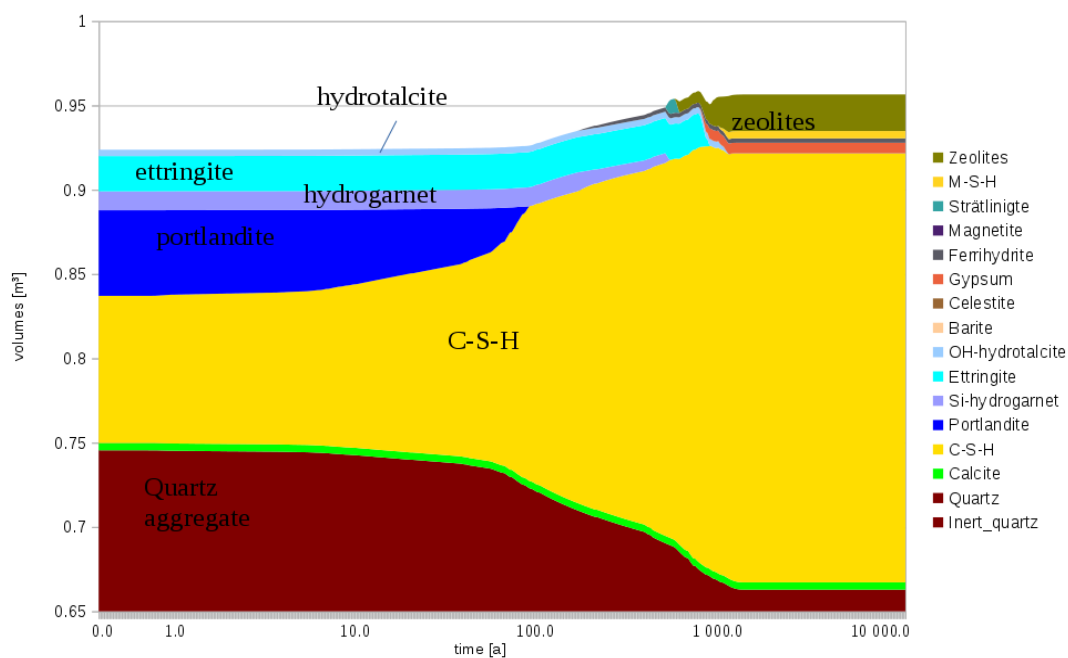


Figure 22.: Mineralogical evolution with time shown as volume fractions. The porosity corresponds to $1 - (\text{sum of solid volume fractions})$. Calcite, quartz, inert phases and some part of C-S-H that make up 80 % of the volume are not shown.

GEM results. The results demonstrate a very good agreement between the two codes. The fully reactive transport model shows additional variations in pH and porosity with time at around 800-1000 years. These variations are not covered by the look-up table, as they are related to increments in SiO_2 which are smaller than the resolution of the look-up table ($\text{SiO}_2 = 0.2 \text{ mol/l}$).

Figure 22 shows the evolution of the batch reaction system in terms of time-dependent mineral volumes calculated by the OpenGeoSys-GEM code. To highlight the minerals with active changes, calcite, quartz, inert phases and some part of C-S-H that make up 80 % of the volume are not shown in this figure. The use of the kinetic rates for aggregate dissolution relates the SiO_2 amounts with a time scale. For this setup portlandite is dissolved after 85 years, hydrogarnet after 380 years, ettringite after 855 years, hydrotalcite after 1075 years and thermodynamic equilibrium is reached after about 1600 years.

Case 2

The case 2 is dedicated to investigate the appropriateness of the look-up table approach for the case of carbonation only. Figure 23 shows spatial profiles for CO_2 concentrations in the gas phase at different times. The pH and porosity profiles at the same times are shown in Fig.24 .

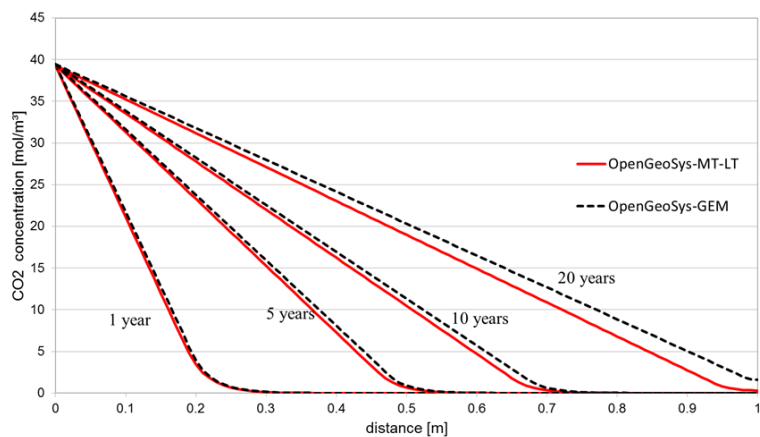


Figure 23.: Gaseous CO_2 concentration profiles at different times for case 2.

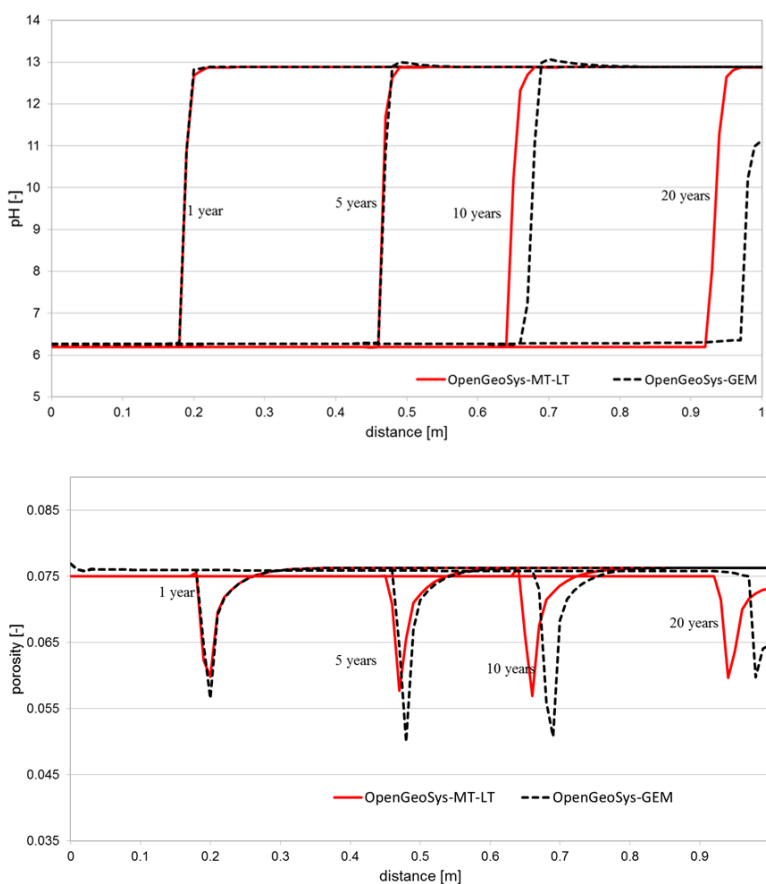


Figure 24.: pH profiles at different times for case 2. (a): Precipitation of quartz is allowed. (b) precipitation of quartz is suppressed.

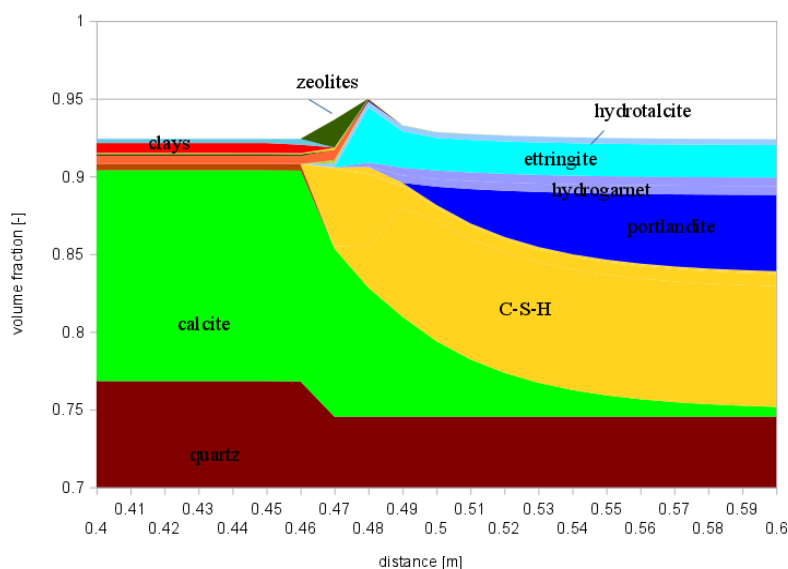


Figure 25.: Mineralogical profile after 5 years of simulation time produced by OpenGeoSys-GEM.

Agreement between both approaches is relatively good, although after 10 to 20 years the reactive transport approach predicts faster progress of the carbonation front compared to the look-up table approach.

It should be noted that the progress of the carbonation front is dependent on the square root of time which is typical for reactive fronts driven by diffusive transport. The pH profiles show some overshooting by OpenGeoSys-GEM at the onset of the carbonation front which coincides with a stronger interim reduction of the porosity. The porosity reduction is caused by the interim formation of zeolite (chabazite), which occurs when portlandite dissolution is completed and ettringite is dissolved (Fig. 25). Chabazite, which is a hydrated calcium aluminum silicate, takes up considerable amounts of H₂O from the pore water. Removal of H₂O from the pore water increases the alkali concentrations and consequently pH. Due to the small stability field of chabazite this effect is not covered by the look-up table and therefore not reproduced by OpenGeoSys-MP-LT. The mineralogical profile in Fig. 25 shows that most mineral transformations follow a step function, except for the dissolution of portlandite. Note that the direction of transport is from left to right, i.e. the completely degraded concrete is on the left and intact concrete is on the right side. The smoothed dissolution profile indicates some effect of numerical diffusion related to the steep concentration gradients for CO₂ in the gas phase and all solutes in liquid phase near the carbonation front. This numerical diffusion might be also responsible for the faster progress of the carbonation front as indicated by the OpenGeoSys-GEM results.

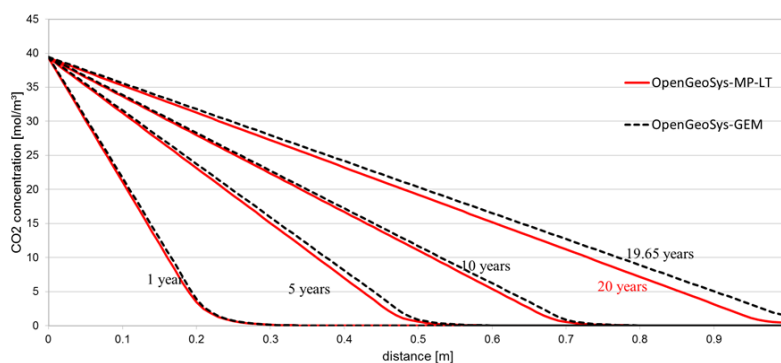


Figure 26.: Gaseous CO_2 concentration profiles at different times for benchmark case 3a.

Case 3a

Case 3a compares the combined effect of carbonation and ASR over a relatively short distance, i.e. in this case concrete degradation due to carbonation is dominant. The system evolution is therefore expected to be very close to case 2. Comparison of the profiles for gaseous CO_2 (Fig. 26), pH (Fig. 27) and porosity (Fig. 28) resemble the corresponding profiles of case 2 (Fig. 23 and Fig. 24) very much. The advancement of the carbonation front is a little bit faster than the one predicted in case 2. Within 20 years, ASR consumes already a portion of the portlandite which reduces slightly the amount of CO_2 necessary to complete carbonation. For the fully reactive transport model the carbonation front passed already the model boundary at 1 m distance and it is not visible anymore. Therefore, the front at time $t = 19.65$ years is plotted for comparison with the look-up table approach. As previously mentioned in connection with case 2, the faster progress of the carbonation front can be explained by an enhanced numerical diffusion in the OpenGeoSys-GEM code. In the porosity profiles (Fig. 28) some oscillations are visible for the OGS-GEM results on the left side, i.e. behind (left of) the carbonation front. These oscillations are induced by numerical oscillations in the transport solver caused by strong temporal variations in the concentrations near the carbonation front. Concentration oscillations are smoothed at the expense of small mineralogical changes as the chemical solver enforces equilibrium between pore water composition and mineralogy. In the specific setup for concrete carbonation it is believed that the solid solution model for C-S-H phase reacts particularly sensitive to changes in the pore water composition. The concentration oscillations from the transport solver are not random. They occur at the same position relative to the carbonation front. The carbonation front moves slowly or even might stay at the same position over a long period of time, which causes an accumulation of mineralogical changes over many time steps.

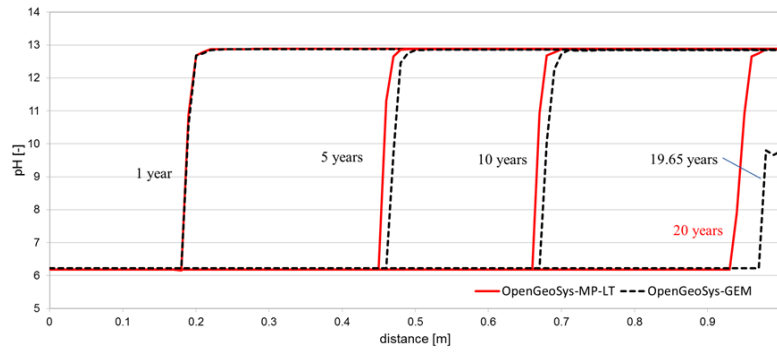


Figure 27.: pH profiles at different times for benchmark case 3a.

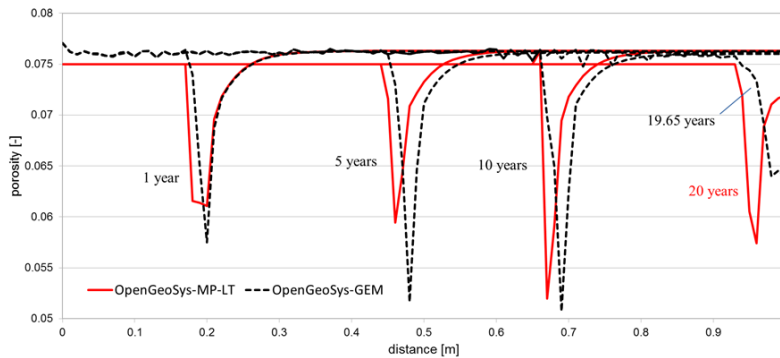


Figure 28.: Porosity profiles at different times for benchmark case 3a.

Case 3b

Case 3b extends case 3a to the full competition between carbonation and ASR. On the left side of the domain, at early times, carbonation dominates, whereas on the right side, ASR is the only process degrading the concrete. This case is a simple extension of case 3a in terms of a 10 times longer simulation domain. This was achieved by simply increasing the FE node distance by 10-fold. As for case 3a on the left side ($x=0$ m) the CO_2 concentration in the gas phase was fixed, whereas the right side of the domain was closed, i.e. a no-flow boundary was applied on both the gas and liquid phase. As the progress of the diffusion driven carbonation front follows a relationship which depends on the square root of time, it would take the carbonation front in the absence of ASR about 2000 years to reach the right boundary. This is 100 times longer than the time obtained in case 3a (20 years). From the calculations performed in connection with case 1 it is clear that the ASR is mostly completed within 2000 years. Results of the calculations are given in terms of CO_2 concentration in the gas phase (Fig. 29), pH profiles (Fig. 30) and porosity profiles (Fig. 31). In general, the same effects for case 3a can be observed in this case, while they are superimposed by the ASR. As a consistency check, the carbonation front progress after 10 years in

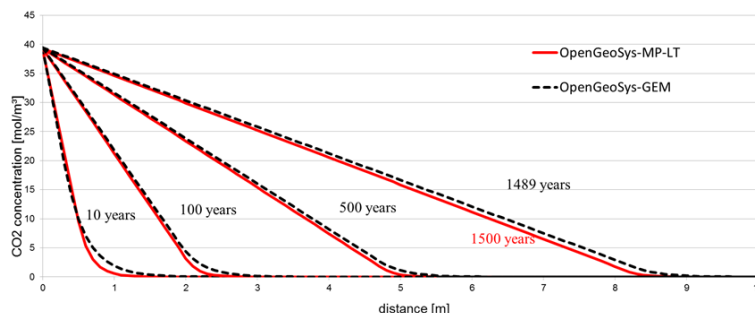


Figure 29.: Gaseous CO₂ concentration profiles at different times for benchmark case 3b.

the cases 3a and 3b are the same, although discretization and time step size were different. This shows that the difference between the look-up table approach and full reactive transport is similar too. In the cases 2 and 3a the carbonation front propagates slightly faster for reactive transport calculations than with the look-up table approach. In addition, variations of pH, mineral transformations and porosity near the carbonation front become stronger with time. With time, diffusive transport of solutes other than CO₂ increasingly influences concrete carbonation. The effect of chemical gradients across the carbonation front becomes more important with time. Over time, CO₂ gradients and fluxes become smaller and the progress of the reaction front decelerates correspondingly. This behavior is described by the well-known square root relation ($x \propto \sqrt{tD_a}$) [68] where D_a is an apparent diffusion coefficient which includes the retardation due to chemical reactions. The slow-down of the front allows geochemical differences across the carbonation front to be equilibrated over longer time steps. The influence of chemical gradients other than CO₂ (in gas and liquid phase) is not covered by the look-up table approach. ASR does not depend on continuum scale spatial gradients in the look-up table it is implemented as an internal source term for SiO₂. Interestingly, small differences in the progress of ASR are more evident from the porosity changes over time than pH evolution. The pH changes with time in a more stepwise way, whereas porosity oscillates more strongly at intermediate pH values due to formation of intermediate phases (compare Sect. 8.3.4-case 1, Fig. 21a and Fig. 21b).

8.3.5 Reference

H. Yonghui, S. Haibing, W. Erich, K. Olaf, and K. Georg. A new approach to coupled two-phase reactive transport simulation for long-term degradation of concrete. submitted.

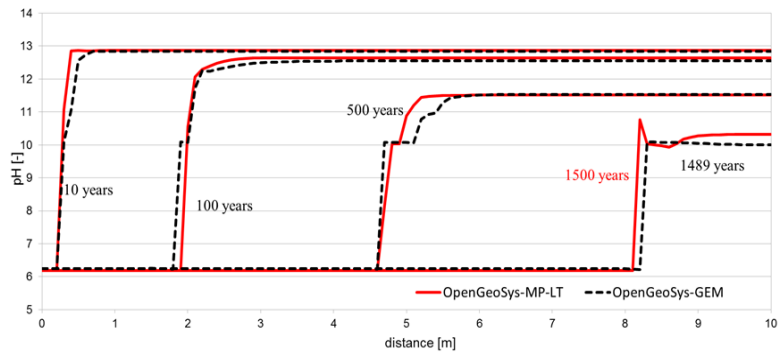


Figure 30.: pH profiles at different times for benchmark case 3b.

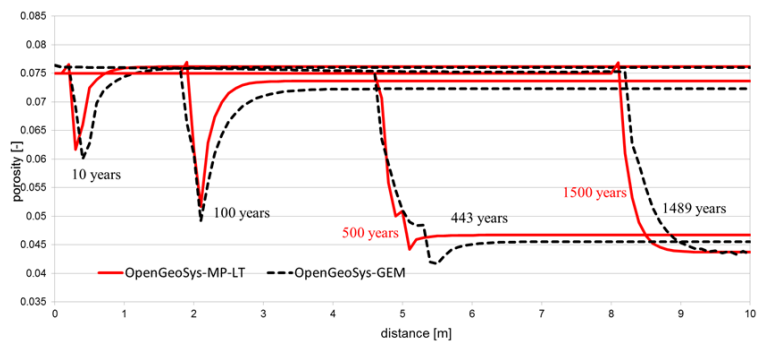


Figure 31.: Porosity profiles at different times for benchmark case 3b.

Part II

SUMMARY AND OUTLOOKS

DISCUSSION AND SUMMARY

In the first part of the thesis, a numerical study of nonisothermal multiphase compositional compressible flow and transport is presented, where an emphasis is placed on the accurate and robust handling of phase change problem. Two different formulations: local NCP and global NCP are addressed and compared. The phase change logic is formulated as nonlinear complimentary problem (NCP) and restructure as algebraic equations using min function or mid function. Both ideal and non-ideal thermodynamics are taken into account. In order to suppress the numerical challenge where the cubic equation of state is involved for the non-ideal properties, a nonsmooth inside-out algorithm proposed by Watson et al.[3] is applied and extended. Different numerical benchmarks related to desaturated process in deep geological repositories of radioactive waste and to CO₂ sequestration demonstrate that both formulations, provide accurate numerical results, and that it is capable of handling the strongly nonlinear coupling of multiphase flow and transport. While the phase change problem can be handled in a efficient and robust way by using the nonlinear complimentary problem.

Furthermore, this newly implemented compositional two-phase flow model is extended into a coupled two-phase reactive transport model framework based on a look-up table approach. For model validation, a variety of applications are addressed for the concrete degradation in the context of long-term safety assessment of the nuclear waste repository.

Firstly(in Section 1.1), several well established cases have been employed to analyze the efficiency and robustness of local and global NCP formulations. It is found that NCP formulations are numerically more robust and efficient in handling phase change compared to conventional approaches. In both homogeneous and heterogeneous media, the global-NCP formulation is around 20% faster than the local one. However, in heterogeneous media, the local NCP formulation delivers a more accurate and stable result. The slightly longer computation time is a good trade-off for suppressing numerical oscillations at the interface of different media or at the location of phase transition. In the near future, it is planned to apply the NCP formulation in more complicated scenarios, such as in reservoir simulation with three phases coexist.

While in Section 1.2, the degradation of concrete in the context of nuclear waste disposal in Switzerland has been investigated based on the validated compositional two-phase model. A special interest has been focused on integrating the chemical reactive processes into the two-phase model via a look-up table approach. It has been demonstrated that the look-up table approach gives simulation results in great agreement with those from the fully coupled reactive transport model. In terms of calculation time, the look-up table approach achieves up to 10 times faster compared to the reactive transport model.

1.1 REMARKS ON THE NON-ISOTHERMAL COMPOSITIONAL TWO-PHASE FLOW MODEL

[P2]: Huang et al.[69]

1.1.1 *Background*

Compositional two-phase flow is considered to be one of the fundamental physical processes in the field of geoscientific research. For example, at sites where groundwater is contaminated by Non-Aqueous Phase Liquids (NAPL), the dispersion of NAPL components occurs in both the aqueous and gas phases [70, 71]. For CO₂ sequestration, the amount of CO₂ dissolved in saline water determines the water-rock interactions and also the long-term geochemical evolution(cf. Nordbotten et al.[72]). For the assessment of nuclear waste repositories, transport of radionuclides driven by the gas production is the focus of a lot of recent research [73, 14].

Phase transition represents one of the most important processes underlying compositional two-phase flow, and it consistently attracts the interest of researchers and engineers. In the first part of the thesis, two different formulations (namely local NCP and global NCP formulations) which incorporate the phase change as nonlinear complementarity problem (NCP) are presented. Different numerical benchmarks related to gas migration in deep geological repository of nuclear waste and to CO₂ sequestration has successfully validated both formulations can handle the phase change problem appropriately in both idealize and non-ideal mixing system.

However, to the authors' knowledge, there has been rarely a detailed analysis of these two nonlinear formulations, with respect to their numerical performance and computational efficiency in solving the compositional two-phase flow problem. In this work, the investigation and comparison is conducted with the scientific simulator OpenGeoSys [24, 25], which is based on the Galerkin Finite Element

method. Both aforementioned NCP formulations have been implemented in it.

1.1.2 Conclusion

Three well established benchmarks have been employed to analyze the efficiency and robustness of these numerical models. It is found that both local and global NCP formulation deliver results in good agreement with those from conventional primary variable switching (PVS) approaches. It is also found that NCP formulations are numerically more robust and efficient for handling phase transition, as shown by the fewer global Newton iterations and larger time step sizes. In both homogeneous and heterogeneous media, the global NCP formulation is around 20% faster than the local one. However, in heterogeneous media, the local NCP formulation is recommended, as it delivers a more accurate and stable evaluation of capillary pressure and relative permeability. The slightly longer computation time is a good trade-off for suppressing numerical oscillations at the interface of different media or at the location of phase transition.

1.1.3 Reference

Huang Y, Nagel T, Shao H. Comparing global and local implementations of nonlinear complementary problems for the modeling of multi-component two-phase flow with phase change phenomena[*J*]. *Environmental Earth Sciences*, 2017, 76(18): 643. (cf. [69], Appendix A.2)

1.2 REMARKS ON THE TWO-PHASE REACTIVE TRANSPORT MODEL WITH LOOK-UP TABLE

This part are mainly adopted from [47]

1.2.1 Discussion

From the benchmarking exercise, two main factors have been identified to cause differences between the look-up table approach and full reactive transport.

- 1) The resolution of the look-up table used for the benchmarks does not cover all variations in porosity, pH or quartz dissolution rates in detail. This is obvious from the temporal evolution of pH and porosity associated with ASR as shown in Fig. 4. The accuracy of the look-up table approach can be improved by including interpolation points for maxima/minima of porosity/pH/rates and/or by covering regions with strong changes with a finer mesh of interpolation

points. As previously mentioned, the look-up table approach does not cover the entire variability of the chemical system. Variability of the parameters below the sampling scale is smoothed out. The absolute minimum porosity for carbonation might not be included in the look-up table as it is reached only for a very narrow intermediate stage of carbonation. The progress of the carbonation front is a direct function of the diffusive CO₂ flux. From Ficks law it is clear that for a given CO₂ concentration gradient the flux is controlled by the effective CO₂ (gas) diffusion coefficient. In our simplified setup effective diffusion coefficient is calculated as the product of porosity and pore diffusion coefficient. A mismatch in the porosity evolution upon concrete degradation should influence the diffusion of CO₂ and might affect the progress of carbonation fronts. The interpretation of the porosity profiles in Fig. 24 (b), Fig. 28 and Fig. 31 is not straightforward, as absolute porosity minima with time are not necessarily present within the plotted time steps. It seems that OpenGeoSys-GEM systematically calculates a slightly bigger intermediate porosity reduction. These values might be even smaller than those calculated with the look-up table as the diffusive transport of reactive species other than CO₂ in the aqueous phase influences transformation of mineral phases. Nevertheless, lower porosity values should reduce diffusive fluxes and slow down the progress of the carbonation front. Note that the opposite was observed which shows that other processes have a bigger influence on the observed diffusive fluxes.

2) Reactive transport calculations with OpenGeoSys-GEM are extremely sensitive to numerical oscillations in the solution of the transport equations. With the standard Galerkin FE methods, as used in OpenGeoSys, undershooting and overshooting of the solution are a common problem at reaction fronts with steep concentration gradients. Often numerical oscillations are quite strong and spread out into the whole calculations domain.

As the magnitude of these oscillations is different for each transport equation the chemical system may become poorly defined and the GEM algorithm fails to reach a solution. We observed this problem at nearly all nodes in several benchmark runs. There are some methods available in OpenGeoSys which enable to suppress the numerical oscillations. For example, for some systems a flux corrected transport (FCT) method was successfully applied [67]. For the current benchmark calculations mass lumping was used. The drawback of this method, like FCT, is that it causes an additional diffusive flux (numerical diffusion) in the transport equations causing reaction fronts to proceed faster.

It is shown from the above benchmark study that in both codes the time step size has to be small in order to properly approximate the progress of the carbonation front. Time step size t depends on the Neumann stability condition [74], which in turn depends on the

spatial discretization \times (FE node distance). With a very refined discretization, the time step size may become a computationally limiting factor.

One way to overcome limitations in time step size for OpenGeoSys-MP-LT is to use source/sink terms derived from the look-up table in a fully implicit way instead of an operator-splitting approach to include the look-up table. The fully implicit method allows achieving improved numerical stability and enabling a larger time step size. This further allows an automatic time stepping regime to be included with time step size not limited by the Neumann stability condition, but rather by changes in the reaction rates (e.g. completion of carbonation at a node).

1.2.2 Conclusion

In this study, a new coupled two-phase reactive transport model derived from the look-up table approach has been presented to simulate the long-term degradation of concrete due to ASR and carbonation. The proposed model is validated by the means of comparison with a full reactive transport model. In general, the proposed approach shows the same system evolution as the reactive transport models. Differences in the propagation speed of carbonation fronts are not necessarily related to the approach itself and can be attributed to numerical diffusion.

In terms of calculation time, it was observed that the serial (not parallelized) version of OpenGeoSys-MP-LT is up to 10 times faster than OpenGeoSys-GEM which employs 32 threads for chemical calculations. Although an exact speedup calculation is not possible due to the use of different compilers, CPUs and operating systems, the approach presented in this study leads to a significant reduction in the computational efforts, while maintaining numerical stable and a good accuracy.

The accuracy of the look-up table approach can be further improved by including interpolation points for maxima/minima of porosity/pH/rates and/or by covering regions with strong changes with a finer mesh of interpolation points. Depending on the way the look-up table is used in the multi-phase multi-component transport codes this might cause problems. With OpenGeoSys-MP-LT the possibility was tested to include the look-up table in terms of rates also for porosity changes. These rates (time derivative of porosity) may strongly vary between interpolation points which could cause convergence problems in case of the non-linear equation solver. In addition, the variability of e.g. porosity very much depends on the specific thermodynamic setup (choice and quality of thermodynamic data for e.g. clay and zeolite minerals).

The look-up table approach can be applied to problems where the transport of CO₂ preferentially in the gas phase is much faster than the transport of other reactive solutes in the liquid phase. There are scenarios in the framework of radioactive waste disposal where macroscopic transport of dissolved silica might influence the long-term performance of the engineered system of a radioactive waste repository. These scenarios are related to skin formation and porosity clogging at clay/cement interfaces with a distinct dependency of clogging time on numerical discretization and kinetic parametrization [75]. Given the very small extend of the influenced volume and the complexity of porosity clogging [76], an approximation of the localized change of transport properties by time-dependent functions seems more appropriate.

Furthermore, the formation and transformations of zeolite and clay minerals at later stages of concrete degradation are kinetically controlled. Here, an additional multiplicative function for accounting of a kinetic slowdown of reactivity needs to be introduced, similar to the function used by Bzant and Najjar [77] for cement hydration.

1.2.3 Reference

H. Yonghui, S. Haibing, W. Erich, K. Olaf, and K. Georg. A new approach to coupled two-phase reactive transport simulation for long-term degradation of concrete. submitted.

1.3 OUTLOOKS

The new functionalities proposed in this work, and implemented in OpenGeoSys, opens a wide array of applications. Therefore, there are plenty of topics of great interests which could developed in the future.

1.3.1 Application

The numerical models presented in this work can be extended to develop some more advanced models that are applicable, not only in the field of nuclear waste storage and CO₂ sequestration, but in some more complex geologic systems and some other energy or environmental problems.

- Deep geothermal system, such as the enhanced geothermal system, has been receiving worldwide attention, and still under intensive study over the last decades. Heat exploitation from the deep geothermal system is subjected to complex physical and chemical processes within the fluid and interaction with high-temperature geological rock formation. It often involves

heat transfer, multiphase flow, rock deformation and chemical reactions. Among these, the non-isothermal compositional two-phase reactive transport model can serve as the basis and will play an important role for better understanding and efficient utilization the deep geothermal energy.

1.3.2 *Model extension*

As one of the future topics of this work, the improved computational efficiency of the chemical reaction part makes the proposed look-up table based model particularly promising in further coupled with the geomechanical model in OpenGeoSys for a multi-scale and multi-chemo-physics analysis of the evolution of the concrete.

Part III

APPENDIX

A

APPENDIX

A.1 PAPER 1

Huang Y, Kolditz O, Shao H. Extending the persistent primary variable algorithm to simulate non-isothermal two-phase two-component flow with phase change phenomena[J]. Geothermal Energy, 2015, 3(1): 1-23.

RESEARCH

Open Access



Extending the persistent primary variable algorithm to simulate non-isothermal two-phase two-component flow with phase change phenomena

Yonghui Huang^{1,2†}, Olaf Kolditz^{1,2} and Haibing Shao^{1,3*†}

*Correspondence:

haibing.shao@ufz.de

†Equal contributors

¹Helmholtz Centre for

Environmental Research - UFZ,

Permoserstr. 15, 04318 Leipzig,

Germany

³Freiberg University of Mining and

Technology, Gustav-Zeuner-Strasse

1, 09596 Freiberg, Germany

Full list of author information is
available at the end of the article

Abstract

In high-enthalpy geothermal reservoirs and many other geo-technical applications, coupled non-isothermal multiphase flow is considered to be the underlying governing process that controls the system behavior. Under the high temperature and high pressure environment, the phase change phenomena such as evaporation and condensation have a great impact on the heat distribution, as well as the pattern of fluid flow. In this work, we have extended the persistent primary variable algorithm proposed by (Marchand et al. *Comput Geosci* 17(2):431–442) to the non-isothermal conditions. The extended method has been implemented into the OpenGeoSys code, which allows the numerical simulation of multiphase flow processes with phase change phenomena. This new feature has been verified by two benchmark cases. The first one simulates the isothermal migration of H₂ through the bentonite formation in a waste repository. The second one models the non-isothermal multiphase flow of heat-pipe problem. The OpenGeoSys simulation results have been successfully verified by closely fitting results from other codes and also against analytical solution.

Keywords: Non-isothermal multiphase flow; Geothermal reservoir modeling; Phase change; OpenGeoSys

Background

In deep geothermal reservoirs, surface water seepages through fractures in the rock and moves downwards. At a certain depth, under the high temperature and pressure condition, water vaporizes from liquid to gas phase. Driven by the density difference, the gas steam then migrates upwards. Along with its path, it will condensate back into the liquid form and release its energy in the form of latent heat. Often, this multiphase flow process with phase transition controls the heat convection in deep geothermal reservoirs. Besides, such multiphase flow and heat transport are considered to be the underlying processes in a wide variety of applications, such as in geological waste repositories, soil vapor extraction of Non-Aqueous Phase Liquid (NAPL) contaminants (Forsyth and Shao 1991), and CO₂ capture and storage (Park et al. 2011; Singh et al. 2012). Throughout the process, different phase zones may exist under different temperature and pressure conditions. At lower temperatures, water flows in the form of liquid. With the rise of temperature, gas

and liquid phases may co-exist. At higher temperature, water is then mainly transported in the form of gas/vapor. Since the physical behaviors of these phase zones are different, they are mathematically described by different governing equations. When simulating the geothermal convection with phase change phenomena, this imposes challenges to the numerical models. To numerically model the above phase change behavior, there exist several different algorithms so far. The most popular one is the so-called primary variable switching method proposed by Wu and Forsyth (2001). In Wu's method, the primary variables are switched according to different phase states. For instance, in the two phase region, liquid phase pressure and saturation are commonly chosen as the primary variables; whereas in the single gas or liquid phase region, the saturation of the missing phase will be substituted by the concentration or mass fraction of one light component. This approach has already been adopted by the multiphase simulation code such as TOUGH (Pruess 2008) and MUFTE (Class et al. 2002). Nevertheless, the governing equations deduced from the varying primary variables are intrinsically non-differentiable and often lead to numerical difficulties. To handle this, Abadpour and Panfilov (2009) proposed the negative saturation method, in which saturation values less than zero and bigger than one are used to store extra information of the phase transition. Salimi et al. (2012) later extended this method to the non-isothermal condition, and also taking into account the diffusion and capillary forces. By their efforts, the primary variable switching has been successfully avoided. Recently, Panfilov and Panfilova (2014) has further extended the negative saturation method to the three-component three-phase scenario. As the negative saturation value does not have a physical meaning, further extension of this approach to general multi-phase multi-component system would be difficult. For deep geothermal reservoirs, it requires the primary variables of the governing equation to be persistent throughout the entire spatial and temporal domain of the model. Following this idea, Neumann et al. (2013) chose the pressure of non-wetting phase and capillary pressure as primary variables. The two variables are continuous over different material layers, which make it possible to deal with heterogeneous material properties. The drawback of Neumann's approach is that it can only handle the disappearance of the non-wetting phase, not its appearance. As a supplement, Marchand et al. (2013) suggested to use mean pressure and molar fraction of the light component as primary variables. This allows both of the primary variables to be constructed independently of the phase status and allows the appearance and disappearance of any of the two phases. Furthermore, this algorithm could be easy to be extended to multi-phases (≥ 3) multi-components (≥ 3) system.

In this work, as the first step of building a multi-component multi-phase reactive transport model for geothermal reservoir simulation, we extend Marchand's component-based multi-phase flow approach (Marchand et al. 2013) to the non-isothermal condition. The extended governing equations ('Governing equations' section), together with the Equation of State (EOS) ('Constitutive laws' section), were solved by nested Newton iterations ('Numerical solution of the global equation system' section). This extended model has been implemented into the OpenGeoSys software. To verify the numerical code, two benchmark cases were presented here. The first one simulates the migration of H₂ gas produced in a waste repository ('Benchmark I: isothermal injection of H₂ gas' section). The second benchmark simulates the classical heat-pipe problem, where a thermal convection process gradually develops itself and eventually reaches equilibrium ('Benchmark II: heat pipe problem' section). The numerical results produced by OpenGeoSys were

verified against analytical solution and also against results from other numerical codes (Marchand et al. 2012). Furthermore, details of numerical techniques regarding how to solve the non-linear EOS system were discussed ('Numerical solution of EOS' section). In the end, general ideas regarding how to include chemical reactions into the current form of governing equations are introduced.

Method

Governing equations

Following Hassanizadeh and Gray (1980), we write instead the mass balance equations of each chemical component by summing up their quantities over every phase. According to Gibbs Phase Rule (Landau and Lifshitz 1980), a simplest multiphase system can be established with two phases and two components. Considering a system with water and hydrogen as constitutive components (with superscript h and w), they distribute in liquid and gas phase, with the subscript $\alpha \in L, G$. The component-based mass balance equations can be formulated as

$$\Phi \frac{\partial(S_L \rho_L^w + S_G \rho_G^w)}{\partial t} + \nabla(\rho_L^w v_L + \rho_G^w v_G) + \nabla(j_L^w + j_G^w) = F^w \quad (1)$$

$$\Phi \frac{\partial(S_L \rho_L^h + S_G \rho_G^h)}{\partial t} + \nabla(\rho_L^h v_L + \rho_G^h v_G) + \nabla(j_L^h + j_G^h) = F^h, \quad (2)$$

where S_L and S_G indicate the saturation in each phase. ρ_α^i ($i \in \{h, w\}, \alpha \in \{L, G\}$) represents the mass density of i -component in α phase. Φ refers to the porosity. F^h and F^w are the source and sink terms. The Darcy velocity v_L and v_G for each fluid phase are regulated by the general Darcy Law

$$v_L = -\frac{KK_{rL}}{\mu_L}(\nabla P_L - \rho_L \mathbf{g}) \quad (3)$$

$$v_G = -\frac{KK_{rG}}{\mu_G}(\nabla P_G - \rho_G \mathbf{g}). \quad (4)$$

Here, K is the intrinsic permeability, and \mathbf{g} refers to the vector for gravitational force. The terms j_L^w, j_L^h, j_G^w , and j_G^h represent the diffusive mass fluxes of each component in different phases, which are given by Fick's Law as

$$j_\alpha^{(i)} = -\Phi S_\alpha \rho_\alpha D_\alpha^{(i)} \nabla C_\alpha^{(i)}. \quad (5)$$

Here $D_\alpha^{(i)}$ is the diffusion coefficient, and $C_\alpha^{(i)}$ the mass fraction. When the non-isothermal condition is considered, a heat balance equation is added, with the assumption that gas and liquid phases have reached local thermal equilibrium and share the same temperature.

$$\begin{aligned} & \frac{\Phi \partial[(1 - S_G)\rho_L u_L + S_G \rho_G u_G]}{\partial t} + \frac{(1 - \Phi)\partial(\rho_S c_S T)}{\partial t} \\ & + \nabla[\rho_G h_G v_G] + \nabla[\rho_L h_L v_L] - \nabla(\lambda_T \nabla T) \\ & = Q_T + \Delta h_{vap} \left(\Phi \frac{\partial(\rho_L S_L)}{\partial t} - \nabla(\rho_L v_L) \right) \end{aligned} \quad (6)$$

In the above equation, the phase density ρ_G, ρ_L , the specific internal energy in different phase u_L, u_G and specific enthalpy in different phase h_L and h_G are all temperature and

pressure dependent. While ρ_S and c_S are the density and specific heat capacity of the soil grain, λ_T refers to the heat conductivity, and Q_T is source term, $\Delta h_{vap}(\Phi \frac{\partial(\rho_L S_L)}{\partial t} - \nabla(\rho_L v_L))$ represents the latent heat term according to (Gawin et al. 1995). Generally, the specific enthalpy in Eq. 6 can be described as follows

$$h_\alpha = c_{p\alpha} T. \quad (7)$$

Here $c_{p\alpha}$ is the specific heat capacity of phase α at given pressure. At the same time, relationship between internal energy and enthalpy can be described as

$$h_\alpha = u_\alpha + P_\alpha V_\alpha, \quad (8)$$

where P_α and V_α are the pressures and volumes of phase α . Since we consider the liquid phase is incompressible, its volume change can be ignored, i.e. $h = u$.

Non-isothermal persistent primary variable approach

Here in this work, we follow the idea of Marchand et al. (2013), where the 'Persistent Primary Variable' concept were adopted. A new choice of primary variables consists of:

- P [Pa] is the weighted mean pressure of gas and liquid phase, with each phase volume as the weighting factor. It depends mainly on the liquid saturation S .

$$P = \gamma(S)P_G + (1 - \gamma(S))P_L \quad (9)$$

Here $\gamma(S)$ stands for a monotonic function of saturation S , with $\gamma(S) \in [0, 1]$, $\gamma(0) = 0$, $\gamma(1) = 1$. In Benchmark I ('Benchmark I: isothermal injection of H₂ gas' section), we choose

$$\gamma(S) = 0$$

In Benchmark II ('Benchmark II: heat pipe problem' section), we choose

$$\gamma(S) = S^2$$

When one phase disappears, its volume converges to zero, making the P value equal to the pressure of the remaining phase. If we assume the local capillary equilibrium, the gas and liquid phase pressure can both be derived based on the capillary pressure P_c , that is also a function of saturation S .

$$P_L = P - \gamma(S)P_c(S) \quad (10)$$

$$P_G = P + (1 - \gamma(S))P_c(S) \quad (11)$$

- X [-] refers to the total molar fraction of the light component in both fluid phases. Similar to the mean pressure P , it is also a continuous function throughout the phase transition zones. We formulate it as

$$X = \frac{SN_G X_G^h + (1 - S)N_L X_L^h}{SN_G + (1 - S)N_L} \quad (12)$$

In a hydrogen-water system, X_L^h and X_G^h refer to the molar fraction of the hydrogen in the two phases, and N_L and N_G are the respective molar densities [mol m⁻³].

Based on the choice of new primary variables, the mass conservation Eqs. 1 and 2 can be transformed to the molar mass conservation. The governing equations of the two-phase two-component system are then written as

$$\frac{\Phi \partial((S N_G + (1 - S) N_L) X^{(i)})}{\partial t} + \nabla \cdot (N_L X_L^{(i)} v_L + N_G X_G^{(i)} v_G) + \nabla \cdot (N_L S_L W_L^{(i)} + N_G S_G W_G^{(i)}) = F^{(i)} \tag{13}$$

with $i \in (h, w)$ and the flow velocity v regulated by the generalized Darcy's law, referred to Eqs. 3 and 4.

The molar diffusive flux can be calculated following Fick's law

$$W_\alpha^i = -D_\alpha^{(i)} \Phi \nabla X_\alpha^{(i)}. \tag{14}$$

- T [K] refers to the Temperature. If we consider the temperature T as the third primary variable, the energy balance equation can then be included.

$$\frac{\Phi \partial \left[(1 - S_G) N_L \left(\sum X_L^{(i)} M^{(i)} \right) u_L + S_G N_G \left(\sum X_G^{(i)} M^{(i)} \right) u_G \right]}{\partial t} + \frac{(1 - \Phi) \partial(\rho_S c_S T)}{\partial t} - \nabla \cdot \left[N_G \left(\sum X_G^{(i)} M^{(i)} \right) h_G v_G \right] - \nabla \cdot \left[N_L \left(\sum X_L^{(i)} M^{(i)} \right) h_L v_L \right] - \nabla \cdot (\lambda_T \nabla T) = Q_T \tag{15}$$

The non-isothermal system can thus be simulated by the solution of combined Eqs. 13 and 15, with P , X , and T as primary variables. Once these three primary variables are determined, the other physical quantities are then constrained by them and can be obtained by the solution of EOS system. These secondary variables were listed in Table 1. Compared to the primary variable switching (Wu and Forsyth 2001) and the negative saturation (Abadpour and Panfilov 2009) approach, the choice of P and X as primary variables fully covers all three possible phase states, i.e., the single-phase gas, two-phase, and single-phase liquid regions. It also allows the appearance or disappearance of any of the two phases. Instead of switching the primary variable, the non-linearity of phase change behavior was removed from the global partial differential equations and was embedded into the solution of EOS.

Closure relationships

Mathematically, the solution for any linear system of equations is unique if and only if the rank of the equation system equals the number of unknowns. In this work, the combined mass conservation of Eqs. 1, 2, and the energy balance Eq. 6 must be determined by three primary variables. Other variables are dependent on them and considered to be secondary. Such nonlinear dependencies form the necessary closure relationships.

Table 1 List of secondary variables and their dependency on the primary variables

Parameters	Symbol	Unit
Gas phase saturation	$S(P, X)$	[-]
Molar density of phase α	$N_\alpha(P, X, T)$	[mol m ⁻³]
Molar fraction of component i in phase α	$X_\alpha^{(i)}(P, X, T)$	[-]
Capillary pressure	$P_c(S)$	[Pa]
Relative permeability of phase α	$K_{r\alpha}(S)$	[-]
Specific internal energy of phase α	$u_\alpha(P, X, T)$	[J mol ⁻¹]
Specific enthalpy of phase α	$h_\alpha(P, X, T)$	[J mol ⁻¹]
Heat conduction coefficient	$\lambda_{pm}(P, X, S, T)$	[W m ⁻¹ K ⁻¹]

Constitutive laws

Dalton's Law regulates that the total pressure of a gas phase is equal to the sum of partial pressures of its constitutive non-reacting chemical component. In our case, a gas phase with two components, i.e., water and hydrogen is considered. Then the gas phase pressure P_G writes as

$$P_G = P_G^h + P_G^w. \quad (16)$$

Ideal Gas Law In our model, the ideal gas law is assumed, where the response of gas phase pressure and volume to temperature is regulated as

$$P_G = \frac{nRT}{V}, \quad (17)$$

where R is the Universal Gas Constant ($8.314 \text{ J mol}^{-1}\text{K}^{-1}$), V is the volume of the gas and n stands for the mole number gas. Reorganizing the above equation gives the molar density of gas phase N_G

$$N_G = \frac{n}{V} = \frac{P_G}{RT}. \quad (18)$$

Combining Dalton's Law of Eq. 16, we have

$$N_G^h = \frac{P_G^h}{RT}, N_G^w = \frac{P_G^w}{RT}. \quad (19)$$

Furthermore, the molar fraction of component i can be obtained by normalizing its partial pressure with the total gas phase pressure,

$$X_G^i = \frac{P_G^i}{P_G}. \quad (20)$$

Incompressible Fluid Unlike the gas phase, the liquid phase in our model is considered to be incompressible, i.e., the density of the fluid is linearly dependent on the molar amount of the constitutive chemical component. By assuming standard water molar density $N_L^{std} = \frac{\rho_w^{std}}{M^w}$, with ρ_w^{std} refers to the standard water mass density (1000 kg m^{-3} in our model), the in-compressibility of the liquid phase writes as

$$N_L = \frac{N_L^{std}}{1 - X_L^h}. \quad (21)$$

Henry's Law We assume that the distribution of light component (hydrogen in our case) can be regulated by the Henry's coefficient $H_W^h(T)$, which is a temperature-dependent parameter.

$$P_G^h H_W^h(T) = N_L X_L^h \quad (22)$$

Raoult's Law For the heavy component (water), we apply Raoult's Law that the partial pressure of the water component in the gas phase changes linearly with its molar fraction in the liquid.

$$P_G^w = X_L^w P_{Gvapor}^w(T) \quad (23)$$

Here X_L^w is the molar fraction of the water component in the liquid phase. $P_{Gvapor}^w(T)$ is the vapor pressure of pure water, and it is a temperature-dependent function in non-isothermal scenarios.

EOS for isothermal systems Based on the constitutive laws discussed in the 'Constitutive laws' section, we have:

$$\frac{X_L^h N_L^{std}}{X_L^w H_W^h(T)} + X_L^w P_{Gvapor}^w(T) = P_G \quad (24)$$

$$P_G X_G^h = \frac{N_L^{std}}{H_W^h(T)} \frac{X_L^h}{X_L^w} \quad (25)$$

According to Eqs. 24 and 25, X_L^h and X_G^h can be calculated explicitly, under the condition:

$$G(T) = \frac{H_W^h(T) P_{Gvapor}^w(T)}{N_L^{std}} < \frac{1}{4} \quad (26)$$

which is obviously satisfied in water-air and water-hydrogen system, i.e., under the condition that the temperature T is 25 °C, with $H_W^h(T) = 7.8 \times 10^{-6} [\text{mol m}^{-3} \text{Pa}^{-1}]$, $P_{Gvapor}^w(T) = 3173.07 [\text{Pa}]$, then we could have $G(T) = 4.54 \times 10^{-7} \ll \frac{1}{4}$. Here, if we only consider isothermal condition, the temperature is assumed to be fixed with T_0 . In summary, X_L^h and X_G^h could be expressed as:

$$X_L^h = X_m(P_L, S, T_0) = \frac{N_L^{std} + (P_L + P_c)H_W^h(T_0)}{2H_W^h(T_0)P_{Gvapor}^w(T_0)} \quad (27)$$

$$+ \frac{\left(\sqrt{(N_L^{std} + (P_L + P_c)H_W^h(T_0))^2 - 4(P_L + P_c)H_W^h(T_0)N_L^{std}P_{Gvapor}^w(T_0)}\right)}{2H_W^h(T_0)P_{Gvapor}^w(T_0)}$$

$$X_G^h = X_M(P_G, S, T_0) = \frac{X_L^h N_L^{std}}{H_W^h(T_0)P_G(1 - X_L^h)} \quad (28)$$

Where S is the saturation of light component, and P_c represents the capillary pressure. The above equations are the most general way of calculating the distribution of molar fraction. In Benchmark I ('Benchmark I: isothermal injection of H₂ gas' section), we follow Marchand's idea (Marchand and Knabner 2014), by assuming there is no water vaporization and the gas phase contains only hydrogen, which indicate $P_G \equiv P_G^h$ and $X_G^h \equiv 1$. Therefore Eqs. 27 and 28 could be reformulated as:

$$X_L^h = X_m(P_L, S, T_0) = \frac{(P_L + P_c)H_W^h(T_0)}{(P_L + P_c)H_W^h(T_0) + N_L^{std}} \quad (29)$$

$$X_G^h \equiv 1 \quad (30)$$

Here, for simplification purpose, if we combined with Eqs. 10 and 11, X_L^h and X_G^h could be expressed as functions of mean pressure P and gas phase saturation S , and the above formulation can be transformed to

$$X_L^h = X_m(P_L(P, S(P, X)), S(P, X), T_0) = X_m(P, S, T_0) \quad (31)$$

$$X_G^h = X_M(P_G(P, S(P, X)), S(P, X), T_0) = X_M(P, S, T_0). \quad (32)$$

Assuming the local thermal equilibrium of the multi-phase system is reached, then the Equations of State (EOS) are formulated accordingly based on the three different phase states.

- In two phase region
Molar fraction of hydrogen (X_L^h and X_G^h) and molar density in each phase (N_G and N_L) are all secondary variables that are dependent on the change of pressure and saturation. They can be determined by solving the following non-linear system.

$$X_L^h = X_m(P, S, T_0) \quad (33)$$

$$X_G^h = X_M(P, S, T_0) \quad (34)$$

$$N_G = \frac{P_G(P, S)}{RT_0} \quad (35)$$

$$N_L = \frac{N_L^{std}}{1 - X_L^h} \quad (36)$$

$$\frac{SN_G(X - X_G^h) + (1 - S)N_L(X - X_L^h)}{SN_G + (1 - S)N_L} = 0 \quad (37)$$

- In the single liquid phase region
In a single liquid phase scenario, the gas phase does not exist, i.e., the gas phase saturation S always equals to zero. Meanwhile, the molar fraction of light component in the gas phase X_G^h can be any value, as it will be multiplied with the zero saturation (see Eqs. 13 to 14) and vanish in the governing equation. This also applies to the gas phase molar density N_G , whereas the two parameters can be arbitrarily given, and have no physical impact. So to determine the EOS, we only need to solve for the liquid phase molar fraction and density.

$$X_L^h = X \quad (38)$$

$$N_L = \frac{N_L^{std}}{1 - X} \quad (39)$$

- In the single gas phase region
Similarly, in a single gas phase scenario, the liquid phase does not exist, i.e., the gas phase saturation S always equals to 1, whereas the liquid phase saturation remains zero. Meanwhile, the molar fraction of light component in the liquid phase X_L^h can be any value, as it will be multiplied with the zero liquid phase saturation (see Eqs. 13 to 14) and vanish in the governing equation. This also applies to the liquid phase molar density N_G , whereas the two parameters can be arbitrarily given, and have no physical meaning. So to determine the EOS, we only need to solve for the gas phase molar fraction and density.

$$X_G^h = X$$

$$N_G = \frac{P}{RT_0}$$

EOS for non-isothermal systems

As the energy balance of Eq. 6 has to be taken into account under the non-isothermal condition, all the secondary variables not only are dependent on the pressure P but also rely on the temperature T . Except for the parameters mentioned above, several other physical properties are also regulated by the T/P dependency. Furthermore, in

a non-isothermal transport, high non-linearity of the model exists in the complex variational relationships between secondary variables and primary variables. Therefore, how to set up an EOS system for each fluid is a big challenge for the non-isothermal multi-phase modeling. In the literature, (Class et al. 2002; Olivella and Gens 2000; Peng and Robinson 1976; Singh et al. 2013a, and Singh et al. 2013b) have given detailed procedures of solving EOS to predicting the gas and liquid thermodynamic and their transport properties. Here in our model, we follow the idea by Kolditz and De Jonge (2004). Detailed procedure regarding how to calculate the EOS system is discussed in the following.

Vapor pressure As we discussed in the ‘Constitutive laws’ section, vapor pressure is a key parameter for determining the molar fractions of different components in each phase. The equilibrium restriction on vapor pressure of pure water is given by Clausius-Clapeyron equation (Çengel and Boles 1994).

$$P_{Gvapor}^w(T) = P_0 \exp \left[\left(\frac{1}{T_0} - \frac{1}{T} \right) \frac{h_G^w M^w}{R} \right] \quad (40)$$

where h_G^w is enthalpy of vaporization, M^w is molar mass of water. P_0 represents the vapor pressure of pure water at the specific Temperature T_0 . In our model, we choose $T_0 = 373\text{K}$, $P_0 = 101,325\text{Pa}$. An alternative method is using the Antoine equation, written as

$$\log_{10}(P_{Gvapor}^w(T)) = A - \frac{B}{C + T} \quad (41)$$

with A, B, and C as the empirical parameters. Details regarding this formulation can be found in Class et al. (2002).

Specific enthalpy Specific enthalpy h_α [J mol^{-1}] is the enthalpy per unit mass. According to Eq. 6, we need to know the specific enthalpy of a certain phase. In particular, since component-based mass balance is considered, we calculate the phase enthalpy as the sum of mole (mass) specific enthalpy of each component in this phase. Here we assume that the energy of mixing is ignored. For instance, the water-air system applied in the second benchmark is formulated as

$$h_G = h_G^{air} X_G^{air} + h_G^{wvap} X_G^{wvap} \quad (42)$$

$$h_L = h_L^{air} X_L^{air} + h_L^{wliq} X_L^{wliq} \quad (43)$$

Here h_G^{air} is the specific enthalpy of air in gas phase, h_G^{wvap} is specific enthalpy of vapor water in gas phase, h_L^{air} represents the specific enthalpy of the air dissolved in the liquid phase, while h_L^{wliq} donates the specific enthalpy of the liquid water in liquid phase. While X_G^{air} , X_G^{wvap} , X_L^{air} and X_L^{wliq} represent molar fraction [-] of each component (air and water) in the corresponding phase (gas and liquid).

Henry coefficient We assume Henry’s Law is valid under the non-isothermal condition. Therefore Henry coefficient is a secondary variable. In the water-air system, it can be defined as (Kolditz and De Jonge 2004)

$$H_W^h(T) = (0.8942 + 1.47 \exp(-0.04394T)) \times 10^{-10} \quad (44)$$

with T the temperature value in $^\circ\text{C}$.

Heat conductivity Since the local thermal equilibrium is assumed, the heat conductivity λ_{pm} [$\text{W m}^{-1} \text{K}^{-1}$] of the fluid-containing porous media is averaged from the heat conductivities of the fluid phases and the solid matrix. Thus, it is a function of saturation only.

$$\lambda_{pm} = \lambda_{pm}^{S_L=S_G=0} + \sqrt{S_L}(\lambda_{pm}^{S_L=1} - \lambda_{pm}^{S_L=0}) + \sqrt{S_G}(\lambda_{pm}^{S_G=1} - \lambda_{pm}^{S_G=0}) \quad (45)$$

Fugacity When the thermal equilibrium is reached, the chemical potentials of component i in gas and liquid phase equal with each other. This equilibrium relationship can be formulated as the equation of chemical potential ν

$$\nu_G^{(i)}(P_G, X_L^{(i)}, X_G^{(i)}, T) = \nu_L^{(i)}(P_L, X_L^{(i)}, X_G^{(i)}, T)$$

In our model, the fugacity was applied instead of chemical potential. The above relationship is then transformed to the equivalence of component fugacities, where

$$f_G^{(i)} = f_L^{(i)}$$

holds for each component i in each phase. In order to compute the fugacity of a component in a particular phase, the following formulation is used

$$f_\alpha^{(i)} = P_\alpha X_\alpha^{(i)} \phi_\alpha^{(i)} \quad (46)$$

where $\phi_\alpha^{(i)}$ is the respective fugacity coefficient of component.

Numerical scheme

Numerical solution of EOS

Physical constraints of EOS

Since the pore space should be fully occupied by either or both the gas and liquid phases, the sum of phase saturation should equal to one. By definition, the saturation for each phase should be no less than zero and no larger than one. This constraint is summarized as

$$\sum_\alpha S_\alpha = 1 \wedge S_\alpha > 0 \quad (\alpha \in G, L) \quad (47)$$

Similarly, the sum of the molar fraction for all components in a single phase should also be in unity, and this second constraint can be formulated as

$$\sum_i X_G^{(i)} = 1 \wedge \sum_i X_L^{(i)} = 1 \quad \text{with } X_G^{(i)} > 0 \wedge X_L^{(i)} > 0 \quad (i \in h, w) \quad (48)$$

Combining these constraints, we have

$$S = 0 \wedge X_L^h \leq X_m(P, 0, T) \quad (49)$$

$$0 \leq S \leq 1 \wedge X_m(P, S, T) - X_L^h = 0, X_G^h - X_m(P, S, T) = 0 \quad (50)$$

$$S = 1 \wedge X_G^h \geq X_m(P, 1, T) \quad (51)$$

For the Eqs. 49 to 51, they contain both equality and inequality relationships, which impose challenges for the numerical solution. In order to solve it numerically, we introduce a minimum function (Kanzow 2004; Kräutle 2011), to transform the inequalities. It is defined as

$$\Psi(a, b) := \min\{a, b\} \quad (52)$$

Combined with Eqs. 49 to 51, they can be transformed to

$$\Psi(S, X_m(P, S, T) - X_L^h) = 0 \quad (53)$$

$$\Psi(1 - S, X_G^h - X_M(P, S, T)) = 0 \tag{54}$$

$$\frac{SN_G(X - X_G^h) + (1 - S)N_L(X - X_L^h)}{SN_G + (1 - S)N_L} = 0 \tag{55}$$

Then Eqs. 53 to 55 formulates the EOS system, which needs to be solved on each mesh node of the model domain.

Numerical scheme of solving EOS

For the EOS, the primary variables P and X are input parameters and act as the external constraint. The saturation S , gas and liquid phase molar fraction of the light component X_G^h and X_L^h are then the unknowns to be solved. Once they have been determined, other secondary variables can be derived from them. When saturation is less than zero or bigger than one, the second argument of the minimization function in Eq. 53 will be chosen. Then it effectively prevents the saturation value from moving into unphysical value. This transformation will result in a local Jacobian matrix that might be singular. Therefore, a pivoting action has to be performed before the Jacobian matrix is decomposed to calculating the Newton step. An alternative approach to handle this singularity is to treat the EOS system as a nonlinear optimization problem with the inequality constraints. Our tests showed that the optimization algorithms such as Trust-Region method are very robust in solving such a local problem, but the calculation time will be considerably longer, compared to the Newton-based iteration method.

Numerical solution of the global equation system

In this work, we solve the global governing equation Eqs. 13 to 15 with all the closure relationships simultaneously satisfied. To handle the non-linearities, a nested Newton scheme was implemented (see the flow chart in Fig. 1). All the derivatives in the EOS system Eqs. 53 to 55 are computed exactly and the local Jacobian matrix is constructed in an analytical way, while the global Jacobian matrix is numerically evaluated based on the finite difference method. For the global equations, the time was discretized with the backward Euler scheme, and the spatial discretization was performed with the Galerkin Finite Element method. In each global Newton iteration, the updated global variables P , X , and T from the previous iteration were passed to the EOS system, and acted as constraints to solve for secondary variables. The solution of Eqs. 53 to 55 was performed one after the other on each mesh node of the model domain.

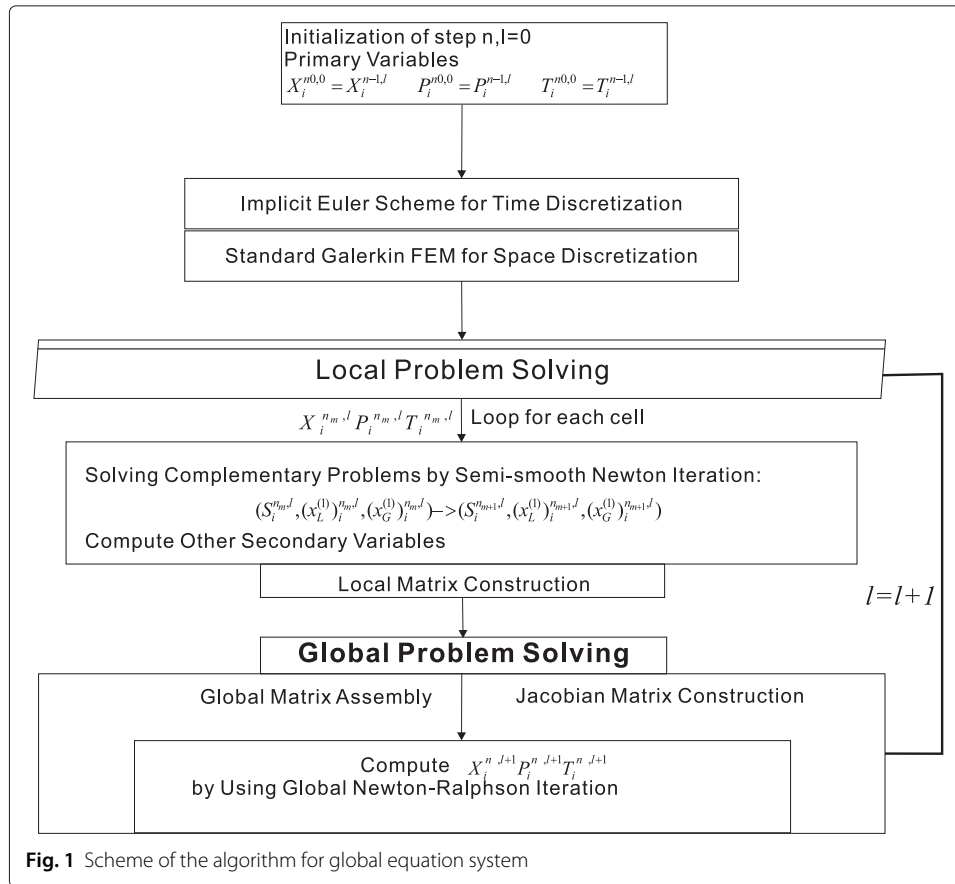
For Newton iterations, the following convergence criteria was applied.

$$\|Residual(Step(k))\|_2 \leq \epsilon \tag{56}$$

where $\|\cdot\|_2$ denotes the Euclidean norm. A tolerance value $\epsilon = 1 \times 10^{-14}$ were adopted for the EOS and 1×10^{-9} for the global Newton iterations.

Handling unphysical values during the global iteration

In the ‘Numerical scheme of solving EOS’ section, we have discussed the procedure of handling physical constraint of the EOS system. However, during the global iterations, if the initial value of X is small enough, it may happen that $X \leq 0$ can appear. Since the negative value of X would cause failures of further iteration, it is necessary to force the non-negativity constraint on X . To achieve this, a widely used method is extending the



definition of the physical variables such as N_G, N_L for $X < 0$, as was done in (Marchand et al. 2013), (Marchand and Knabner (2014), and (Abadpour and Panfilov 2009). In our implementation, we chose an alternative and more straightforward method, which is adding a damping factor in each global Newton iteration when updating the unknown vector. The damping factor δ are chosen as follows,

$$\frac{1}{\delta} = \max\left\{1, 2 * \frac{\Delta P(j)}{P(j)}, 2 * \frac{\Delta X(j)}{X(j)}, 2 * \frac{\Delta T(j)}{T(j)}\right\} \tag{57}$$

where $P(j), X(j)$ and $T(j)$ denote pressure/molar fraction/temperature at node j .

Results and Discussions

In our work, the model verification was carried out in two separate cases, one under isothermal and the other under non-isothermal conditions. In the first case, a simple benchmark case was proposed by GNR MoMaS (Bourgeat et al. 2009). We simulated the same H_2 injection process with the extended OpenGeoSys code (Kolditz et al. 2012), and compared our results against those from other code (Marchand and Knabner 2014). For the non-isothermal case, there exists no analytical solution, which explicitly involves the phase transition phenomenon. Therefore, we compared our simulation result of the classical heat pipe problem to the semi-analytical solution from Udell and Fitch (1985). This semi-analytical solution was developed for the steady state condition without the consideration of phase change phenomena. Despite of this discrepancy, the OpenGeoSys code delivered very close profile as by the analytical approach.

Benchmark I: isothermal injection of H₂ gas

The background of this benchmark is the production of hydrogen gas due to the corrosion of the metallic container in the nuclear waste repository. Numerical model is built to illustrate such gas appearance phenomenon. The model domain is a two-dimensional horizontal column representing the bentonite backfill in the repository tunnel, with hydrogen gas injected on the left boundary. This benchmark was proposed in the GNR MoMaS project by French National Radioactive Waste Management Agency. Several research groups has made contributions to test the benchmark and provided their reference solutions (Ben Gharbia and Jaffré 2014; Bourgeat et al. 2009; Marchand and Knabner 2014; Neumann et al. 2013). Here we adopted the results proposed in Marchand’s paper Marchand and Knabner 2014 for comparison.

Physical scenario

Here a 2D rectangular domain $\Omega = [0, 200] \times [-10, 10]$ m (see Fig. 2) was considered with an impervious boundary at $\Gamma_{imp} = [0, 200] \times [-10, 10]$ m, an inflow boundary at $\Gamma_{in} = \{0\} \times [-10, 10]$ m, and an outflow boundary at $\Gamma_{out} = \{200\} \times [-10, 10]$ m. The domain was initially saturated with water, hydrogen gas was injected on the left-hand-side boundary within a certain time span ($[0, 5 \times 10^4 \text{century}]$). After that the hydrogen injection stopped and no flux came into the system. The right-hand-side boundary is kept open throughout the simulation. The initial condition and boundary conditions were summarized as

- $X(t = 0) = 10^{-5}$ and $P_L(t = 0) = P_L^{out} = 10^6$ [Pa] on Ω .
- $q^w \cdot v = q^h \cdot v = 0$ on Γ_{imp} .
- $q^w \cdot v = 0, q^h \cdot v = Q_d^h = 0.2785$ [mol century⁻¹m⁻²] on Γ_{in} .
- $X = 0$ and $P_L = P_L^{out} = 10^6$ [Pa] on Γ_{out} .

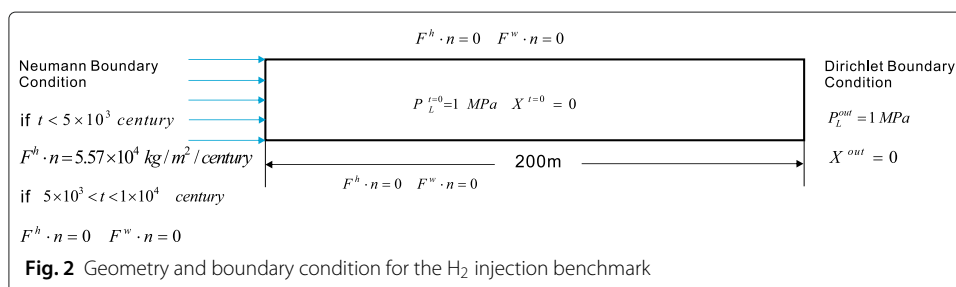
Model parameters and numerical settings

The capillary pressure P_c and relative permeability functions are given by the van-Genuchten model (Van Genuchten 1980).

$$P_c = P_r \left(S_{le}^{-\frac{1}{m}} - 1 \right)^{\frac{1}{n}}$$

$$K_{rL} = \sqrt{S_{le}} \left(1 - \left(1 - S_{le}^{\frac{1}{m}} \right)^m \right)^2$$

$$K_{rG} = \sqrt{1 - S_{le}} \left(1 - S_{le}^{\frac{1}{m}} \right)^{2m}$$



where $m = 1 - \frac{1}{n}$, P_r and n are van-Genuchten model parameters and the effective saturation S_{le} is given by

$$S_{le} = \frac{1 - S_g - S_{lr}}{1 - S_{lr} - S_{gr}} \quad (58)$$

here S_{lr} and S_{gr} indicate the residual saturation in liquid and gas phases, respectively. Values of parameters applied in this model are summarized in Table 2.

We created a 2D triangular mesh here with 963 nodes and 1758 elements. The mesh element size varies between 1m and 5m. A fixed time step size of 1 century is applied. The entire simulated time from 0 to 10^4 centuries were simulated. The entire execution time is around 3.241×10^4 s.

Results and analysis

The results of this benchmark are depicted in Fig. 3. The evolution of gas phase saturation and the gas/liquid phase pressure at the inflow boundary Γ_{in} over the entire time span are shown. In addition, we compare results from our model against those given in Marchand's paper (Marchand and Knabner 2014). In Fig. 3, solid lines are our simulation results while the symbols are the results from Marchand et al. It can be seen that a good agreement has been achieved. Furthermore, the evolution profile of the gas phase saturation S_g , the liquid phase pressure P_L , and the total molar fraction of hydrogen X are plotted at different time ($t = 150, 1 \times 10^3, 5 \times 10^3, 6 \times 10^3$ centuries) in Fig. 4a–c, respectively.

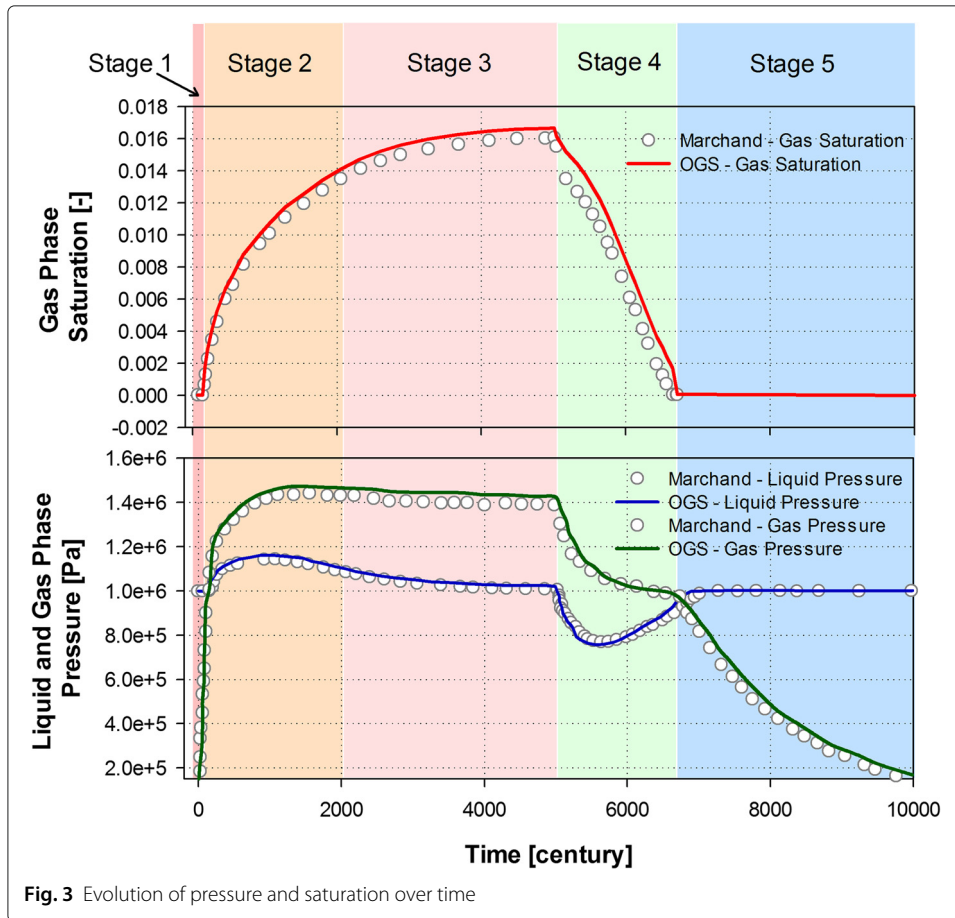
By observing the simulated saturation and pressure profile, the complete physical process of H_2 injection can be categorized into five subsequent stages.

1) The dissolution stage: After the injection of hydrogen at the inflow boundary, the gas first dissolved in the water. This was reflected by the increasing concentration of hydrogen in Fig. 4c. Meanwhile, the phase pressure did not vary much and was kept almost constant (see Fig. 4b).

2) Capillary stage: Given a constant temperature, the maximal soluble amount of H_2 in the water liquid is a function of pressure. In this MoMaS benchmark case, our simulation showed that this threshold value was about 1×10^{-3} mol H_2 per mol of water at a pressure of 1×10^6 [Pa]. Once this pressure was reached, the gas will emerge and formed a continuous phase. As shown in Fig. 4a, at approximately 150 centuries, the first phase transition happens. Beyond this point, the gas and liquid phase pressure quickly increase, while hydrogen gas is transported towards the right boundary driven by the pressure and concentration gradient. In the meantime, the location of this phase transition point also slowly shifted towards the middle of the domain.

Table 2 Fluid and porous medium properties applied in the H_2 migration benchmark

Parameters	Symbol	Value	Unit
Intrinsic permeability	K	5×10^{-20}	[m ²]
Porosity	Φ	0.15	[-]
Residual saturation of liquid phase	S_{lr}	0.4	[-]
Residual saturation of gas phase	S_{gr}	0	[-]
Viscosity of liquid	μ_l	10^{-3}	[Pa · s]
Viscosity of gas	μ_g	9×10^{-6}	[Pa · s]
van Genuchten parameter	P_r	2×10^6	[Pa]
van Genuchten parameter	n	1.49	[-]



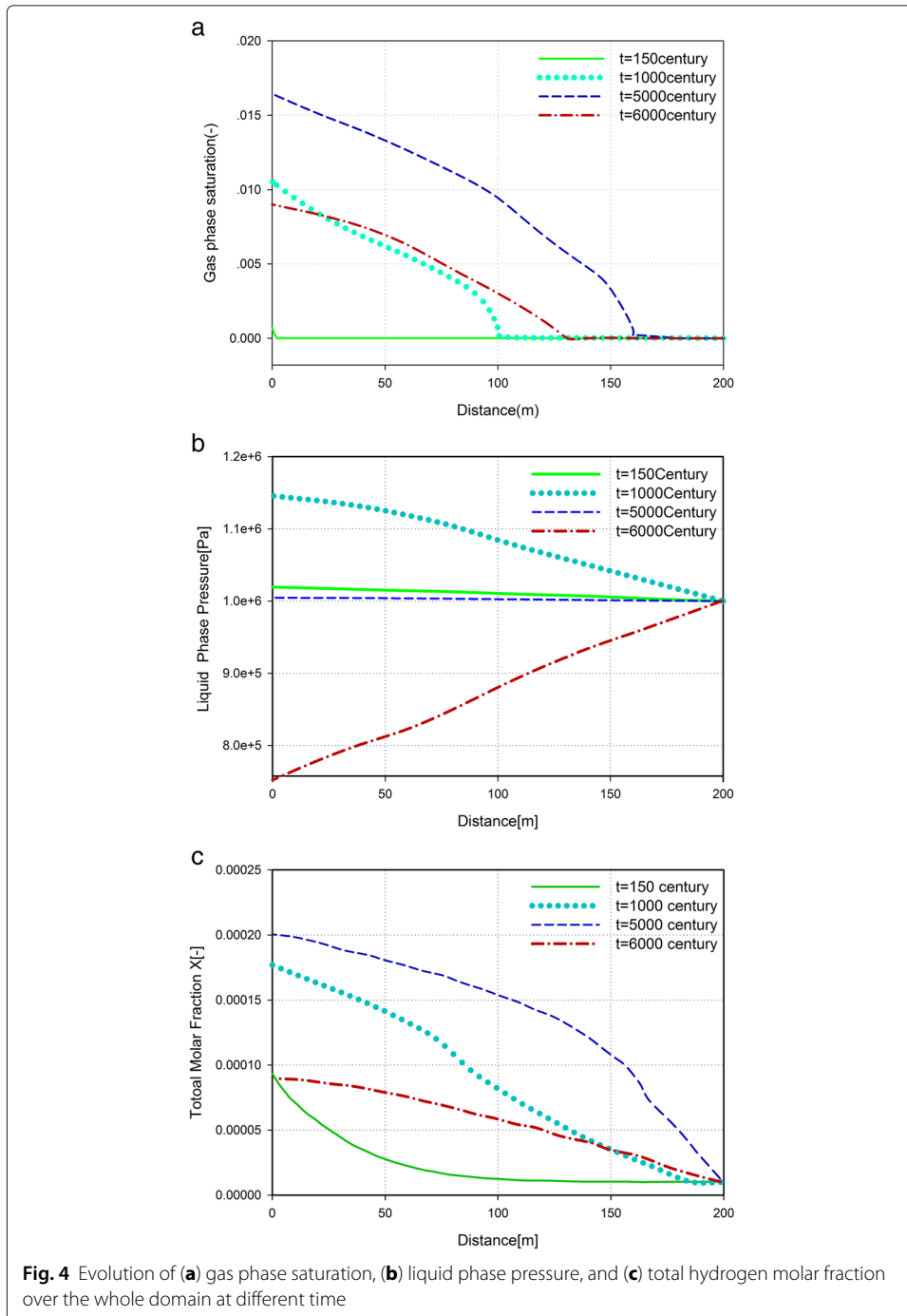
3) Gas migration stage: The hydrogen injection process continued until the 5000th century. Although the gas saturation continues to increase, pressures in both phases begin to decline due to the existence of the liquid phase gradient. Eventually, the whole system will reach steady state with no liquid phase gradient.

4) Recovery stage: After hydrogen injection was stopped at the 5000th century, the water came back from the outflow boundary towards the left, which was driven by the capillary effect to occupy the space left by the disappearing gas phase. During this stage, the gas phase saturation begins to decline, and both phase pressures drop even below the initial pressure. The whole process will not stop until the gas phase completely disappeared.

5) Equilibrium stage: After the complete disappearance of the gas phase, the saturation comes to zero again, and the whole system will reach steady state, with pressure and saturation values same as the ones given in the initial condition.

Benchmark II: heat pipe problem

To verify our model under the non-isothermal condition, we adopted the heat pipe problem proposed by Udell and Fitch (1985). They have provided a semi-analytical solution for a non-isothermal water-gas system in porous media, where heat convection, heat conduction as well as capillary forces were considered. A heater installed on the right-hand-side of the domain generated constant flux of heat, and it was then transferred through the



porous media by conduction, as well as the enthalpy transport of the fluids. The semi-analytical solution was developed for the steady state condition, and the liquid phase flowed in the opposite direction to the gas phase. If gravity was neglected, the system can be simplified to a system of six ordinary differential equations (ODE), the solution of which was then be obtained in the form of semi-analytical solution. Detailed derivation procedure is available in (Helmig 1997), and the parameters used in our comparison

are listed in Table 3. Interested readers may also refer to the supplementary material regarding how this solution was deducted (see Additional file 1-6).

Physical scenario

As shown in Fig. 5, the heat pipe was represented by a 2D horizontal column (2.25 m in length and 0.2 m in diameter) of porous media, which was partially saturated with a liquid phase saturation value of 0.7 at the beginning. A constant heat flux ($Q_T = 100 [W m^{-2}]$) was imposed on the right-hand-side boundary Γ_{in} , representing the continuously operating heating element. At the left-hand-side boundary Γ_{out} , Dirichlet boundary conditions were imposed for Temperature $T = 70 \text{ }^\circ\text{C}$, liquid phase pressure $P_G = 1 \times 10^5 [Pa]$, effective liquid phase saturation $S_{le} = 1$, and air molar fraction in the gas phase $X_G^a = 0.71$. Detailed initial and boundary condition are summarized as follows.

- $P(t = 0) = 1 \times 10^5 [Pa]$, $S_L(t = 0) = 0.7$, $T(t = 0) = 70 [^\circ C]$ on the entire domain.
- $q^w \cdot \nu = q^h \cdot \nu = 0$ on Γ_{imp} .
- $q^w \cdot \nu = q^h \cdot \nu = 0$, $q^T \cdot \nu = Q_T$ on Γ_{in} .
- $P = 1 \times 10^5 [Pa]$, $S_L = 0.7$, $T = 70 [^\circ C]$ on Γ_{out} .

Model parameters and numerical settings

For the capillary pressure–saturation relationship, van Genuchten model was applied. The parameters used in the van Genuchten model are listed in Table 3. The water–air relative permeability relationships were described by the Fatt and Klikoffv formulations (Fatt and Klikoff Jr 1959).

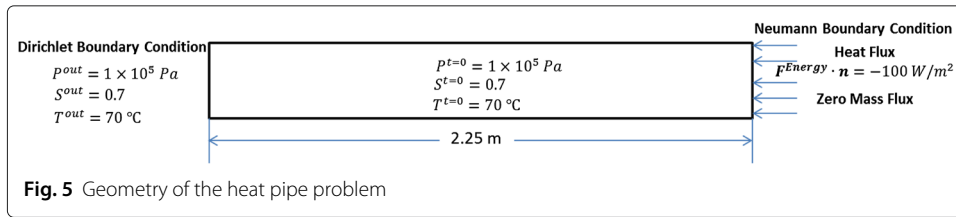
$$K_{rG} = (1 - S_{le})^3 \tag{59}$$

$$K_{rL} = S_{le}^3 \tag{60}$$

where S_{le} is the effective liquid phase saturation, referred to Eq. 58.

Table 3 Parameters applied in the heat pipe problem

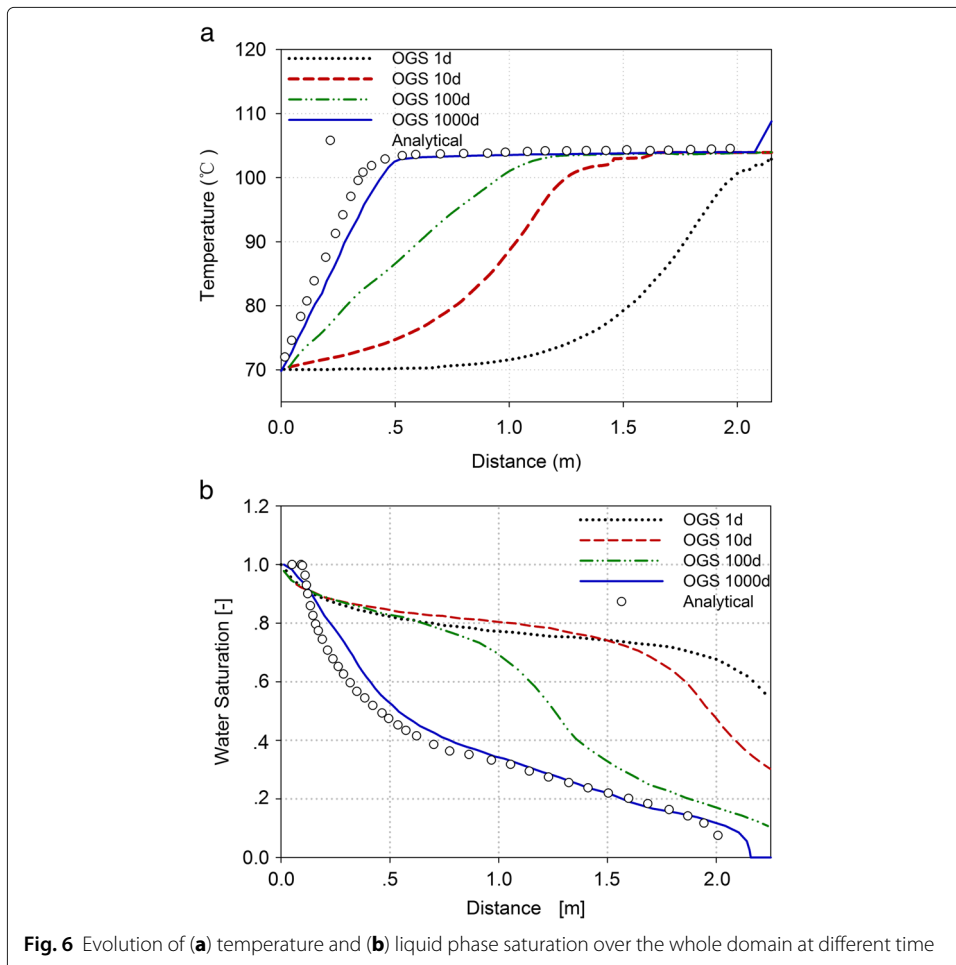
Parameters name	Symbol	Value	Unit
Permeability	K	10^{-12}	$[m^2]$
Porosity	Φ	0.4	[-]
Residual liquid phase saturation	S_{lr}	0.4	[-]
Heat conductivity of fully saturated porous medium	$\lambda_{pm}^{S_w=1}$	1.13	$[W m^{-1} K^{-1}]$
Heat conductivity of dry porous medium	$\lambda_{pm}^{S_w=0}$	0.582	$[W m^{-1} K^{-1}]$
Heat capacity of the soil grains	c_s	700	$[J kg^{-1} K^{-1}]$
Density of the soil grain	ρ_s	2600	$[kg m^{-3}]$
Density of the water	ρ_w	1000	$[kg m^{-3}]$
Density of the air	ρ	0.08	$[kg m^{-3}]$
Dynamic viscosity of water	μ_w	2.938×10^{-4}	$[Pa \cdot s]$
Dynamic viscosity of air	μ_g^a	2.08×10^{-5}	$[Pa \cdot s]$
Dynamic viscosity of steam	μ_g^w	1.20×10^{-5}	$[Pa \cdot s]$
Diffusion coefficient of air	D_g^a	2.6×10^{-5}	$[m^2 s^{-1}]$
van Genuchten parameter	P_r	1×10^4	$[Pa]$
van Genuchten parameter	n	5	[-]



We created a 2D triangular mesh here with 206 nodes and 326 elements. The averaged mesh element size is around 6m. A fixed size time stepping scheme has been adopted, with a constant time step size of 0.01 day. The entire simulated time from 0 to 10^4 day were simulated.

Results

The results of our simulation were plotted along the central horizontal profile over the model domain at $y = 0.1$ m, and compared against semi-analytical solution. Temperature and saturation profiles at day 1, 10, 100, 1000 are depicted in Fig. 6a, b respectively. As the heat flux was imposed on the right-hand-side boundary, the temperature kept rising there. After 1 day, the boundary temperature already exceeded $100 \text{ }^\circ\text{C}$, and the water in the soil started to boil. Together with the appearance of steam, water saturation



on the right-hand-side began to decrease. After 10 days, the boiling point has almost moved to the middle of the column. Meanwhile, the steam front kept boiling and shifted to the left-hand-side, whereas liquid water was drawn back to the right. After about 1000 days, the system reached a quasi-steady state, where the single phase gas, two phase and single phase liquid regions co-exist and can be distinguished. A pure gas phase region can be observed on the right and liquid phase region dominates the left side.

Discussion

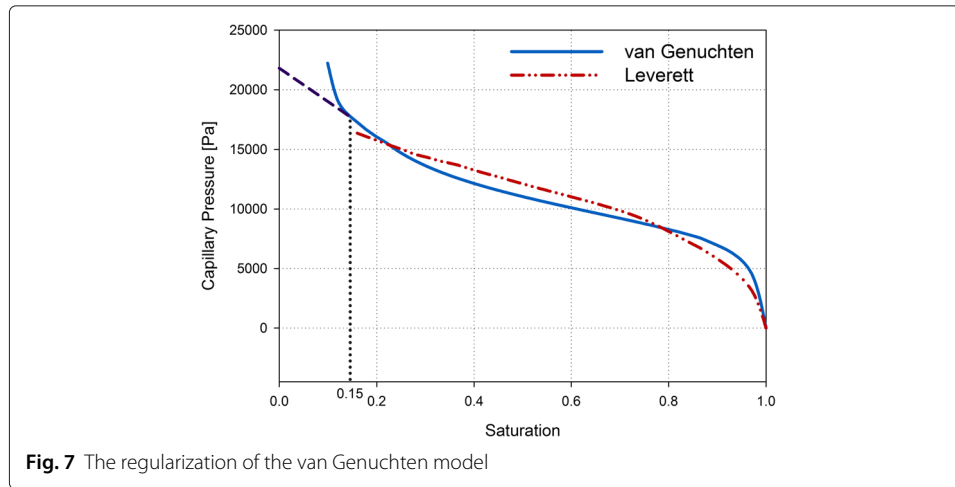
Analysis of the differences in benchmark II

From Fig. 6a, b, some differences can still be observed in comparison to the semi-analytical solution. Our hypothesis is this difference originates from the capillary pressure–saturation relationship adopted in our numerical implementation. In the original formulation of Udell and Fitch (1985), the Leverett model was applied to produce the semi-analytical solution. It is assumed that the liquid and gas are immiscible and thus there is no gas component dissolved in the liquid phase, and vice versa. In our work, we cannot precisely follow the same assumption, since the dissolution of chemical component in both phases is a requirement for the calculation of phase equilibrium. When considering phase change, we need to allow the saturation S to drop below the residual saturation, so that the evaporation as well as the condensation process can occur. In the traditional van Genuchten model, infinite value of capillary pressure may occur in the lower residual saturation region. Therefore we have made regularization that allows water saturation to fall below the residual saturation, as demonstrated in Fig. 7. Every time the capillary pressure needs to be evaluated, an if-else judgment is performed.

$$\begin{array}{l}
 \text{if } S_{lr} < S < 1 \text{ then} \\
 \quad \bar{P}_c(S) = P_c(S) \\
 \text{end}
 \end{array} \tag{61}$$

$$\begin{array}{l}
 \text{else} \\
 \quad \text{if } 0 < S < S_{lr} \text{ then} \\
 \quad \quad \bar{P}_c(S) = P_c(S_{lr}) - P'_c(S_{lr})(S - S_{lr}) \\
 \quad \text{end} \\
 \text{end}
 \end{array} \tag{62}$$

Here $\bar{P}_c(S)$ indicates the modified van Genuchten model, and $P'_c(S_{lr})$ represents the slope of P_c - S curve at the point of residual water phase saturation. The above modified van Genuchten model approximates the same behavior as the original Leverett one in majority part of the saturation region (see Fig. 7), yet still allowing the phase change behavior. However, it is not exactly same as the one in the semi-analytical solution. This is considered to be the reason why the quasi steady-state profile by our numerical model (Fig. 6) deviates from the analytical one.



Continuity of the global system and convergence of the iteration

In this work, we have only considered the homogeneous medium, where the primary variables of P and X are always continuous over the entire domain. For some primary variables, their derivatives in the governing Eqs. (13)–(15) are discontinuous at locations where the phase transition happens, i.e., $X = X_m(P, S = 0, T)$ and $X = X_M(P, S = 1, T)$. For instance, $\frac{\partial S}{\partial X}$ and $\frac{\partial S}{\partial P}$ might produce singularities at $S = 0$ and $S = 1$, and they can cause trouble on the conditioning of the global Jacobian matrix. In our simulation, a damped Newton iterations with line search has been adopted (see the ‘Handling unphysical values during the global iteration’ section). We observed that such derivative terms will result in an increased number of global Newton iterations, and the linear iteration number to solve the Newton step as well. It does not alter the convergence of the Newton scheme, as long as the function is Lipschitz continuous.

We are aware of the fact that this issue may be more difficult to handle for the heterogeneous media, where the primary variable P and X could not be directly applied any more because of the non-continuity over the heterogeneous interface (Park et al. 2011). In that case, choosing the primary variables which are continuous over any interface of the medium is a better option. Based on the analysis by Ern and Mozolevski (2012), if we assume Henry’s law is valid, concentration, or in another word, the molar or mass fraction of the hydrogen in the liquid phase ρ_L^h (X_L^h), gas/liquid phase pressure P_G/P_L , as well as the capillary pressure are all continuous over the interface. Therefore, they are the potential choices of primary variable which can be applied in the heterogeneous media (see (Angelini et al. 2011); (Neumann et al. 2013), and (Bourgeat et al. 2013)). We are currently investigating these options and will report on the results in subsequent work.

Conclusions

In this work, based on the persistent primary variable algorithm proposed by Marchand et al. (2013), we extended the isothermal multi-phase flow formulation to the non-isothermal condition. The extended governing equation is based on the mass balance of each chemical component and is nonlinearly coupled with the non-isothermal EOS. The numerical scheme has been implemented into the open source code OpenGeoSys. The verification of our model were carried out in two benchmark cases.

- For the GNR MoMaS (Bourgeat et al. 2009) benchmark ('Benchmark I: isothermal injection of H₂ gas' section), the extended model is capable of simulating the migration of H₂ gas including its dissolution in aqueous phase. The simulated results fitted well with those from other codes (Marchand et al. 2013; Marchand and Knabner 2014).
- For the non-isothermal benchmark, we simulated the heat pipe problem and verified our result against the semi-analytical solution ('Benchmark II: heat pipe problem' section). Furthermore, our numerical model extended the original heat pipe problem to include the phase change behavior.

Currently, we are working on the incorporation of equilibrium reactions, such as the mineral dissolution and precipitation, into the EOS system. As our global mass-balance equations are already component based, one governing equation can be written for each basis component. Pressure, temperature, and molar fraction of the chemical components can be chosen as primary variables. Inside the EOS problem, the amount of secondary chemical components can be calculated based on the result of basis, which can further lead to the phase properties as density and viscosity. The full extension of including temperature-dependent reactive transport system will be the topic of a separate work in the near future.

Nomenclature

Greek symbols

ϵ	Tolerance value for Newton iteration.	[-]
λ_T	Heat Conductivity.	[W m ⁻¹ K ⁻¹]
μ_α	Viscosity in α phase.	[Pa · s]
v_α^i	Chemical potential of i-component in α phase.	[Pa]
Φ	Porosity.	[-]
ϕ_α^i	fugacity coefficient of i-component in α phase.	[-]
ρ_α^i	Mass density of i-component in α phase.	[Kg m ⁻³]

Operators

\wedge	Logical "and"
$\ \cdot \ _2$	Euclidean norm
$\Psi(a, b)$	Minimum function

Roman symbols

\mathbf{g}	Vector for gravitational force.	[m s ⁻²]
$c_{p\alpha}$	Specific heat capacity in phase α at given pressure.	[J Kg ⁻¹ K ⁻¹]
c_S	Specific heat capacity of soil grain.	[J Kg ⁻¹ K ⁻¹]
D_α^i	Diffusion coefficient of i-component in phase α .	[m ² s ⁻¹]
F^i	Mass source/sink term for i-component.	[Kg m ⁻³ s ⁻¹]
f_α^i	Fugacity of i-component in α phase.	[Pa]
H_W^h	Henry coefficient.	[mol Pa ⁻¹ m ⁻³]
h_α	Specific enthalpy.	[J Kg ⁻¹]
j_α^i	Diffusive mass flux of i-component in α phase.	[mol m ⁻² s ⁻¹]
K	Intrinsic Permeability.	[m ²]
N_α	Molar density in α phase.	[mol m ⁻³]
P_α	Pressure in α phase.	[Pa]
P_{Gvapor}^w	Vapor pressure of pure water.	[Pa]
P_c	Capillary pressure.	[Pa]
Q_T	Heat source/sink term.	[W s ⁻²]

R	Universal Gas Constant.	$[J\ mol^{-1}\ K^{-1}]$
$S_{\alpha r}$	Residual saturation in α phase.	[-]
S_{α}	Saturation in α phase.	[-]
S_{le}	Effective saturation.	[-]
T	Temperature.	[K]
u_{α}	Specific internal energy.	$[J\ Kg^{-1}]$
V_{α}	Volume in α phase.	$[m^3]$
v_{α}	Darcy velocity in α phase.	$[m\ s^{-1}]$
X	Total molar fraction of light component in two phases.	[-]
X_{α}^i	Molar Fraction of i-component in α phase.	[-]

Additional files

- Additional file 1:** This document introduces how this analytical solution is deduced.
- Additional file 2:** This is the main matlab script file, which will be executed to produce the analytical solution.
- Additional file 3:** This file constructs the four coupled differential equations.
- Additional file 4:** This file calculates the relative permeability of gas phase.
- Additional file 5:** This file calculates the relative permeability of liquid phase.
- Additional file 6:** This file calculates the capillary pressure, with water saturation as the input parameter.

Competing interests

The authors declare that they have no competing interests.

Authors' contributions

YH implemented the extended method into the OpenGeoSys software, produced simulation results of the two benchmarks, and also drafted this manuscript. HS designed the numerical algorithm of solving the coupled PDEs, and also contributed to the code implementation. OK coordinated the development of OpenGeoSys, and contributed to the manuscript writing. All authors read and approved the final manuscript.

Acknowledgements

We would thank to Dr. Norihito Watanabe for his thoughtful scientific suggestions and comments on this paper. This work has been funded by the Helmholtz Association through the program POF III-R41 'Geothermal Energy Systems'. The first author would also like to acknowledge the financial support from Chinese Scholarship Council (CSC).

Author details

¹Helmholtz Centre for Environmental Research - UFZ, Permoserstr. 15, 04318 Leipzig, Germany. ²Technical University of Dresden, Helmholtz-Strane 10, 01062 Dresden, Germany. ³Freiberg University of Mining and Technology, Gustav-Zeuner-Strasse 1, 09596 Freiberg, Germany.

Received: 17 December 2014 Accepted: 7 May 2015

Published online: 09 July 2015

References

- Abadpour A, Panfilov M (2009) Method of negative saturations for modeling two-phase compositional flow with oversaturated zones. *Transp Porous Media* 79(2):197–214
- Angelini O, Chavant C, Chénier E, Eymard R, Granet S (2011) Finite volume approximation of a diffusion–dissolution model and application to nuclear waste storage. *Math Comput Simul* 81(10):2001–2017
- Ben Gharbia I, Jaffré J (2014) Gas phase appearance and disappearance as a problem with complementarity constraints. *Math Comput Simul* 99:28–36
- Bourgeat A, Jurak M, Smäi F (2009) Two-phase, partially miscible flow and transport modeling in porous media; application to gas migration in a nuclear waste repository. *Comput Geosci* 13(1):29–42
- Bourgeat A, Jurak M, Smäi F (2013) On persistent primary variables for numerical modeling of gas migration in a nuclear waste repository. *Comput Geosci* 17(2):287–305
- Çengel YA, Boles MA (1994) Thermodynamics: an engineering approach. Property Tables, Figures and Charts to Accompany. McGraw-Hill Ryerson, Limited, Singapore. <https://books.google.de/books?id=u2-SAAAACAAJ>
- Class H, Helmig R, Bastian P (2002) Numerical simulation of non-isothermal multiphase multicomponent processes in porous media: 1. an efficient solution technique. *Adv Water Resour* 25(5):533–550
- Ern A, Mozolevski I (2012) Discontinuous galerkin method for two-component liquid–gas porous media flows. *Comput Geosci* 16(3):677–690
- Fatt I, Klikoff Jr WA (1959) Effect of fractional wettability on multiphase flow through porous media. *Trans., AIME (Am. Inst. Min. Metall. Eng.)*, 216:426–432
- Forsyth P, Shao B (1991) Numerical simulation of gas venting for NAPL site remediation. *Adv Water Resour* 14(6):354–367
- Gawin D, Baggio P, Schrefler BA (1995) Coupled heat, water and gas flow in deformable porous media. *Int J Numer Methods Fluids* 20(8–9):969–987. doi:10.1002/flid.1650200817
- Hassanizadeh M, Gray WG (1980) General conservation equations for multi-phase systems: 3. constitutive theory for porous media flow. *Adv Water Resour* 3(1):25–40

- Helmig R (1997) Multiphase flow and transport processes in the subsurface: a contribution to the modeling of hydrosystems. Springer, Berlin
- Kanzow C (2004) Inexact semismooth newton methods for large-scale complementarity problems. *Optimization Methods Softw* 19(3-4):309–325
- Kolditz O, De Jonge J (2004) Non-isothermal two-phase flow in low-permeable porous media. *Comput Mech* 33(5):345–364
- Kolditz O, Bauer S, Bilke L, Böttcher N, Delfs JO, Fischer T, Görke UJ, Kalbacher T, Kosakowski G, McDermott CI, Park CH, Radu F, Rink K, Shao H, Shao HB, Sun F, Sun YY, Singh AK, Taron J, Walther M, Wang W, Watanabe N, Wu Y, Xie M, Xu W, Zehner B (2012) Opengeosys: an open-source initiative for numerical simulation of thermo-hydro-mechanical/chemical (THM/C) processes in porous media. *Environ Earth Sci* 67(2):589–599. <http://dx.doi.org/10.1007/s12665-012-1546-x>
- Krättele S (2011) The semismooth newton method for multicomponent reactive transport with minerals. *Adv Water Resour* 34(1):137–151
- Landau L, Lifshitz E (1980) Statistical physics, part i. *Course Theoretical Phys* 5:468
- Marchand E, Müller T, Knabner P (2012) Fully coupled generalised hybrid-mixed finite element approximation of two-phase two-component flow in porous media. part ii: numerical scheme and numerical results. *Comput Geosci* 16(3):691–708
- Marchand E, Müller T, Knabner P (2013) Fully coupled generalized hybrid-mixed finite element approximation of two-phase two-component flow in porous media. part i: formulation and properties of the mathematical model. *Comput Geosci* 17(2):431–442
- Marchand E, Knabner P (2014) Results of the momas benchmark for gas phase appearance and disappearance using generalized mhfe. *Adv Water Resour* 73:74–96
- Neumann R, Bastian P, Ippisch O (2013) Modeling and simulation of two-phase two-component flow with disappearing nonwetting phase. *Comput Geosci* 17(1):139–149
- Olivella S, Gens A (2000) Vapour transport in low permeability unsaturated soils with capillary effects. *Transp Porous Media* 40(2):219–241
- Park CH, Taron J, Görke UJ, Singh AK, Kolditz O (2011) The fluidal interface is where the action is in CO_2 sequestration and storage: Hydro-mechanical analysis of mechanical failure. *Energy Procedia* 4:3691–3698
- Panfilov M, Panfilova I (2014) Method of negative saturations for flow with variable number of phases in porous media: extension to three-phase multi-component case. *Comput Geosci*:1–15
- Park CH, Böttcher N, Wang W, Kolditz O (2011) Are upwind techniques in multi-phase flow models necessary?. *J Comput Phys* 230(22):8304–8312
- Pruess K (2008) On production behavior of enhanced geothermal systems with CO_2 as working fluid. *Energy Convers Manag* 49(6):1446–1454
- Peng DY, Robinson DB (1976) A new two-constant equation of state. *Ind Eng Chem Fundam* 15(1):59–64
- Salimi H, Wolf KH, Bruining J (2012) Negative saturation approach for non-isothermal compositional two-phase flow simulations. *Transp Porous Media* 91(2):391–422
- Singh A, Baumann G, Hennings J, Görke UJ, Kolditz O (2012) Numerical analysis of thermal effects during carbon dioxide injection with enhanced gas recovery: a theoretical case study for the altmark gas field. *Environ Earth Sci* 67(2):497–509
- Singh A, Delfs JO, Böttcher N, Taron J, Wang W, Görke UJ, Kolditz O (2013a) A benchmark study on non-isothermal compositional fluid flow. *Energy Procedia* 37:3901–3910
- Singh A, Delfs JO, Shao H, Kolditz O (2013b) Characterization of CO_2 leakage into the freshwater body. In: EGU General Assembly Conference Abstracts Vol. 15, p 11474
- Udell K, Fitch J (1985) Heat and mass transfer in capillary porous media considering evaporation, condensation, and non-condensable gas effects. In: 23rd ASME/AIChE National Heat Transfer Conference, Denver, CO. pp 103–110
- Van Genuchten MT (1980) A closed-form equation for predicting the hydraulic conductivity of unsaturated soils. *Soil Sci Soc Am J* 44(5):892–898
- Wu YS, Forsyth PA (2001) On the selection of primary variables in numerical formulation for modeling multiphase flow in porous media. *J Contam Hydrol* 48(3):277–304

Submit your manuscript to a SpringerOpen® journal and benefit from:

- Convenient online submission
- Rigorous peer review
- Immediate publication on acceptance
- Open access: articles freely available online
- High visibility within the field
- Retaining the copyright to your article

Submit your next manuscript at ► springeropen.com

A.2 PAPER 2

Huang Y, Nagel T, Shao H. Comparing global and local implementations of nonlinear complementary problems for the modeling of multi-component two-phase flow with phase change phenomena[J]. Environmental Earth Sciences, 2017, 76(18): 643.

Comparing global and local implementations of nonlinear complementary problems for the modeling of multi-component two-phase flow with phase change phenomena

Yonghui Huang^{1,4} · Thomas Nagel^{1,2} · Haibing Shao^{1,3} 

Received: 8 August 2017 / Accepted: 6 September 2017
© Springer-Verlag GmbH Germany 2017

Abstract Compositional multiphase flow is considered to be one of the fundamental physical processes in the field of water resources research. The strong nonlinearity and discontinuity emerging from phase transition phenomena pose a serious challenge for numerical modeling. Recently, Lauser et al. (Adv Water Resour 34(8):957–966, 2011) have proposed a numerical scheme, namely the nonlinear complementary problem (NCP), to handle this strong nonlinearity. In this work, the NCP is implemented at both local and global levels of a finite element algorithm. In the former case, the NCP is integrated into the local thermodynamic equilibrium calculation, while in the latter one, it is formulated as one of the governing equations. The two different formulations have been investigated through three well-established benchmarks and analyzed for their efficiency and robustness. It is found that both globally and locally implemented NCP formulations are numerically more efficient and robust in comparison with

traditional primary variable switching approach. In homogeneous media, the globally implemented NCP formulation leads to an approximately 20% faster simulation compared to the local NCP. This is because a nested Newton iteration for the local phase state identification can be avoided, and thus, the overall computational resources are saved accordingly. However, for problems involving strongly heterogeneous media, the locally integrated NCP formulation suppresses numerical oscillations and delivers more accurate and robust results, especially at the phase boundary.

Keywords Phase transition · Multiphase flow · Nonlinear complementary problem · Numerical efficiency and accuracy · OpenGeoSys

Greek symbols

μ_α	Dynamic viscosity of phase α (Pa s)
λ_T	Effective heat conductivity tensor [W (m K) ⁻¹]
Ω	(sub)domains
ω	Test function
ϕ	Porosity (–)
Φ^i	Fugacity coefficient (–)
ρ	Mass density (kg m ⁻³)
τ	Overall computational time (s)

Operators

\wedge	Logical and
div	Divergence operator
∇	Gradient operator
\perp	Complement operator

Roman symbols

$c_{p\alpha}$	Specific heat capacity of fluid phase α (J (kg K) ⁻¹)
c_{pS}	Specific heat capacity of soil grain (J (kg K) ⁻¹)

This article is part of a Topical Collection in Environmental Earth Sciences on “Subsurface Energy Storage II”, guest edited by Zhonghe Pang, Yanlong Kong, Haibing Shao, and Olaf Kolditz.

Throughout the article, bold face symbols denote tensors and vectors. Normal face letters represent scalar quantities.

✉ Haibing Shao
haibing.shao@ufz.de

¹ Department of Environmental Informatics, Helmholtz Centre for Environmental Research - UFZ, Permoserstraße 15, 04318 Leipzig, Germany

² Department of Mechanical and Manufacturing Engineering, Trinity College Dublin, Dublin 2, Ireland

³ Freiberg University of Mining and Technology, Gustav-Zeuner-Straße 1, 09596 Freiberg, Germany

⁴ Applied Environmental Systems Analysis, Dresden University of Technology, Dresden, Germany

D_{α}^i	Diffusivity tensor ($\text{m}^2 \text{s}^{-1}$)
F^i	Source or sink term of component i ($\text{kg} (\text{m}^3 \text{s})^{-1}$)
f_{α}^i	Fugacity of component i in α phase (Pa)
g	Gravitational acceleration (m s^{-2})
H	Henry constant ($\text{mol} (\text{Pa m}^3)^{-1}$)
h_{α}	Specific enthalpy of phase α (J kg^{-1})
J_{α}^i	Diffusive flux of component i in phase α (m s^{-1})
K	Intrinsic permeability tensor (m^2)
$k_{r\alpha}$	Relative permeability of phase α ($-$)
M^i	Molar mass of i th component (kg mol^{-1})
N_{α}	Molar density of phase α (mol m^{-3})
N_c	Total number of components existing in the system
P_{α}	Pressure in phase α (Pa)
P_C	Capillary pressure (Pa)
P_{sat}	Vapor saturation pressure (Pa)
P_{vap}	Vapor pressure (Pa)
q	Darcy velocity (m s^{-1})
Q_T	Heat source or sink (W m^{-3})
S	Saturation ($-$)
T	Temperature (K)
u_{α}	Specific internal energy (J kg^{-1})
U^P	Primary variable set
U^S	Secondary variable set
x_{α}^i	Molar fraction of i th component in phase α ($-$)

Introduction

Compositional two-phase flow is considered to be one of the fundamental physical processes in the field of geoscientific research. For example, at sites where groundwater is contaminated by Non-Aqueous Phase Liquids (NAPL), the dispersion of NAPL components occurs in both the aqueous and gas phases (Sleep and Sykes 1989; Forsyth 1994). For CO_2 sequestration, the amount of CO_2 dissolved in saline water determines the water–rock interactions and also the long-term geochemical evolution (Nordbotten and Celia 2011; Zhang and Agarwal 2013). For the assessment of nuclear waste repositories, transport of radionuclides driven by the gas production is the focus of a lot of recent research (Xu et al. 2008; Bourgeat et al. 2009b).

Phase transition represents one of the most important processes underlying compositional two-phase flow, and it consistently attracts the interest of researchers and engineers. Compositional two-phase flow incorporating the phase transition is difficult to simulate due to several reasons. Firstly, the equations that describe two-phase zones and single-phase zones are qualitatively different, since the composition in two-phase zones is controlled by thermodynamic equilibrium, while it is not the case in single-

phase zones (Panfilov and Panfilova 2014). Moreover, the pore fluid mixture can be in either a single-phase or two-phase state, depending on the local pressure, temperature, and phase composition conditions. Such phase transition creates discontinuities in the primary or secondary variables such as the phase saturation. Additionally, phase change-induced latent heat effects introduce nonlinearities in the energy balance equation, which tends to cause numerical difficulties (Siavashi et al. 2014).

In order to overcome these challenges, several numerical approaches have been proposed. The conventional approach is to alter the combination of primary variables based on the present phase state, which is also known as the primary variable switching (PVS) scheme (Coats et al. 1980; Wu and Forsyth 2001; Class et al. 2002). Another widely known alternative is performing two-stage flash calculations, termed phase stability analysis and phase splitting (Firoozabadi 1999; Moortgat et al. 2012). Recently, the persistent primary variable (PPV) approach was proposed to detect the gas phase appearance and disappearance in the context of nuclear waste repositories (Bourgeat et al. 2009b). In this approach, either nonstandard primary variables such as generalized mass density are applied (Bourgeat et al. 2009a), or the definition of variables such as saturation or capillary pressure is extended to incorporate information on phase transitions (Abadpour and Panfilov 2009; Neumann et al. 2013).

The aforementioned approaches have demonstrated the capability of modeling phase transition, yet some specific restrictions remain. For example, in the PVS scheme, numerical oscillation might be introduced within Newton iterations due to frequent switching of primary variables, which often leads to irregular convergence behavior, whereas for the flash calculation approach, although it delivers stable results in terms of phase transition (Hoteit and Firoozabadi 2008; Zidane and Firoozabadi 2015), the minimization of Gibbs free energy required by phase stability analysis usually leads to an expensive computation. With regard to the PPV scheme, Neumann et al. (2013) pointed out that it suffers from numerical difficulties when liquid phase is allowed to vanish. To alleviate these issues, Lauser et al. (2011) introduced a new approach which formulates the process of phase disappearance or emergence as so-called nonlinear complementary problems (NCPs). This numerical scheme results in intrinsically non-differentiable but semi-smooth equation systems, which can be solved by semi-smooth Newton scheme (Hager and Wohlmuth 2010). The main advantage of NCP approach is avoiding the variable switching by using a fixed set of primary unknowns and nonlinear equations. Another advantage is no phase stability analysis is necessary due to the presence of complementarity conditions. To the

authors’ understanding, the NCP can be implemented in two different ways.

Local NCP formulation

In this formulation, the NCP is combined with thermodynamic model to construct the local problems (Marchand et al. 2013). A local nonlinear solver of the semi-smooth Newton type is applied to determine the phase status and phase compositions, while standard Newton algorithm is employed to solve the global mass and energy conservations for all primary unknowns.

Global NCP formulation

As proposed by Lauser et al. (2011), when combined NCP with mass and energy balance equations, the extended global system can be solved by an iterative semi-smooth Newton algorithm without requiring nested Newton iterations to identify the local phase state.

To our knowledge, there has been rarely a detailed analysis of these two nonlinear formulations, with respect to their numerical performance and computational efficiency in solving the compositional two-phase flow problem. In this work, the investigation is conducted with the scientific simulator OpenGeoSys (Kolditz et al. 2012; Huang et al. 2015), which is based on the Galerkin finite element method. Both aforementioned NCP formulations have been implemented in it. The paper is structured as follows. In “The mathematical framework” section, the mathematical formulation of non-isothermal multi-component two-phase flow is presented, together with the thermodynamic equilibrium model. The details of local and global NCP formulations are introduced in “Nonlinear formulations” section. Following that, “Numerical solution strategy” section focuses on the technical issues regarding the discretization, linearization, and numerical solution strategies. In “Numerical experiments” section, three benchmarks are defined for the performance analysis of different numerical implementations. The results are compared and discussed in “Results” section. Finally, the advantages and drawbacks of the two NCP formulations are summarized.

The mathematical framework

Throughout this work, the following assumptions have been made for the compositional two-phase flow model.

- Pressure remains at the order of magnitude of atmospheric pressure.
- Temperature ranges from 10 to 300 °C.
- Low mutual miscibility.
- Local thermal and chemical equilibrium are assumed to hold at all times.
- Gas phase is assumed to behave as an ideal gas. Liquid phase is an incompressible fluid.

Governing equation

Let $\alpha \in \{G, L\}$ denote the set of gas and liquid phases. N_c indicates the total number of components present in the system. The mass conservation for each component can be written as

$$\phi \frac{\partial}{\partial t} \left(\sum_{\alpha \in \{G,L\}} N_\alpha S_\alpha x_\alpha^i \right) + \text{div} \left[\sum_{\alpha \in \{G,L\}} N_\alpha (x_\alpha^i \mathbf{q}_\alpha + \mathbf{J}_\alpha^i) \right] = F^i, \tag{1}$$

where x_α^i is the molar fraction of component i in phase α , S_α is the saturation of phase α , and N_α represents the phase molar density. For a particular phase α , its velocity \mathbf{q}_α is given by the generalized Darcy’s law

$$\mathbf{q}_\alpha = - \frac{K k_{r\alpha}(S)}{\mu_\alpha} (\nabla P_\alpha - \rho_\alpha \mathbf{g}), \tag{2}$$

with ρ_α indicating the mass density, and the diffusive flux \mathbf{J}_α^i is governed by Fick’s law

$$\mathbf{J}_\alpha^i = -\phi S_\alpha \mathbf{D}_\alpha^i \nabla x_\alpha^i \quad i \in [1, \dots, N_c]. \tag{3}$$

Note that in a compositional system, the diffusive fluxes for all components should sum to zero. When thermal effects need to be considered, the energy balance equation is then augmented along with the above mass balance formulations

$$\begin{aligned} &\phi \frac{\partial}{\partial t} [(1 - S_G) \rho_L u_L + S_G \rho_G u_G] \\ &+ (1 - \phi) \frac{\partial}{\partial t} (\rho_S c_{pS} T) + \text{div} [\rho_G h_G \mathbf{q}_G] + \text{div} [\rho_L h_L \mathbf{q}_L] \\ &- \text{div} (\lambda_T \nabla T) = Q_T, \end{aligned} \tag{4}$$

where c_{pS} denotes the specific heat capacity of solids. u_L and u_G stand for the specific internal energy. The specific enthalpy h_α in phase α can be computed as

$$h_\alpha = \int_{T_0}^T c_{p\alpha} dT. \tag{5}$$

Note that the enthalpy of gas phase is higher than that of the liquid, and the difference between them equals to the

latent heat of vaporization at given pressure and temperature, which guarantees the phase changes from liquid to gas or vice versa.

The relationship between specific internal energy u_α and specific enthalpy h_α is related to the pressure volume work. Since the liquid phase is assumed to be incompressible, i.e., the volume change in the liquid phase is neglected ($u_L = h_L$). For the compressible gas phase, however, the specific enthalpy is given by

$$h_G = u_G + \frac{P_G}{\rho_G}. \tag{6}$$

Equations (1)–(4) provide a general mathematical framework for compositional two-phase flow. Yet, their solution has to be complemented by the requirement of local thermodynamic equilibrium.

Phase behavior

In a compositional two-phase flow model, phase equilibrium calculation claims a most critical part. The calculation is required to detect the phase transition and obtain the correct phase composition. Here, the thermodynamic equilibrium is represented as the equality of fugacities in the gas and liquid phases

$$f_G^i(P_G, T, x_G^i) = f_L^i(P_L, T, x_L^i), \tag{7}$$

with f_G^i and f_L^i indicating the fugacity of component i in gas and liquid phase, respectively. Following the definition of fugacity, the above equation can be extended

$$f_\alpha^i = \Phi^i x_\alpha^i P_\alpha, \quad \alpha \in \{G, L\}, \quad \text{and } i \in [1, \dots, N_c], \tag{8}$$

with Φ^i denoting the fugacity coefficient. Meanwhile, the mass balance for a particular component within any elements is represented by a set of material balance equations (Whitson and Michelsen 1989)

$$X^i \sum_{\alpha \in \{G, L\}} N_\alpha S_\alpha = \sum_{\alpha \in \{G, L\}} x_\alpha^i N_\alpha S_\alpha. \tag{9}$$

Here, X^i represents the overall molar fraction of component i . In order to close the system, phase constraints and saturation constraints must be applied

$$\sum_\alpha S_\alpha = 1, \tag{10}$$

$$\sum_{i=1}^{N_c} (x_G^i - x_L^i) = 0. \tag{11}$$

The conventional approach to handling the phase transition can be achieved in several different ways. One commonly applied strategy is the primary variable switching (PVS) approach (Coats et al. 1980). Within each Newton iteration per time step, the phase appearance and disappearance are

determined by solving equation system (1)–(4) and (7). In case the solution yields saturation value $S_\alpha < 0$, it indicates the phase α vanishes, and the saturation has to be set to zero. Since S_α is no longer free, the component molar fraction for the present phase x_γ^i ($\gamma \in \{G, L\}, \gamma \neq \alpha$) becomes the primary variable and replace the saturation S_α . The same principle applies when $S_\alpha > 1$, which suggests phase α is over-saturated and the other phase disappears. With regard to the phase appearance, a saturation pressure is calculated and compared with the pressure of the present phase. If the calculated saturation pressure is larger, it suggests the two-phase will coexist, and saturation S_α will be the primary variable again.

Nonlinear complementarity problem (NCP)

Different from the conventional approaches, a new approach has recently been introduced by utilizing the so-called nonlinear complimentary problem (NCP) (Facchinei and Pang 2007). In optimization theory, complementarity conditions usually arise as the Karush–Kuhn–Tucker (KKT) condition of a constrained nonlinear optimization problem (Gopal and Biegler 1999), and they can be used to represent the switches between mathematical models. Its general form can be written as

$$0 \leq \psi_1(x) \perp \psi_2(x) \geq 0. \tag{12}$$

This indicates $\psi_1(x) \cdot \psi_2(x) = 0$, and both $\psi_1(x)$ and $\psi_2(x)$ are nonnegative. Operator \perp denotes $\psi_1(x)$ complements with $\psi_2(x)$. Such nonlinear complementarity constrains can also be applied to the phase transition problem, in which they serve as the KKT conditions for the phase equilibrium model. For a two-phase system that involves gas and liquid phases, there are three possible combinations of phase status.

(1) When only the liquid phase is present, the gas phase saturation S_G is 0. The composition distribution in the single liquid phase is no longer controlled by thermodynamic equilibrium. According to Michelsen (1982), the liquid phase is stable at the given pressure and temperature, if the following stationarity criterion is satisfied:

$$1 + \sum_{i=1}^{N_c} x_G^i (\ln x_G^i + \ln \Phi_G^i - \ln x_L^i - \ln \Phi_L^i - 1) \geq 0. \tag{13}$$

Based on thermodynamic equilibrium Eq. (7), the following relationships can be formulated:

$$\begin{cases} x_G^i = K^i x_L^i, & i \in [1, \dots, N_c] \\ \Phi_G^i = \frac{\Phi_L^i P_L}{K^i P_G} \end{cases}. \tag{14}$$

where K^i is known as the equilibrium ratio. Substituting

Eq. (14) into criterion (13), we obtain that the liquid phase is stable if and only if the sum of gas phase composition should not exceed 1, i.e., $\sum_{i=1}^{N_c} x_G^i \leq 1$. Therefore, the stability condition for single liquid phase can be written as:

$$S_G = 0 \quad \wedge \quad \sum_{i=1}^{N_c} x_G^i \leq 1. \tag{15}$$

(2) A similar relationship holds when a single gas phase is present in the system.

$$S_L = 0 \quad \wedge \quad \sum_{i=1}^{N_c} x_L^i \leq 1. \tag{16}$$

(3) When both phases are present, the constituent phase composition has to satisfy the thermodynamic equilibrium (Eq. 7), and their molar fractions should sum up to one:

$$S_\alpha > 0 \quad \wedge \quad \sum_{i=1}^{N_c} x_\alpha^i = 1, \quad \alpha \in \{G, L\}. \tag{17}$$

Equations (15)–(17) can be summarized into the complementarity constraints:

$$0 \leq S_\alpha \quad \perp \quad \left(1 - \sum_{i=1}^{N_c} x_\alpha^i\right) \geq 0, \quad \alpha \in \{G, L\}. \tag{18}$$

The complementarity constraints (18), consisting of equations and inequalities, can be further expressed equivalently by a nonlinear complementarity function, such that the inequalities can be avoided. In this work, a minimum function is adopted:

$$\min\left(S_\alpha, \left(1 - \sum_{i=1}^{N_c} x_\alpha^i\right)\right) = 0, \quad \alpha \in \{G, L\}. \tag{19}$$

At locations where the first argument S_α and the second argument $(1 - \sum_{i=1}^{N_c} x_\alpha^i)$ are equal, the min-function is known to be discontinuous. Yet at all other places, the min-function has the attractive property that it is both smooth and differentiable. The piecewise differentiable and semi-smooth features are perfectly suited for the semi-smooth Newton algorithm (Masson et al. 2014). In Sect. 6.1, it will be further discussed why in certain cases the NCP approach is advantageous over the conventional approaches.

Nonlinear formulations

In a finite element implementation, the thermodynamic equilibrium model can either be solved as a constraint equation coupled with the governing Eqs. (1)–(4), or being handled as a separate flash calculation routine (Cao 2002). Based on these two strategies, two different nonlinear formulations will be presented in terms of incorporating the

thermodynamic equilibrium model along with the complementarity constraints.

Local NCP formulation

This formulation was first proposed by Marchand et al. (2012), in which the primary variables are chosen to be a “molar variable” set (Voskov and Tchelepi 2012). It includes:

- the reference phase pressure P ,
- overall molar fraction X^i , $i \in [1, \dots, N_c - 1]$, with $(N_c - 1)$ degrees of freedom,
- the temperature T .

The local NCP is embedded within the solution procedure of the local thermodynamic equilibrium, and it is constructed as part of the local problems for solving all secondary variables on each integration points. For a given set of primary variables P , X^i ($i \in [1, \dots, N_c - 1]$) and T , the local problem reads,

$$\begin{cases} f_G^i(P_G, T, x_G^i) - f_L^i(P_L, T, x_L^i) = 0 \\ X^i - \left[\frac{(1 - S_G)N_L x_L^i + S_G N_G x_G^i}{(1 - S_G)N_L + S_G N_G}\right] = 0 \\ \min\left(S_\alpha, \left(1 - \sum_{i=1}^{N_c} x_\alpha^i\right)\right) = 0. \quad \alpha \in \{G, L\} \end{cases} \tag{20}$$

In total, there are $2N_c + 2$ equations, along with $2N_c + 2$ secondary variables, including S_α, x_α^i , $\alpha \in \{G, L\}$, $i \in [1, \dots, N_c]$. Within each global Newton iteration, Eq. (20) is solved with the updated primary variable. In return, the updated S_α and x_α^i will be cast in the next round of global Newton iteration to solve Eqs. (1)–(4). The details of the so-called nested Newton procedure can also be found in Marchand et al. (2013).

Global NCP formulation

An alternative to the local NCP formulation was proposed by Lauser et al. (2011), who directly combined the complementary constraints with the global governing equations. In this work, the “natural variable” set (Coats et al. 1980) is chosen as primary variables. They are

- the reference phase pressure P ,
- the gas phase saturation S_G ,
- the gas phase composition x_G^i , $i \in [1, \dots, N_c]$, with (N_c) degrees of freedom,
- the temperature T .

The liquid phase compositions x_L^i , which are selected as secondary variables, can be uniquely described in terms of primary variables by reformulating Eqs. (7) and (8)

$$x_L^i = K^i(P, T, x_G^i)x_G^i, \quad i \in [1, \dots, N_c]. \tag{21}$$

To summarize, let $\mathcal{H} : \mathbb{R}^{(N_c+3)} \rightarrow \mathbb{R}^{(N_c+1)}$ represent the mass and energy balance Eqs. (1)–(4), the global governing equation system reads

$$\begin{cases} \mathcal{H}(U) = 0 \\ \min \left(S_\alpha, \left(1 - \sum_{i=1}^{N_c} x_\alpha^i \right) \right) = 0. \quad \alpha \in \{G, L\}, \end{cases} \tag{22}$$

where U represents the primary variable set: $U = [P, S_G, x_G^i, T]^T \in \mathbb{R}^{(N_c+3)}$.

Within the global NCP formulation, the phase state identification no longer requires additional local Newton iterations on each element or integration point. This means less computational resources are required on the local level, at the price that the global linear equation system is larger. Nevertheless, due to the piecewise linearity of the min-function, a Schur complement strategy (Ouellette 1981) can be further applied on the Jacobian matrix to minimize the size of global system. More details regarding this procedure will be discussed in Sect. 3.2.

Numerical solution strategy

Discretization

In this work, the Galerkin finite element method is employed for spacial discretization, with a backward Euler fully implicit scheme for the time integration. On each (sub)domain Ω , the weighted residual method is used to derive the weak form of mass and energy balance Eqs. (1)–(4). It reads

$$\begin{aligned} & \frac{\phi}{\Delta t} \sum_{\alpha \in \{G,L\}} \int_{\Omega} \left[(N_\alpha S_\alpha x_\alpha^i)^{k+1} - (N_\alpha S_\alpha x_\alpha^i)^k \right] \omega d\Omega \\ & + \sum_{\alpha \in \{G,L\}} \int_{\Omega} \text{div} [N_\alpha x_\alpha^i (q_\alpha + J_\alpha^i)]^{k+1} \omega d\Omega \\ & = \int_{\Omega} (F^i)^{k+1} \omega d\Omega \end{aligned} \tag{23}$$

for component-based mass balance and

$$\begin{aligned} & \frac{\phi}{\Delta t} \sum_{\alpha \in \{G,L\}} \int_{\Omega} \left[(\rho_\alpha S_\alpha u_\alpha)^{k+1} - (\rho_\alpha S_\alpha u_\alpha)^k \right] \omega d\Omega \\ & + \frac{(1-\phi)\rho_S c_{pS}}{\Delta t} \sum_{\alpha \in \{G,L\}} \int_{\Omega} [T^{k+1} - T^k] \omega d\Omega \\ & - \int_{\Omega} \text{div}(\lambda \nabla T^{k+1}) \omega d\Omega \\ & + \sum_{\alpha \in \{G,L\}} \int_{\Omega} \text{div}(\rho_\alpha h_\alpha q_\alpha)^{k+1} \omega d\Omega = \int_{\Omega} (Q_T)^{k+1} \omega d\Omega \end{aligned} \tag{24}$$

for energy balance of the fluid mixtures. Here, $\omega \in H_0^1$ represents the test function. The superscripts \cdot^k and \cdot^{k+1} are employed here to represent the previous (t^k) and current (t^{k+1}) time step, and Δt denotes the actual time-step size ($\Delta t = t^{k+1} - t^k$).

The Laplacian-related terms in the above formulations have the general form of $\int_{\Omega} \text{div} \nabla \omega d\Omega$, and they yield second-order differentials in Euclidean space of the respective primary variables. The reduction in the differentiation order of the Laplacian-related terms can be realized via integration by parts and Green–Gauss theorem as follows:

$$\int_{\Omega} \text{div} \nabla \omega d\Omega = \int_{\Gamma} \nabla \cdot \mathbf{n}_\Gamma \omega d\Gamma - \int_{\Omega} \nabla \cdot \nabla \omega d\Omega, \tag{25}$$

where Γ represents the domain boundary $\partial\Omega$ and \mathbf{n}_Γ is the unit outward normal at the boundary surface.

In this work, a special attention is paid to the discretization of complementary problem (Eq. 19). In global NCP formulation, the NCP is cast as governing equations coupled with mass and energy balance equations. Here, the nodal discretized version for NCP is given as follows:

$$C((U^P)^{k+1}) := \begin{bmatrix} C_G((U^P)^{k+1}) \\ C_L((U^P)^{k+1}) \end{bmatrix} = \mathbf{0} \tag{26}$$

with

$$C_\alpha = \min \left\{ (S_\alpha)^{k+1}, 1 - \sum_{i=1}^{N_c} (x_\alpha^i)^{k+1} \right\}, \quad \alpha \in \{G, L\}. \tag{27}$$

Linearization strategy

Semi-smooth Newton scheme

In non-isothermal two-phase flow problems, nonlinearities can emerge from the conservation Eqs. (1)–(4), from the thermodynamic equilibrium Eqs. (7)–(11), as well as from the NCP Eq. (19). Mathematically, these nonlinearities can be categorized into smooth or non-smooth types. In the conservation equations and thermodynamic equilibrium formulations, the function itself, as well its first-order derivatives, is continuous with respect to the primary unknowns. Therefore, the nonlinearities originated from them are considered to be smooth. On the contrary, the minimum functions of Eq. (19) are considered to be semi-smooth, as discussed in Sect. 2.3. For the two types of nonlinearities, the corresponding linearization strategies are also different. Smooth nonlinearities can be directly handled by standard Newton scheme, while a semi-smooth Newton scheme (Krättele 2011) must be employed to

handle the complementary constraints. This algorithm is proven to achieve local convergence while keeping the quadratic convergence rate.

In the local NCP formulation, the local problem (20) is of semi-smooth type. Therefore, in each time step, semi-smooth Newton scheme is performed on each integration point, while the standard Newton method is used to solve the global mass and energy conservations [Eqs. (1)–(4)]. In contrast, for the global NCP implementation, equation system (22) requires a semi-smooth Newton scheme on the global level.

Construction of Jacobian matrix

To construct the global Jacobian matrix, the derivatives of governing equations with respect to the primary variables are required. In the global NCP scheme, the derivatives are straightforward to calculate, whereas in the local NCP, the derivatives calculation is very complicated, due to a nested thermodynamic model. In this work, the partial derivatives of the secondary variable set U^S with respect to the primary variable set U^P can be obtained by:

$$\frac{\partial U^S}{\partial U^P} = \left(\frac{\partial F}{\partial U^S} \right)^{-1} \frac{\partial F}{\partial U^P}, \tag{28}$$

where function F represents the equation system (20), and the square matrix $\frac{\partial F}{\partial U^S}$ is the local Jacobian matrix for equation system (20).

Jacobian matrix reduction

As already mentioned in Sect. (2.4.2), for global NCP formulation, the Schur complement strategy can be applied on the global Jacobian matrix, such that the size of global linear system can be minimized. Special attention has to be paid to the minimum function. For a Newton iteration l , the Newton equation for NCP (27) can be easily obtained:

$$C_G : \begin{cases} (\delta S_G)^l = -(S_G)^l & \text{if } S_G \leq 1 - \sum_{i=1}^{N_c} (x_G^i)^l \\ \sum_{i=1}^{N_c} (\delta x_G^i)^l = 1 - \sum_{i=1}^{N_c} (x_G^i)^l & \text{if } S_G > 1 - \sum_{i=1}^{N_c} (x_G^i)^l \end{cases} \tag{29}$$

$$C_L : \begin{cases} (\delta S_G)^l = 1 - (S_G)^l, & \text{if } 1 - S_G \leq 1 - \sum_{i=1}^{N_c} (x_G^i)^l \\ x_G^i \frac{\partial K^i}{\partial P} (\delta P)^l + x_G^i \frac{\partial K^i}{\partial T} (\delta T)^l \\ + \sum_{i=1}^{N_c} \left(\frac{\partial}{\partial x_G^i} (K^i x_G^i) \right) (\delta x_G^i)^l = 1 - \sum_{i=1}^{N_c} (K^i x_G^i)^l & \text{if } 1 - S_G > 1 - \sum_{i=1}^{N_c} (x_G^i)^l \end{cases} \tag{30}$$

Here $\delta \cdot$ indicates the change of primary variable in each Newton iteration. Function K is defined in Eq. (21). Substituting (29) and (30) into the global Jacobian matrix leads to a linear system with $(N_c + 1)$ primary unknowns, while the secondary unknowns can be computed in the local post-processing procedure, which are summarized as follows

- In the single-phase zone, the following linear system needs to be solved

$$\begin{bmatrix} \frac{\partial \mathcal{H}}{\partial P} & \frac{\partial \mathcal{H}}{\partial x_G^i} & \frac{\partial \mathcal{H}}{\partial T} \end{bmatrix} \begin{bmatrix} \delta P \\ \delta x_G^i \\ \delta T \end{bmatrix} = -\mathcal{H} \tag{31}$$

$$- \delta S_G \frac{\partial \mathcal{H}}{\partial S_G} - \delta x_G^{N_c} \frac{\partial \mathcal{H}}{\partial x_G^{N_c}}, \quad i \in [1, \dots, N_c - 1].$$

- While in the two-phase zone, the linear equation is given as

$$\begin{bmatrix} \frac{\partial \mathcal{H}}{\partial P} & \frac{\partial \mathcal{H}}{\partial S_G} & \frac{\partial \mathcal{H}}{\partial x_G^i} & \frac{\partial \mathcal{H}}{\partial T} \end{bmatrix} \begin{bmatrix} \delta P \\ \delta S_G \\ \delta x_G^i \\ \delta T \end{bmatrix} = -\mathcal{H} - \delta x_G^{N_c-1} \frac{\partial \mathcal{H}}{\partial x_G^{N_c-1}} - \delta x_G^{N_c} \frac{\partial \mathcal{H}}{\partial x_G^{N_c}}, \quad i \in [1, \dots, N_c - 2]. \tag{32}$$

Therefore, by conducting the Schur complement procedure in global NCP formulation, the reduced linear system holds the same size as local NCP formulation, i.e., $(N_c + 1)$. After the linearization of the global governing equations, a sparse and asymmetric linear system is assembled and needs to be solved. The BiCGStab solver from the LIS library (Nishida 2010) is employed with an ILU preconditioner to obtain the solution.

Interface continuity requirement

When the model domain is heterogeneous, the neighboring materials can have highly contrasted physical properties, such as the capillary pressure and relative permeability. Therefore, an accurate treatment of the interface condition should be addressed in the model in order to account for the saturation jump at the material interface.

Let $\Omega^{(1)}$ and $\Omega^{(2)}$ be the two neighboring materials characterized by two different Brooks–Corey type capillary pressure relationships $P_c^{(1)}$ and $P_c^{(2)}$. The corresponding entry pressures $P_e^{(j)}$ ($j \in \{1, 2\}$) are assumed with: $P_e^{(1)} < P_e^{(2)}$, i.e., $\Omega^{(1)}$ holds a smaller entry pressure. With the requirement of cell-wise continuity, the capillary pressure at the interface can be reformulated with the known entry pressure value, following Bastian (2014).

$$\begin{cases} P_c^{(2)} = P_c^{(1)} & \text{if } P_c^{(1)} \geq P_e^{(2)} \\ P_c^{(2)} = P_e^{(2)} & \text{if } P_c^{(1)} \leq P_e^{(2)}. \end{cases}$$

In the case of global NCP formulation, the saturation is treated as primary variable which therefore requires the capillary pressure to be prescribed at each node. Then, in order to account for the saturation discontinuity, the saturation at the interface should be regulated as the following form:

$$S_G^{(2)} = \left(P_c^{(2)}\right)^{-1} \left[P_c^{(1)}\left(S_G^{(1)}\right)\right], \quad (33)$$

where $\left(P_c^{(2)}\right)^{-1}$ indicates the inverse function of the capillary pressure relationship at sub-material domain $\Omega^{(2)}$. For the local NCP formulation, the overall molar fraction (X^i) is chosen as the primary variable. A similar strategy is applied to formulate the interface condition for X^i :

$$X^{i,(2)} = \frac{N_L^{(2)} x_L^{i,(2)} \left(1 - S_G^{(2)}\right) + N_G^{(2)} x_G^{i,(2)} S_G^{(2)}}{N_L^{(2)} \left(1 - S_G^{(2)}\right) + N_G^{(2)} S_G^{(2)}}, \quad (34)$$

where $S_G^{(2)}$ is defined following Eq. (33). Besides, due to the fact that saturation is selected as a secondary variable, it is calculated in local problem by the primary variable P, X^i, T .

$$\begin{cases} S_G^{(2)} = \left(P_c^{(2)}\right)^{-1} \left[P_c^{(1)}\left(S_G^{(1)}\right)\right] \\ S_G^{(1)} = S_G^{(1)}\left(P^{(1)}, X^{i,(1)}, T^{(1)}\right) \end{cases}$$

For the local NCP formulation, the interface conditions have already been incorporated into the local problem and solved on each integration point, and these conditions are further guaranteed at each node throughout the global Newton iterations.

Numerical experiments

In order to analyze the accuracy and computational performance of the two aforementioned numerical formulations, three benchmarks have been adopted with increasing complexity. First, the MoMaS benchmark simulates gas migration through a homogeneous bentonite formation (“[Benchmark I: The MoMaS benchmark](#)” section). Second, the thermal effect is taken into account in the heat pipe problem (“[Benchmark II: heat pipe problem](#)” section), in which both gas and liquid phases are allowed to emerge or disappear. Finally, the Kueper experiment (“[Benchmark III: Kueper experiment](#)” section) is modeled to investigate the influence of heterogeneous media properties and strong gravitational effects. The detailed constitutive relationships of the model with regard to the benchmarks are given in “[Appendix](#)”.

Implementation

All numerical experiments are conducted with the OpenGeoSys software (Kolditz et al. 2012; Huang et al. 2015). Both fixed and adaptive time-stepping features are employed. With the later case, the successive time-step size is doubled when the number of Newton iterations in the previous time step is less than 7, and it will be cut into half if more than 15 iterations are required. Meanwhile, the nonlinear solver convergence criteria for the L_2 -norm of the residual vectors are set to 10^{-14} for the local problem and 10^{-7} for the global one. Note that local tolerance must be lower because solution accuracy of the local problem is crucial for the convergence on global level. All benchmarks are performed on a computer equipped with 8 GB of memory and an Intel(R) Core(TM) I5-3230 processor @2.6 GHz. It is noted although the OpenGeoSys software has the capability of running parallel simulations (Wang et al. 2009), only single-CPU core serial computation is performed here, so that the time spent in different parts of the simulation can be more directly analyzed.

Benchmark I: The MoMaS benchmark

The MoMaS benchmark was proposed by Bourgeat et al. (2009a), aiming to simulate the gas phase appearance and disappearance in a nuclear waste repository. The model is composed of a 2D rectangular domain of 20×200 m, representing the bentonite back-fill in the repository. The domain is initially water saturated (\cdot^w) and bears a liquid pressure $P_L = 1 \times 10^6$ Pa. The gas phase consists of hydrogen (\cdot^h) and water vapor. Dirichlet conditions are imposed on the outflow side with $P_L = 1 \times 10^6$ Pa, $S_G = 0$, $X^h = 0.0$. A hydrogen injection flux of $5.57 \times 10^{-6} \text{ kg} \cdot \text{m}^{-2} \cdot \text{a}^{-1}$ is applied on the inflow boundary for the first 5×10^5 a, and no flow applied afterward. These boundary settings enable the gas phase to first appear and then vanish from the system. The model parameters used in this benchmark are listed in Table 1. Two tests are performed within this benchmark.

- In the first test, the primary variable switching (PVS) approach (Coats et al. 1980), the local and global NCP formulations are all applied with adaptive time-stepping (“[Implementation](#)” section) control. The initial and minimal time-step size Δt_{\min} is set to 100 a, and the maximum allowed time-step size Δt_{\max} is 5×10^4 a. The comparison aims at investigating the impact of NCP implementation on the speed of convergence, especially in the presence of phase transitions.
- The second test is performed with a fixed time-step size of 5000 a. A special focus is placed on the comparison of the computational complexity and distribution.

Table 1 Parameter values used in the MoMaS benchmark

Parameter	Symbol	Value	Unit
Water density	ρ^w	1×10^3	kg m^{-3}
Molar mass of water	M^w	18×10^{-3}	kg mol^{-1}
Molar mass of hydrogen	M^h	2×10^{-3}	kg mol^{-1}
Henry constant	H	7.65×10^{-6}	$\text{mol (Pa m}^3)^{-1}$
Viscosity of gas	μ_G	9×10^{-6}	Pas
Viscosity of water	μ_L	1×10^{-3}	Pas
Diffusion coefficient	D_L^h	3×10^{-9}	$\text{m}^2 \text{ s}^{-1}$
Porosity	ϕ	0.15	–
Intrinsic permeability	K	5×10^{-20}	m^2
van Genuchten parameter	n	1.49	–
Residual saturation	$S_{L,\text{res}}$	0.4	–

Note that in this work, the overall computational cost consists of three major components: the time dedicated to the solution of the local problem, the assembly of the Jacobian matrix and residual vector, and the solution of the linear equation system.

$$\tau = \tau_{\text{loc}} + \tau_{\text{asm}} + \tau_{\text{solver}}. \tag{35}$$

The local problem τ_{loc} mainly refers to the secondary variable calculation, including the thermodynamic calculation, and all derivatives of secondary variable with respect to the primary unknowns. The assembly time τ_{asm} also includes the Schur complement reduction (“Linearization strategy” section).

Benchmark II: heat pipe problem

The heat pipe problem was proposed by Udell and Fitch (1985). In this benchmark, a heater is installed on the right-hand side of the horizontal column with an initial water saturation of 0.5. It generates a constant heat flux of 100 W m^{-2} and raises the temperature gradually above the boiling point. Here, both thermal convection and conduction are considered along with the latent heat transfer, i.e., evaporation and condensation. In this context, the parameters used in this benchmark are listed in Table 2. The heat conductivity for an unsaturated medium is given as

$$\lambda(S_G) = \lambda_{\text{pm}}^{S_L=0} + \sqrt{(1 - S_G)} \left(\lambda_{\text{pm}}^{S_L=1} - \lambda_{\text{pm}}^{S_L=0} \right). \tag{36}$$

The Leverett function (Leverett et al. 1941) and Brooks–Corey relationship (Brooks and Corey 1964) are applied to describe the dependency of capillary pressure and relative permeability on saturation. For the fluid properties of water, the IAPWS (Wagner et al. 2000) formulation is applied.

In this simulation, the comparison is made with adaptive time-stepping control. The initial and minimal time-step size Δt_{min} is set to 100 s, and the maximum time-step size Δt_{max} is allowed to be 10^9 s.

Benchmark III: Kueper experiment

Kueper and Frind (1991) performed an experiment where the DNAPL phase penetrated into an initially water-saturated ($S_L = 0$) heterogeneous porous medium. A 50×70 cm tank is packed with four types of sand. The Brooks–Corey model is applied to describe the dependency of capillary pressure and relative permeability on saturation. The simulation is performed on an unstructured meshes with varying number of elements. A fixed time-step size $\Delta t = 20$ s is adopted and lasts for a span of 800 s. The parameters used in this benchmark are listed in Tables 3 and 4. Both NCP formulations are applied in comparison with the PVS approach. In the simulation, a modification is made regarding the original experiment assumption by allowing the dissolution of DNAPL which enables the gradual phase appearance. The focus therefore lies on the DNAPL phase appearance in heterogeneous porous medium, as well as the influence of highly contrasted capillary pressure and relative permeability properties. Special interests are also focused on the numerical dispersion, which tends to occur at the interface of different materials, as well as phase boundaries.

Results

The MoMaS benchmark

In Fig. 1, the simulated saturation and liquid phase pressure are compared against reference values obtained by PVS approach. Both the local and global NCP formulations are able to correctly reproduce the characteristic features of the MoMaS benchmark, as shown by the excellent agreement of simulated and reference solutions.

Regarding the efficiency, two phenomena are observed. (1) In comparison with the PVS approach, both NCP formulations exhibit better efficiency in terms of Newton convergence speed (Fig. 2b; Table 5). In particular with the most refined mesh (4×10^5 elements), both NCP formulations cost roughly 15% fewer Newton iterations. (2) As shown in Fig. 3, when phase transition occurs (gas phase appears at around 1.4×10^5 a, and vanishes at 7×10^5 a), the minimum time-step size of the PVS approach decreases to about 600 a. In comparison, the two NCP formulations are able to take time-step sizes of 4000 a. The possibility of larger time steps illustrates both efficiency and robustness,

Table 2 Parameters applied in the heat pipe problem

Parameters name	Symbol	Value	Unit
Intrinsic permeability	K	10^{-12}	m^2
Porosity	ϕ	0.4	–
Latent heat of vaporization of water	$h_{\Delta e}$	2258	$kJ\ kg^{-1}$
Heat conductivity of fully saturated porous medium	$\lambda_{pm}^{S_L=1}$	1.13	$W\ (m\ K)^{-1}$
Heat conductivity of dry porous medium	$\lambda_{pm}^{S_L=0}$	0.582	$W\ (m\ K)^{-1}$
Heat capacity of the soil grains	c_s	700	$J\ (kg\ K)^{-1}$
Density of the soil grain	ρ^s	2600	$kg\ m^{-3}$
Density of the water	ρ^w	1000	$kg\ m^{-3}$
Density of the air	ρ^a	0.08	$kg\ m^{-3}$
Dynamic viscosity of water	μ^w	2.938×10^{-4}	Pas
Dynamic viscosity of air	μ_G^a	2.08×10^{-5}	Pas
Dynamic viscosity of steam	μ_G^w	1.20×10^{-5}	Pas
Diffusion coefficient of air in gas	D_G^a	2.6×10^{-5}	$m^2\ s^{-1}$
Diffusion coefficient of air in liquid water	D_L^a	3×10^{-9}	$m^2\ s^{-1}$

Table 3 Fluid and medium properties in Kueper experiment

Parameter	Symbol	Value	Unit
Density of water	ρ^w	1000	$kg\ m^{-3}$
Density of DNAPL	ρ^D	1460	$kg\ m^{-3}$
Viscosity of liquid phase	μ_L	1×10^{-3}	Pas
Viscosity of non-wetting phase	μ_N	0.9×10^{-3}	Pas
Molar mass of water	M^w	0.01	$kg\ mol^{-1}$
Molar mass of DNAPL	M^D	0.1414	$kg\ mol^{-1}$
Porosity	ϕ	0.3	–
Henry constant	H	1×10^{-3}	$mol\ (Pa\ m^3)^{-1}$
Gravitational acceleration	g	9.8	$m\ s^{-2}$

Table 4 Hydraulic properties of sands for the Brooks–Corey model

Property	P_e (Pa)	$\lambda(-)$	$S_{wr}(-)$	$k(m^2)$	$n(-)$
1	369.73	3.86	0.078	5.04×10^{-10}	0.40
2	434.45	3.51	0.069	2.05×10^{-10}	0.39
3	1323.95	2.49	0.098	5.26×10^{-11}	0.39
4	3246.15	3.30	0.189	8.19×10^{-12}	0.41

and this feature is not altered by the increasing number of elements (Fig. 2a).

In the second test, both NCP formulations require similar Newton iterations with a slightly better behavior of local NCP on the finer mesh (Table 6). We further plot the number of Newton iterations per time step required by two formulations in Fig. 4. When the phase transition occurs, the global NCP requires one more iterations per time step over the local one.

Furthermore, the computational time dedicated to the local problem-solving, the assembly, and linear solver is

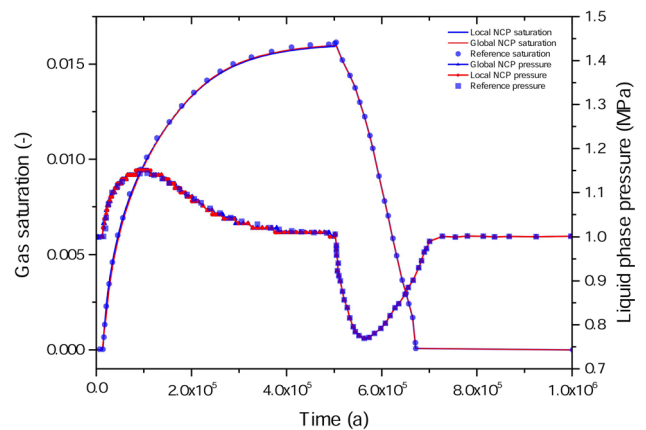


Fig. 1 Evolution of gas phase saturation (left axis) and liquid phase pressure (right axis) at the inflow boundary over the total simulation time for global and local NCP formulation, compared against the results generated by PVS approach

listed in Table 6 and depicted in Fig. 5, to reveal their different requirements on computational resources. The global NCP formulation is observed to be consistently 10–

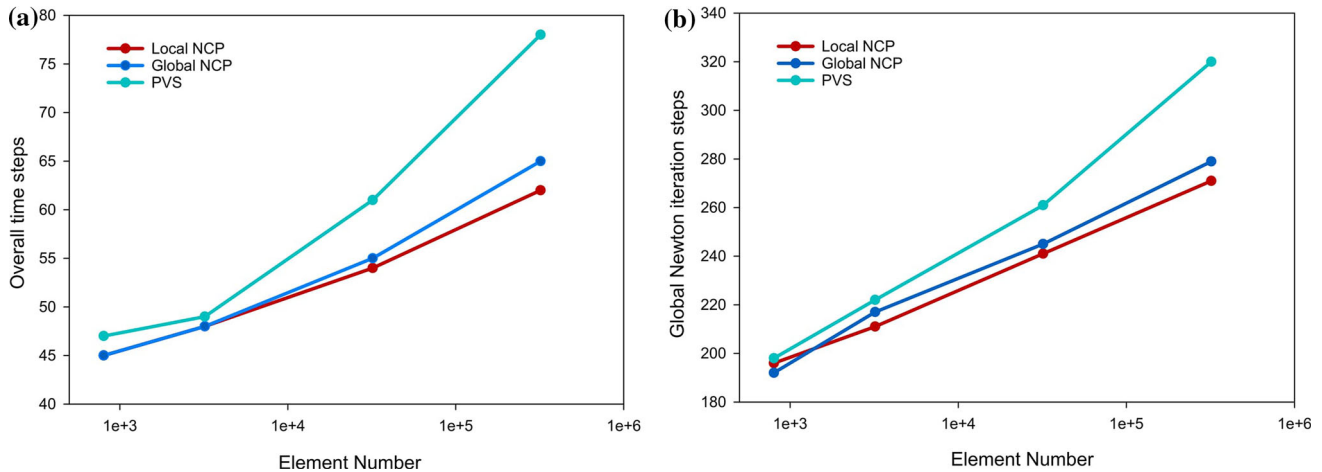


Fig. 2 Overall time steps (a) and global Newton iteration steps evolution (b) for varying number of elements, compared against the results produced by primary variable switching (PVS) model

Table 5 Comparison of numerical behavior between two NCP formulations and PVS approach under adaptive time-stepping control for the simulation of MoMaS benchmark (GNCP and LNCP indicate the global and local NCP formulations, respectively)

Element	Newton iterations			CPU time (s): total/per Newton		
	GNCP	LNCP	PVS	GNCP	LNCP	PVS
800	192	196	198	134/0.683	141.4/0.734	136/0.681
4000	217	211	222	387/1.834	443/2.041	391/1.76
40,000	245	241	264	16,158/67.05	19,305/78.8	16,793/63.061
400,000	279	271	314	227,480/839.41	254,560.8/912.40	260,925/830.79

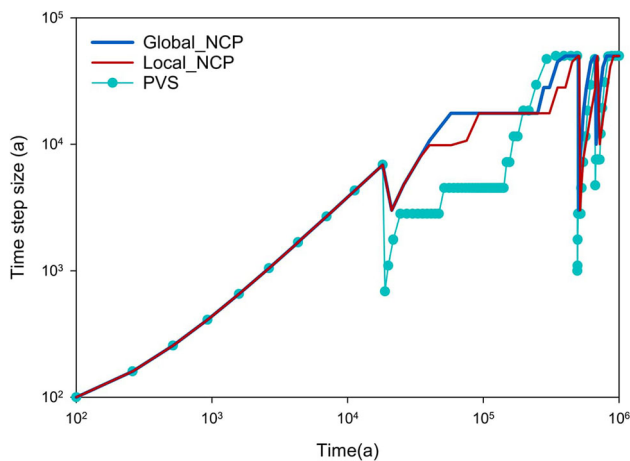


Fig. 3 Evolution of time-step size with respect to the overall simulation time required by three different numerical schemes to simulate the heat pipe problem with a mesh of 4000 elements

20% faster than the local one. As no nested Newton iterations are required to solve local thermodynamic equilibrium, it leads to an approximately 20% faster local problem solution. The global NCP requires about 10% more time for the linear solver. Such a difference can be attributed to

the fact that, in global NCP, the variation of the Jacobian matrix structure (Sect. 3.2) degrades the performance of preconditioner operation prior to the linear solver. With regard to the assembly time, the global NCP requires up to 5% more time over the local one. That might be because of using the Schur complement strategy. However, such difference only accounts for 3% of overall computational time. It is further observed that the local problem-solving represents about 60–70% of the entire computational time, which favors the global NCP. Further tests with different mesh sizes show that the advantage of the global NCP is consistent from a coarse mesh of 800 elements up to a refined mesh of 4×10^5 elements (Table 6).

The heat pipe problem

In Fig. 6, the evolution of liquid saturation and temperature under steady state is plotted over the domain. Figure 7 presents the relative deviation of liquid saturation and temperature compared against the analytical solution in terms of global and local NCP formulation. A good agreement can be found between NCP formulations and the semi-analytical solution. The numerical performance and

Table 6 Comparison of numerical behavior between global and local NCP formulation under constant time-step size for the simulation of MoMaS benchmark

Element	Newton		Linear solver (s)		Local problem (s)		Global assembly (s)	
	GNCP	LNCP	GNCP	LNCP	GNCP	LNCP	GNCP	LNCP
800	581	584	69.186	66.85	378.78	421.502	6.345	5.08
4000	611	608	364.34	384.34	1585.13	1816.48	89.997	80.23
40,000	661	648	5311.9	5129.96	19,845.12	23,159.98	3201.91	3020.65
400,000	839	811	64,370.8	63381.5	163,110.9	201,079	27,161.9	25,614

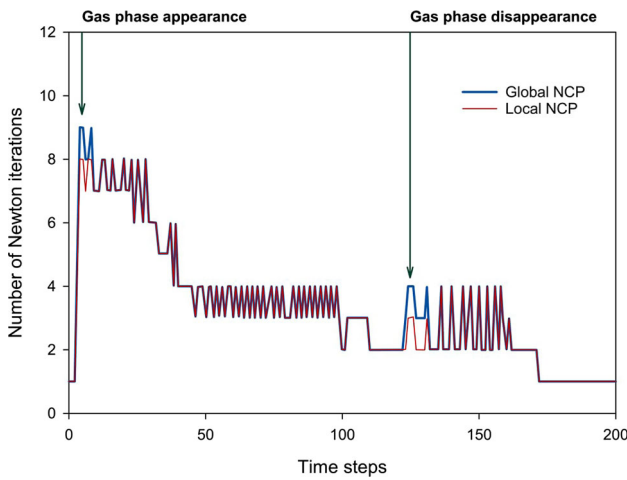


Fig. 4 The number of global Newton iterations per time step for two NCP formulations with a mesh of 40,000 elements

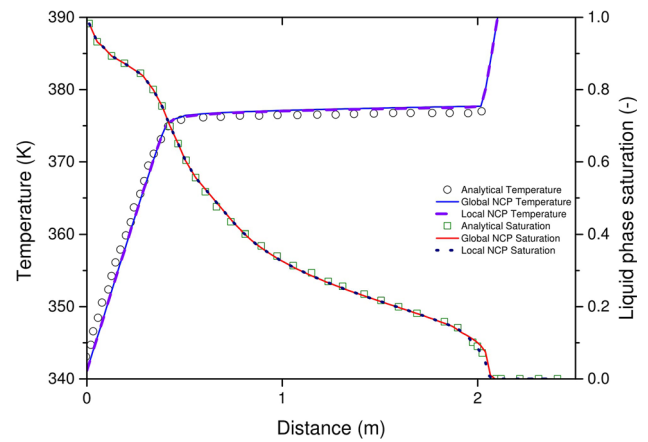


Fig. 6 Evolution of liquid saturation (right axis) and temperature (left axis) over the whole domain at the steady state, compared against semi-analytical solution (scatter symbol) as well as the results of PVS scheme (dot curve)

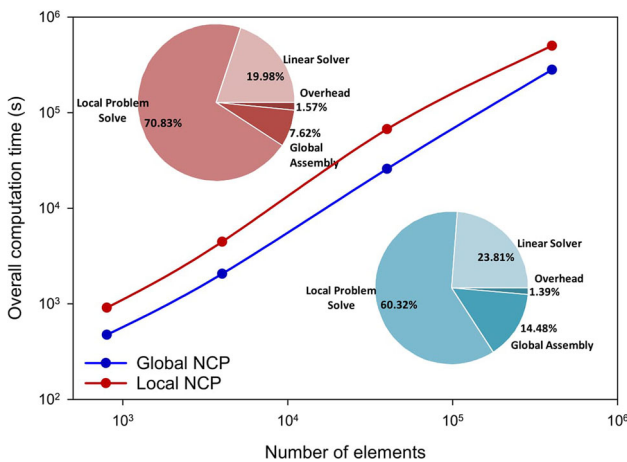


Fig. 5 Comparison of overall computation time for varying number of elements. The Pie charts represent the computation time distribution on a mesh with 4×10^5 elements for local NCP scheme (upper-left) and global NCP scheme (bottom-right), respectively

computational cost of both NCP formulations are compared against that of the PVS approach. Detailed information regarding mesh size, overall computation time, total time steps, and global Newton iterations is listed in Table 7. It is observed that both NCP formulations require

approximately 15% fewer overall time steps and 25% fewer Newton iterations in comparison with the PVS approach. Figure 8 exhibits the overall and averaged Newton iterations required by the three different models. Although the local NCP requires a lower number of total time steps and Newton iterations, the global NCP is the most efficient formulation in all considered cases with the least computational time. Besides, Fig. 9 provides the time-step size evolution with respect to the simulation time for three models. It highlights that after about 0.8×10^6 s, the time-step size in PVS scheme starts to break down to a very small value (around 1000 s), which is triggered by the complete evaporation of the liquid phase in the vicinity of the heated boundary. Similar trend can be observed in both NCP formulations. Yet, the allowed step sizes are much larger (around 5000 s).

Moreover, the distribution of time spent on different parts of the simulation produces identical results to those obtained in the MoMaS benchmark. Figure 10 demonstrates that the global NCP consumes around 30% less time on the local problem at the expense of spending approximately 15% more time on linear solver and 10% more assembly time over the local one. This again leads to 25% savings in the overall computational time.

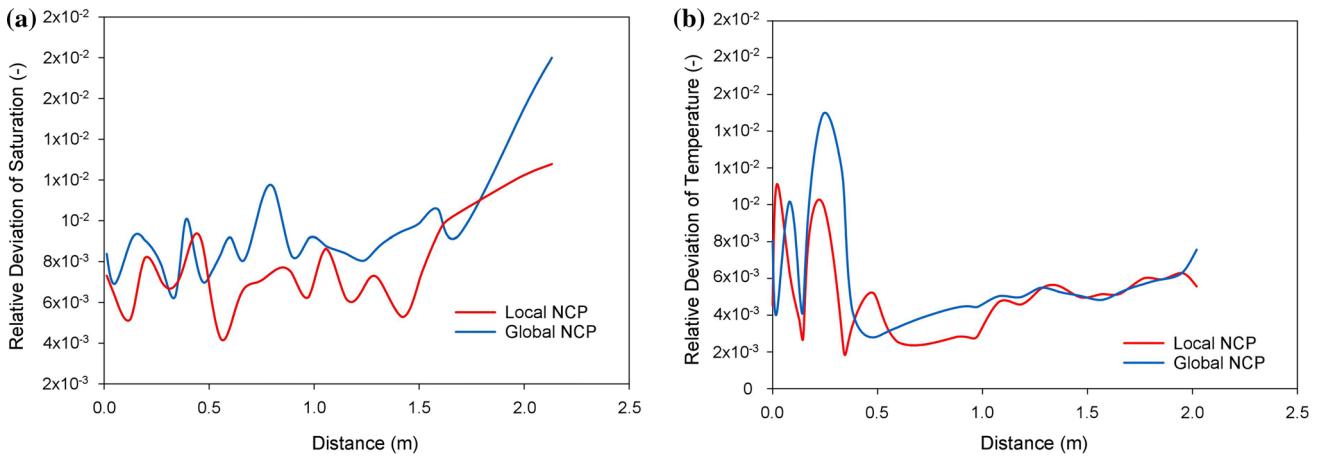


Fig. 7 Relative deviation of saturation and temperature compared against the semi-analytical solution

Table 7 Comparison of numerical behavior between global and local NCP formulations and the PVS model for heat pipe problem under adaptive time-stepping control

Elements	Total steps			Newton iterations			CPU time (s)		
	GNCP	LNCP	PVS	GNCP	LNCP	PVS	GNCP	LNCP	PVS
1600	214	211	334	746	735	1534	8592	10,840.1	17,430.7
3200	329	325	503	1216	1195	2154	31,984	35,820.4	47,812
6400	351	347	516	1421	1401	2214	71,550	89,781	102,308
12,800	579	570	745	2120	2081	3052	246,317	294,521	332,521

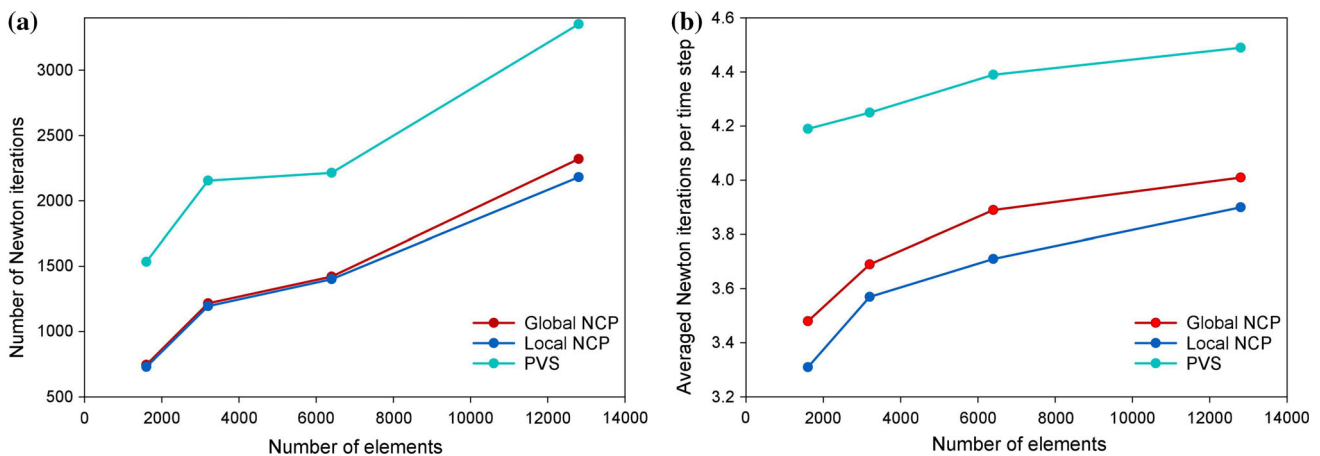


Fig. 8 Overall Newton iterations and averaged Newton iterations per time step required by both NCP formulations for varying number of elements, compared against the results generated by PVS model

Kueper experiment

Figure 11 demonstrates that both NCP formulations are capable of reproducing the DNAPL plume propagation through heterogeneous permeable sandy layers while bypassing the impermeable ones. To compare the numerical dispersion at the interface of different media and phase boundary, Fig. 12 plots the horizontal profile capillary pressure at a depth of 0.45 m at $t = 320$ s, generated by the two NCP formulations and the PVS approach. The results

produced by the PVS approach are observed to exhibit severe over- and undershooting. The oscillating capillary pressure can be clearly identified at phase boundary. In both NCP formulations, these oscillations are reduced significantly, as shown by the red and green profiles in Fig. 12. The minimum capillary pressure simulated by global and local NCP formulations is 365.46 and 369.06 Pa at the phase boundary, while the entry pressure is 369 Pa. Such numerical oscillation imposes challenge in nonlinear solver which can be represented in the Newton iterations

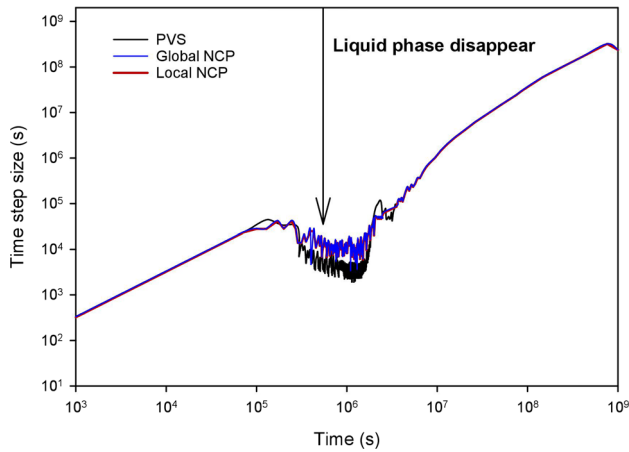


Fig. 9 Evolution of time-step size for three different models on a mesh with 1600 elements

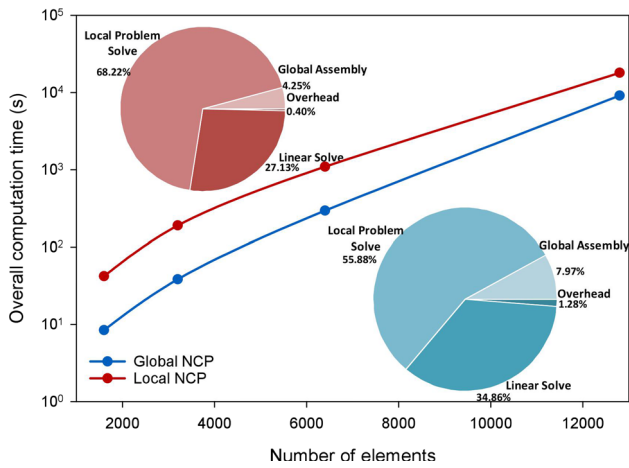


Fig. 10 Comparison of overall computation time for varying number of elements. The pie charts represent the computational time distribution on a mesh with 12,800 elements for the local NCP (upper-left) and global NCP formulations (bottom-right), respectively

required by different models. Table 8 illustrates local NCP is the most robust model with the least number of Newton iteration required. Nevertheless, the global NCP delivers the fastest simulation due to the least CPU time cost, although up to 10% more Newton iterations are required over the local NCP.

Furthermore, the overall computational effort is also compared in terms of detailed computational complexity, as shown in Fig. 13. The same tendency is observed as in the previous benchmarks. The global NCP consumes 10% more linear solver time, while it benefits from 25% less time spent on solving local constitutive problems. All these contribute to approximately 15% savings in the overall computation time (cf. Table 9).

Discussion

Comparison between NCP formulations and PVS approach

With the conventional PVS approach, when phase transition occurs, primary variables have to be switched between saturation S_α and phase composition x_α^i . On the one hand, the local switch of primary variables associated within different elements, which might degrade convergence of the nonlinear solver or even failure. On the other hand, primary variable switching might result in the conservation equations becoming redundant. Therefore, the rank of global Jacobian matrix is constantly changing along with the phase status, which further degrades the linear solver performance. Such problems are obviously addressed in the simulated benchmarks. In comparison, a fixed set of primary unknowns and governing equations are adopted in both NCP formulations. This feature enables the nonlinear system produced by NCP to be solved by semi-smooth Newton iterations with quadratic convergence.

Furthermore, with the NCP constraints, all state variables remain within the physical boundary during Newton iterations. Such feature enables the NCP formulations to be robust when only a small amount of a certain component is present in the system. One example is the heat pipe problem. At the heated boundary, after the boiling temperature is reached (about 2×10^5 s), air is driven away by the water vapor such that its molar fraction approaches zero (cf. Fig. 9). In this case, the air molar fraction can be easily driven into negative values during the global Newton iterations. Such non-physical values can result in more nonlinear iterations or even divergence. The conventional strategy that is applied in the PVS approach is to decrease the time-step size and set a small tolerance, e.g., 10^{-9} , for the global Newton iteration. Nevertheless, by applying the NCP constraints on the molar fraction, non-physical values can be avoided and a relatively larger time-step size is allowed in comparison with the PVS approach. The improvements are demonstrated in Fig. 9.

It is worth noting that in terms of the computational time per Newton iteration, the NCP formulations are slower than the PVS approach (cf. Tables 5, 7, 8). That is because, when phase disappearance occurs, the NCP formulations still require the calculation of the phase composition in the absent phase, which is achieved by assuming the thermodynamic equilibrium between the present phase and the absent phase. Such calculations can be skipped in PVS approach by simply setting the state variables to zero. However, in most cases of compositional two-phase flow, the higher computational cost per Newton iteration can be amortized by fewer time steps and fewer global Newton iterations.

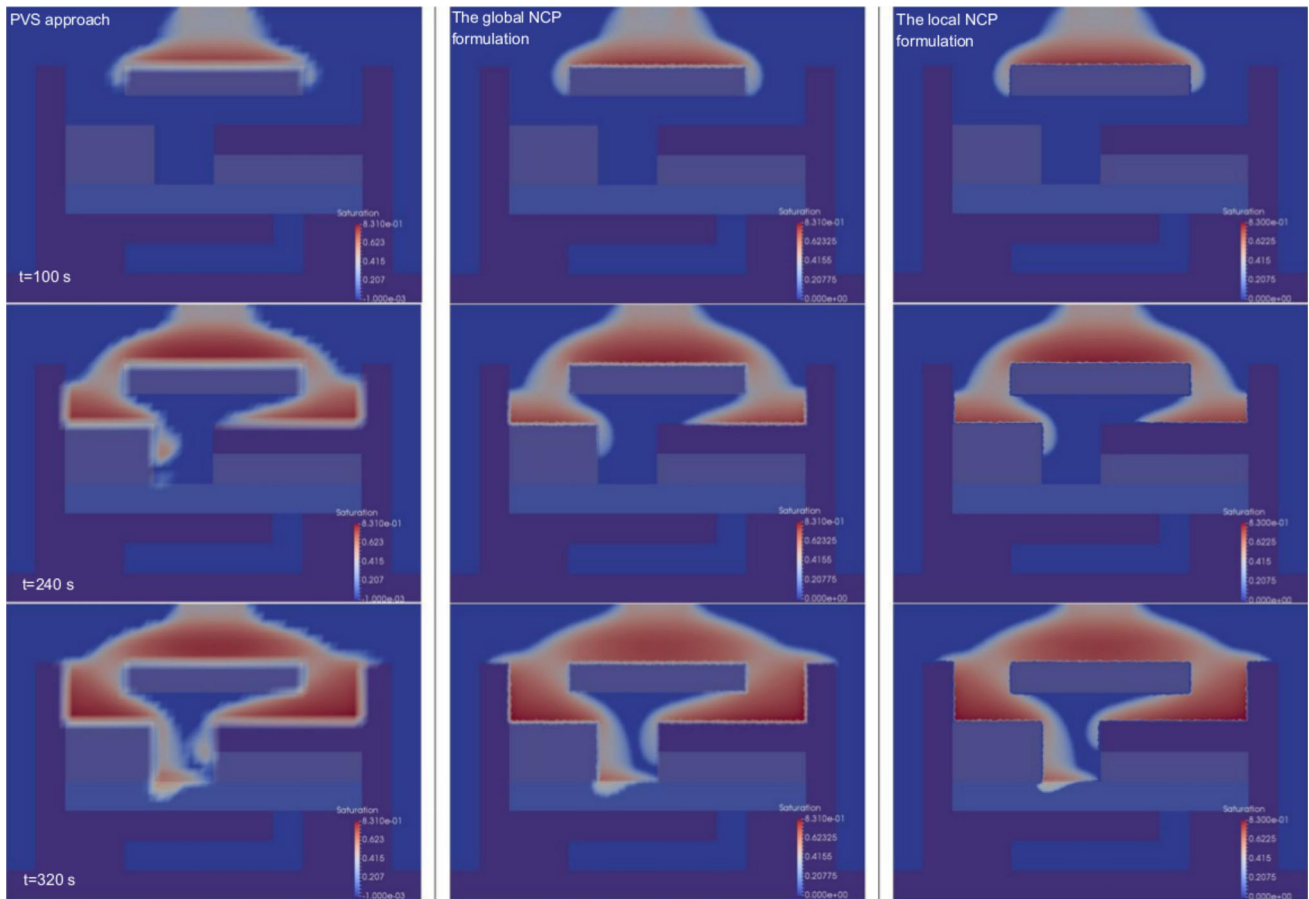


Fig. 11 Comparison of the DNAPL saturation obtained by different models with respect to different time steps (100, 240, 320 s) on a coarse mesh (2000 elements). The left column is the results from PVS

approach. The middle column shows the results of global NCP formulation. The right column represents the results of local NCP formulation

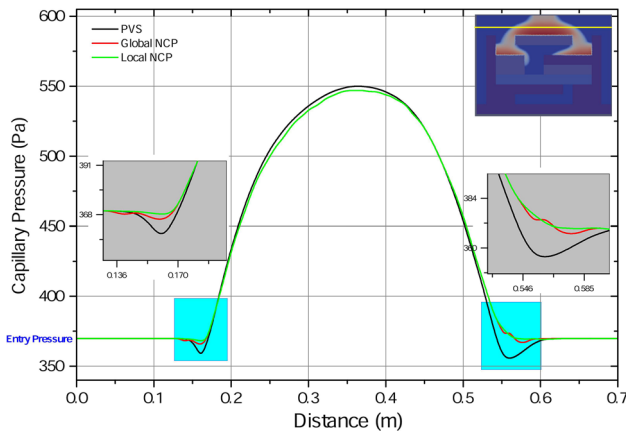


Fig. 12 Comparison of horizontal capillary pressure profile at $z = 0.45$ m

Comparison of local and global NCP implementations

In this section, the advantages and drawbacks of both NCP formulations are discussed in several aspects.

Computational cost

In the local NCP formulation, a nested Newton scheme is required to handle the nonlinearity associated with thermodynamic model and NCP constraints, whereas in global NCP, the thermodynamic model and NCP constraints are coupled with conservation equations and solved within the same Newton loop. Such consistent treatment has the advantage that no nested iteration is necessary for capturing phase transition. This feature significantly relieve the nonlinearity on local level; therefore, global NCP exhibits a higher computational efficiency for local problem-solving.

After applying the Schur complement procedure, the linear system in the global NCP is in the same size as the local one. Such operation is demonstrated to only account for a small computational resources (remains below 3% of the entire computational time). However, it can be observed that an implicit “switch” of the secondary variables is included in the linear equation system [Eqs. (31) and (32)], which could potentially degrade the

Table 8 Comparison of numerical behavior between different models in Kueper benchmark

Elements	Newton steps			CPU time (s): total/per Newton		
	GNCP	LNCP	PVS	GNCP	LNCP	PVS
500	122	129	143	41.85/0.34	79.12/0.61	45.78/0.32
2000	154	143	175	131.28/0.85	187.81/1.071	151.6/0.846
8000	179	175	197	1081.9/6.045	1248.19/7.133	1353.41/5.868
40,000	201	191	244	13,997.73/69.63	15,701.3/81.2	17,154.41/66.58
400,000	214	198	318	278,511.4/1201.6	319,724.9/1604.4	337,562.47/1061.5

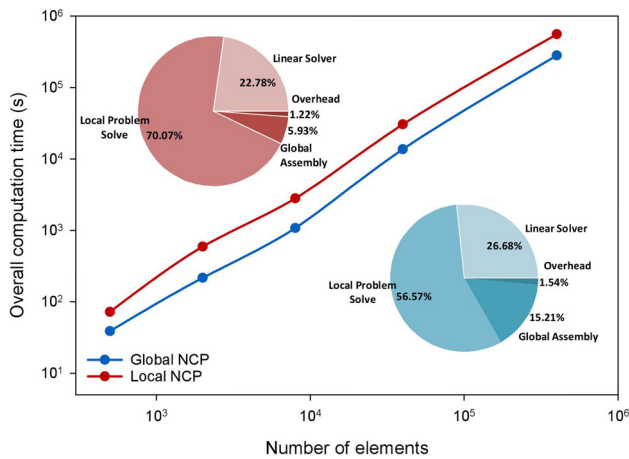


Fig. 13 Comparison of overall computation time for varying number of elements in the simulation of Kueper problem. The pie charts represent the computation time distribution on a mesh with 4×10^5 elements for local NCP (upper-left) and global NCP formulations (bottom-right)

preconditioner performance during the linear solve. Meanwhile, the entries in the global Jacobian matrix of the global NCP have a wider range in magnitudes. Such difference can potentially cause a singular or ill-conditioned matrix, and the resulting linear system requires a strong preconditioner for solution, and also more iterations during it. Such challenges are evident in all simulated cases as more linear solver time is required by the global NCP formulation.

To summarize, due to the tight coupling and strong nonlinearity incorporated in compositional two-phase flow, local problem-solving often claims the majority of total computational effort, which makes the global NCP

formulation the most efficient. However, as pointed out by Lauser (2013), the linear solver is the main limiting factor for the parallel performance, whereas the local problem-solving and the assembly can achieve more than 100% speedup with up to 256 cores. This suggests that, with the parallel scheme applied, the local NCP formulation might again be favorable.

Model robustness

The benchmarks simulated here show that material heterogeneity has a big impact on the model accuracy and robustness. Within a homogeneous medium, both local and global NCP formulations give smooth and accurate results; meanwhile, similar Newton iterations and time steps are required with a slightly better behavior of the local NCP formulation. Such advantages are further increased in heterogeneous medium (e.g., the Kueper problem). The local NCP gives more stable and accurate results compared to the global one, as reflected by the smooth curve shown at the material interfaces and phase boundary in Figs. 11 and 12. The oscillation at the material interface and phase boundary originates from the nature of the problem. In heterogeneous media, all secondary variables as well as the NCP formulations have to be calculated within a representative volume holding the same material properties. In the local NCP, saturation and all its dependencies are clearly defined in each material domain, while in the global NCP, the saturation is a compound value defined on the nodal level, reflecting the contributions from all neighboring material domains simultaneously.

Table 9 Comparison of distribution of overall computation resources between global and local NCP formulation in Kueper benchmark

Elements	Linear solve (s)		Local problem (s)		Global assembly (s)	
	GNCP	LNCP	GNCP	LNCP	GNCP	LNCP
500	7.93	7.35	31.8	39.38	1.1	0.9
2000	32.95	30.53	182.83	224.43	5.3	3.8
8000	171.7	160.17	801.02	1017.15	38.27	32.9
40,000	3313.73	3013.75	9185.62	10,344.41	1501.8	1350.69
400,000	78,684.47	72,033.9	162,744.95	213,430	37,083.21	34,410.9

Conclusions

In this work, two different implementations of the nonlinear complementary problems (NCP) have been compared for simulating (non)-isothermal compositional two-phase flow with phase transition phenomena. Three well-established benchmarks have been employed to analyze the efficiency and robustness of these numerical models. It is found that both local and global NCP formulations deliver results in good agreement with those from conventional primary variable switching (PVS) approaches. It is also found that NCP formulations are numerically more robust and efficient for handling phase transition, as shown by the fewer global Newton iterations and larger time-step sizes. In both homogeneous and heterogeneous media, the global NCP formulation is around 20% faster than the local one. However, in heterogeneous media, the local NCP formulation is recommended, as it delivers a more accurate and stable evaluation of capillary pressure and relative permeability. The slightly longer computation time is a good trade-off for suppressing numerical oscillations at the interface of different media or at the location of phase transition.

Acknowledgements This work is funded by the Helmholtz Association through the program POF III-R41 “Geothermal Energy Systems.” The first author would also like to acknowledge the Chinese Scholarship Council (CSC) for financially supporting his Ph.D. study in Germany.

Appendix

The constitutive relationships

We consider a generic system consisting of two phases $\alpha \in [G, L]$ and two components $i \in [a, b]$, in which a denotes the gas component which is allowed to dissolve in the liquid phase and b indicates the water component and can vaporize into the gas phase. The local thermodynamic equilibrium is described by fugacity equalities for each component:

$$f_G^i = f_L^i, \quad i \in [a, b], \tag{37}$$

where f_G^i and f_L^i are the fugacities of i th component in gas and liquid phase, respectively. They can be described as follows:

$$f_\alpha^i = \Phi_\alpha^i x_\alpha^i P_\alpha, \tag{38}$$

Here, Φ_α^i indicates the fugacity coefficient. Due to the assumption that the gas behaves as an ideal gas, we have $\Phi_G^i = 1$. Then, in the gas phase, we have:

$$f_G^i = x_G^i P_G, \quad i \in [a, b]. \tag{39}$$

If the solubility of gas component in the liquid phase is assumed to be low, the molar fraction x_L^a can be determined by Henry’s law

$$x_L^a = \frac{P_G H^a(T)}{N_L} x_G^a, \tag{40}$$

where N_L indicates the molar density of liquid phase and $H^a(T)$ is the Henry coefficient for gas component a , which is only dependent on temperature T . For example, in heat pipe problem (Sect. 4.3), the temperature dependence of the Henry coefficient of air dissolved in water is given by (Helmig et al. 1997)

$$H^a(T) = (0.8942 + 1.47 \exp(-0.04394T)) \times (1e - 10). \tag{41}$$

Then, the molar fraction of the water component b in the liquid phase is characterized by the Raoult law:

$$x_L^b = \frac{P_G}{P_{\text{vap}}} x_G^b, \tag{42}$$

with P_{vap} standing for the vapor pressure of water component, and it is further regulated as follows:

$$P_{\text{vap}} = P_{\text{sat}} \exp\left(\frac{P_G - P_L}{N_L R T}\right) \tag{43}$$

with P_{sat} indicating the vapor saturation pressure of pure water, which is given by Clausius–Clapeyron equation

$$P_{\text{sat}}(T) = P_0 \exp\left[\left(\frac{1}{T_0} - \frac{1}{T}\right) \frac{h_{\Delta e} M^w}{R}\right], \tag{44}$$

where $T_0 = 373\text{K}$, $P_0 = 10^5\text{Pa}$, $h_{\Delta e}$ is enthalpy of vaporization, and M^w is molar mass of water.

References

Abadpour A, Panfilov M (2009) Method of negative saturations for modeling two-phase compositional flow with oversaturated zones. *Transp Porous Media* 79(2):197–214

Bastian P (2014) A fully-coupled discontinuous Galerkin method for two-phase flow in porous media with discontinuous capillary pressure. *Comput Geosci* 18(5):779–796

Bourgeat A, Jurak M, Smaï F (2009a) Two-phase, partially miscible flow and transport modeling in porous media; application to gas migration in a nuclear waste repository. *Comput Geosci* 13(1):29–42

Bourgeat A et al (2009b) Numerical test data base. http://math.univ-lyon1.fr/homes-www/bourgeat/MoMaS/cas_test.html. Accessed 20 Sept 2017

Brooks RH, Corey AT (1964) Hydraulic properties of porous media and their relation to drainage design. *Trans ASAE* 7(1):26–0028

Cao H (2002) Development of techniques for general purpose simulators. Ph.D. Thesis, Stanford University Stanford, CA

- Class H, Helmig R, Bastian P (2002) Numerical simulation of non-isothermal multiphase multicomponent processes in porous media: 1. an efficient solution technique. *Adv Water Resour* 25(5):533–550
- Coats KH et al (1980) An equation of state compositional model. *Soc Pet Eng J* 20(05):363–376
- Facchinei F, Pang JS (2007) *Finite-dimensional variational inequalities and complementarity problems*. Springer, Berlin
- Firoozabadi A (1999) *Thermodynamics of hydrocarbon reservoirs*. McGraw-Hill, New York
- Forsyth P (1994) Three-dimensional modelling of steam flush for dnapl site remediation. *Int J Numer Methods Fluids* 19(12):1055–1081
- Gopal V, Biegler LT (1999) Smoothing methods for complementarity problems in process engineering. *AIChE J* 45(7):1535–1547
- Hager C, Wohlmuth BI (2010) Semismooth newton methods for variational problems with inequality constraints. *GAMM-Mitteilungen* 33(1):8–24
- Helmig R et al (1997) *Multiphase flow and transport processes in the subsurface: a contribution to the modeling of hydrosystems*. Springer, Berlin
- Hoteit H, Firoozabadi A (2008) Numerical modeling of two-phase flow in heterogeneous permeable media with different capillarity pressures. *Adv Water Resour* 31(1):56–73
- Huang Y, Kolditz O, Shao H (2015) Extending the persistent primary variable algorithm to simulate non-isothermal two-phase two-component flow with phase change phenomena. *Geotherm Energy* 3(1):1–23
- Kolditz O, Bauer S, Bilke L, Böttcher N, Delfs JO, Fischer T, Görke UJ, Kalbacher T, Kosakowski G, McDermott C et al (2012) OpenGeoSys: an open-source initiative for numerical simulation of thermo-hydro-mechanical/chemical (THM/C) processes in porous media. *Environ Earth Sci* 67(2):589–599
- Kräutle S (2011) The semismooth newton method for multicomponent reactive transport with minerals. *Adv Water Resour* 34(1):137–151
- Kueper BH, Frind EO (1991) Two-phase flow in heterogeneous porous media: 1. Model development. *Water Resour Res* 27(6):1049–1057
- Lauser A (2013) *Theory and numerical applications of compositional multi-phase flow in porous media*. Dissertation Zugl.: Stuttgart University
- Lauser A, Hager C, Helmig R, Wohlmuth B (2011) A new approach for phase transitions in miscible multi-phase flow in porous media. *Adv Water Resour* 34(8):957–966
- Leverett M et al (1941) Capillary behavior in porous solids. *Trans AIME* 142(01):152–169
- Marchand E, Müller T, Knabner P (2012) Fully coupled generalised hybrid-mixed finite element approximation of two-phase two-component flow in porous media. part ii: numerical scheme and numerical results. *Comput Geosci* 16(3):691–708
- Marchand E, Müller T, Knabner P (2013) Fully coupled generalized hybrid-mixed finite element approximation of two-phase two-component flow in porous media. part i: formulation and properties of the mathematical model. *Comput Geosci* 17(2):431–442
- Masson R, Trenty L, Zhang Y (2014) Formulations of two phase liquid gas compositional Darcy flows with phase transitions. *Int J Fin Vol* 11:34
- Michelsen ML (1982) The isothermal flash problem. part i. stability. *Fluid Phase Equilib* 9(1):1–19
- Moortgat J, Li Z, Firoozabadi A (2012) Three-phase compositional modeling of CO₂ injection by higher-order finite element methods with CPA equation of state for aqueous phase. *Water Resour Res* 48(12):W12511
- Neumann R, Bastian P, Ippisch O (2013) Modeling and simulation of two-phase two-component flow with disappearing nonwetting phase. *Comput Geosci* 17(1):139–149
- Nishida A (2010) Experience in developing an open source scalable software infrastructure in Japan. In: *Computational science and its applications—ICCSA 2010*, Springer, pp 448–462
- Nordbotten JM, Celia MA (2011) *Geological storage of CO₂: modeling approaches for large-scale simulation*. Wiley, New York
- Ouellette DV (1981) Schur complements and statistics. *Linear Algebra Appl* 36:187–295
- Panfilov M, Panfilova I (2014) Method of negative saturations for flow with variable number of phases in porous media: extension to three-phase multi-component case. *Comput Geosci* 18(3–4):385–399
- Siavashi M, Blunt MJ, Raisee M, Pourafshary P (2014) Three-dimensional streamline-based simulation of non-isothermal two-phase flow in heterogeneous porous media. *Comput Fluids* 103:116–131
- Sleep B, Sykes J (1989) Modeling the transport of volatile organics in variably saturated media. *Water Resour Res* 25(1):81–92
- Udell K, Fitch J (1985) Heat and mass transfer in capillary porous media considering evaporation, condensation, and non-condensable gas effects. In: *23rd ASME/AIChE national heat transfer conference*, Denver, CO, pp 103–110
- Voskov DV, Tchalepi HA (2012) Comparison of nonlinear formulations for two-phase multi-component eos based simulation. *J Pet Sci Eng* 82:101–111
- Wagner W, Cooper J, Dittmann A, Kijima J, Kretschmar HJ, Kruse A, Mares R, Oguchi K, Sato H, Stocker I et al (2000) The IAPWS industrial formulation 1997 for the thermodynamic properties of water and steam. *J Eng Gas Turbines Power* 122(1):150–184
- Wang W, Kosakowski G, Kolditz O (2009) A parallel finite element scheme for thermo-hydro-mechanical (thm) coupled problems in porous media. *Comput Geosci* 35(8):1631–1641
- Whitson CH, Michelsen ML (1989) The negative flash. *Fluid Phase Equilib* 53:51–71
- Wu YS, Forsyth PA (2001) On the selection of primary variables in numerical formulation for modeling multiphase flow in porous media. *J Contam Hydrol* 48(3):277–304
- Xu T, Senger R, Finsterle S (2008) Corrosion-induced gas generation in a nuclear waste repository: Reactive geochemistry and multiphase flow effects. *Appl Geochem* 23(12):3423–3433
- Zhang Z, Agarwal R (2013) Numerical simulation and optimization of CO₂ sequestration in saline aquifers. *Comput Fluids* 80:79–87
- Zidane A, Firoozabadi A (2015) An implicit numerical model for multicomponent compressible two-phase flow in porous media. *Adv Water Resour* 85:64–78

A.3 CODE AVAILABILITY

All the numerical algorithms and models are implemented in the framework of OpenGeoSys (V.6). OpenGeoSys is an open source scientific software and freely available to use. The source codes corresponded to each benchmark or application case are listed in the follow, and they can be freely accessed by following the instruction at: <http://www.opengeosys.org/>.

- The Benchmark I: Drying by gas injection presented in Section 8.1.1 adopts the source code at:
https://github.com/Yonghui56/ogs/tree/Andra_case
 Note that it is a modified version of "TwoPhaseComponentPP" process in official OpenGeoSys (V.6). The difference is a modified van Genuchten curve is adopted in order to keep consistent with the original benchmark concept.
- All the benchmark cases presented in Section 8.2 adopt the source code at:
 1. For the isothermal cases: https://github.com/Yonghui56/ogs/tree/twophasecomponentpp_co2.
 Note that it is a modified version of "TwoPhaseComponentPP" process in official OpenGeoSys (V.6). The Equation of State (EoS) for CO₂ as described in 5.2 is adopted in this model.
 2. For the non-isothermal case: <https://github.com/ufz/ogs/tree/master/ProcessLib/ThermalTwoPhaseFlowWithPP>
- The benchmarks presented in Section.8.3 adopts a modified version – OpenGeoSys-MP-LT which is also based on the framework of OpenGeoSys (V.6). The source code can be freely acquired via the link: https://github.com/Yonghui56/ogs/tree/carbonation_ncomp_altern. Meanwhile, the version of OpenGeoSys-GEM modified for the comparison and validation of the look-up table based model is available from <http://github.com/kosakowski/OGS5GEMDEV.git>. The repository also includes the input files for the benchmark calculations in the folder: `./benchmarks/LookUp-Table`. The GEM-Selektor V₃ software package used to calculate the look-up table is available from <http://gems.web.psi.ch>. The GEM-Selektor V₃ project with the thermodynamic setup and the process script is available from the last author (georg.kosakowski@psi.ch) upon request.
- The benchmarks presented in Section 1.1 adopt the source code which can be freely accessed via the following links:
 1. The local-NCP model can be found at: <https://github.com/ufz/ogs/tree/master/ProcessLib/TwoPhaseFlowWithPrho>
 2. The global-NCP model can be found at: <https://github.com/Yonghui56/ComponentialMultiphase/tree/master/UserModules/>

FemCompMultiPhaseGlobalComplementary

3. The referenced P-P model can be accessed at: <https://github.com/Yonghui56/ComponentialMultiphase/tree/master/UserModules/FemCompMultiPhasePressureForm>

- The Richards flow model which is not presented in this work but can be served as complementary model to the current work, is also implemented in the OpenGeoSys (V.6) software. The source code can be found at: <https://github.com/ufz/ogs/tree/master/ProcessLib/RichardsFlow>

LIST OF FIGURES

Figure 1	Results for varying pressure in the hydrocarbon mixture problem described in Example 1, compared against the results proposed in Watson et al. (circle symbols)	19
Figure 2	Results for varying pressure in the hydrocarbon mixture problem described in benchmark 2, compared against the results proposed in Watson et al. paper (circle symbols)	20
Figure 3	Comparison of gas phase fraction between simulation results in this work and reference results generated by conventional flash calculation method which are reported in Watson et al. for the hydrocarbon mixture	21
Figure 4	The solubility of CO ₂ in water phase at different temperature.	31
Figure 5	The solubility of brine in the gas phase at different temperature	31
Figure 6	The mass density of pure CO ₂ at different temperature	32
Figure 7	The viscosity of CO ₂ phase at different temperature	33
Figure 8	3D surface plots for the combined effects of CO ₂ addition (carbonation) and SiO ₂ addition (ASR) on pH (a), porosity (b), fluid volume (c) and quartz dissolution rate (d).[47]	47
Figure 9	Schematic illustration of the coupling strategy between two-phase multi-component transport and chemical processes via the look-up table approach[47]	48
Figure 10	The regularized van Genuchten curve for the relationship of liquid saturation and capillary pressure.	51
Figure 12	Spatial Domain of the Synthetic CO ₂ Injection Problem	55
Figure 13	Gas phase saturation profile after the CO ₂ injection of 7, 20, and 65 days	57
Figure 15	Evolution of temperature, CO ₂ saturation at different observation points	62
Figure 17	The geometry for 2-D problem	65
Figure 19	Molar fraction profile of multiple gas components at t=2, 6, 10 years	69

Figure 20	The geometry for the concrete degradation application	71
Figure 22	Mineralogical evolution with time shown as volume fractions. The porosity corresponds to $1 - (\text{sum of solid volume fractions})$. Calcite, quartz, inert phases and some part of C-S-H that make up 80 % of the volume are not shown.	73
Figure 23	Gaseous CO_2 concentration profiles at different times for case 2.	74
Figure 24	pH profiles at different times for case 2. (a): Precipitation of quartz is allowed. (b) precipitation of quartz is suppressed.	74
Figure 25	Mineralogical profile after 5 years of simulation time produced by OpenGeoSys-GEM.	75
Figure 26	Gaseous CO_2 concentration profiles at different times for benchmark case 3a.	76
Figure 27	pH profiles at different times for benchmark case 3a.	77
Figure 28	Porosity profiles at different times for benchmark case 3a.	77
Figure 29	Gaseous CO_2 concentration profiles at different times for benchmark case 3b.	78
Figure 30	pH profiles at different times for benchmark case 3b.	79
Figure 31	Porosity profiles at different times for benchmark case 3b.	79

LIST OF TABLES

Table 1	Setup and properties of generic mortar[47]	45
Table 2	The parameters used for the benchmark case of drying by gas injection	52
Table 3	Computational Performance comparison between both NCP formulation and PVS scheme	54
Table 4	The parameters used for the 2-D CO ₂ injection problem.	56
Table 5	Comparison of numerical behavior between two NCP formulations and PPC approach	58
Table 6	Parameters applied in the cold CO ₂ injection problem	59
Table 7	Parameters used for 2-D problem of co-injection CO ₂ and impurities.	66
Table 8	Maximum time step sizes for simulation cases in OpenGeoSys-GEM and fixed time step sizes in OpenGeoSys-MP-LT.	72

BIBLIOGRAPHY

- [1] A. Lauser, C. Hager, R. Helmig, and B. Wohlmuth. "A new approach for phase transitions in miscible multi-phase flow in porous media". In: *Advances in Water Resources* 34.8 (2011), pp. 957–966.
- [2] N. Spycher, K. Pruess, and J. Ennis-King. "CO₂-H₂O mixtures in the geological sequestration of CO₂. I. Assessment and calculation of mutual solubilities from 12 to 100 C and up to 600 bar". In: *Geochimica et cosmochimica acta* 67.16 (2003), pp. 3015–3031.
- [3] H. A. Watson and P. I. Barton. "Modeling phase changes in multistream heat exchangers". In: *International Journal of Heat and Mass Transfer* 105 (2017), pp. 207–219.
- [4] A. Lauser. *Theory and numerical applications of compositional multi-phase flow in porous media*. 2014.
- [5] A. S. Odeh et al. "Comparison of solutions to a three-dimensional black-oil reservoir simulation problem (includes associated paper 9741)". In: *Journal of Petroleum Technology* 33.01 (1981), pp. 13–25.
- [6] M. Chien, H. Yardumian, E. Chung, W. Todd, et al. "The formulation of a thermal simulation model in a vectorized, general purpose reservoir simulator". In: *SPE Symposium on Reservoir Simulation*. Society of Petroleum Engineers. 1989.
- [7] K. H. Coats et al. "An equation of state compositional model". In: *Society of Petroleum Engineers Journal* 20.05 (1980), pp. 363–376.
- [8] M. Panfilov and I. Panfilova. "Method of negative saturations for flow with variable number of phases in porous media: extension to three-phase multi-component case". In: *Computational Geosciences* 18.3-4 (2014), pp. 385–399.
- [9] A. Firoozabadi. *Thermodynamics of hydrocarbon reservoirs*. McGraw-Hill, 1999.
- [10] D. V. Voskov and H. A. Tchelepi. "Comparison of nonlinear formulations for two-phase multi-component EoS based simulation". In: *Journal of Petroleum Science and Engineering* 82 (2012), pp. 101–111.

- [11] Y.-S. Wu and P. A. Forsyth. "On the selection of primary variables in numerical formulation for modeling multiphase flow in porous media". In: *Journal of contaminant hydrology* 48.3 (2001), pp. 277–304.
- [12] H. Class, R. Helmig, and P. Bastian. "Numerical simulation of non-isothermal multiphase multicomponent processes in porous media.: 1. An efficient solution technique". In: *Advances in Water Resources* 25.5 (2002), pp. 533–550.
- [13] A. Abadpour and M. Panfilov. "Method of negative saturations for modeling two-phase compositional flow with oversaturated zones". In: *Transport in Porous Media* 79.2 (2009), pp. 197–214.
- [14] A. Bourgeat et al. "Numerical test data base". In: URL: http://momas.univ-lyon1.fr/cas_test.html (2009).
- [15] R. Neumann, P. Bastian, and O. Ippisch. "Modeling and simulation of two-phase two-component flow with disappearing non-wetting phase". In: *Computational Geosciences* 17.1 (2013), pp. 139–149.
- [16] B. Amaziane, M. Jurak, and A. Ž. Keko. "Modeling compositional compressible two-phase flow in porous media by the concept of the global pressure". In: *Computational Geosciences* 18.3-4 (2014), pp. 297–309.
- [17] I. Ben Gharbia and J. Jaffré. "Gas phase appearance and disappearance as a problem with complementarity constraints". In: *Mathematics and Computers in Simulation* 99 (2014), pp. 28–36.
- [18] I. B. Gharbia, E. Flauraud, A. Michel, et al. "Study of compositional multi-phase flow formulations with cubic eos". In: *SPE Reservoir Simulation Symposium*. Society of Petroleum Engineers. 2015.
- [19] G. Singh and M. F. Wheeler. "Compositional flow modeling using a multi-point flux mixed finite element method". In: *Computational Geosciences* (2015). ISSN: 1420-0597. DOI: 10.1007/s10596-015-9535-2. URL: <http://link.springer.com/10.1007/s10596-015-9535-2>.
- [20] J. Boston and H. Britt. "A radically different formulation and solution of the single-stage flash problem". In: *Computers & Chemical Engineering* 2.2-3 (1978), pp. 109–122.
- [21] R. Zaydullin, D. V. Voskov, S. C. James, H. Henley, and A. Lucia. "Fully compositional and thermal reservoir simulation". In: *Computers & Chemical Engineering* 63 (2014), pp. 51–65.
- [22] L. C. Young, R. E. Stephenson, et al. "A generalized compositional approach for reservoir simulation". In: *Society of Petroleum Engineers Journal* 23.05 (1983), pp. 727–742.

- [23] E. Marchand, T. Müller, and P. Knabner. “Fully coupled generalized hybrid-mixed finite element approximation of two-phase two-component flow in porous media. Part I: formulation and properties of the mathematical model”. In: *Computational Geosciences* 17.2 (2013), pp. 431–442.
- [24] O. Kolditz, S. Bauer, L. Bilke, N. Böttcher, J.-O. Delfs, T. Fischer, U. J. Görke, T. Kalbacher, G. Kosakowski, C. McDermott, et al. “*OpenGeoSys*: an open-source initiative for numerical simulation of thermo-hydro-mechanical/chemical (*THM/C*) processes in porous media”. In: *Environmental Earth Sciences* 67.2 (2012), pp. 589–599.
- [25] Y. Huang, O. Kolditz, and H. Shao. “Extending the persistent primary variable algorithm to simulate non-isothermal two-phase two-component flow with phase change phenomena”. In: *Geothermal Energy* 3.1 (2015), pp. 1–23.
- [26] J. Bear. *Dynamics of fluids in porous media*. Courier Corporation, 2013.
- [27] D.-Y. Peng and D. B. Robinson. “A new two-constant equation of state”. In: *Industrial & Engineering Chemistry Fundamentals* 15.1 (1976), pp. 59–64.
- [28] R. Masson, L. Trenty, and Y. Zhang. “Formulations of two phase liquid gas compositional Darcy flows with phase transitions”. In: *MAMERN13: 5th International Conference on Approximation Methods and Numerical Modelling in Environment and Natural Resources* September (2014), pp. 1–22. URL: papers3://publication/uuid/07126E7E-5CCF-4F9A-9EAC-76809C548DA3.
- [29] C. H. Whitson and M. L. Michelsen. “The negative flash”. In: *Fluid Phase Equilibria* 53 (1989), pp. 51–71.
- [30] R. Okuno, R. Johns, K. Sepehrnoori, et al. “A new algorithm for Rachford-Rice for multiphase compositional simulation”. In: *SPE Journal* 15.02 (2010), pp. 313–325.
- [31] M. L. Michelsen. “The isothermal flash problem. Part I. Stability”. In: *Fluid phase equilibria* 9.1 (1982), pp. 1–19.
- [32] A. M. Sahlodin, H. A. Watson, and P. I. Barton. “Nonsmooth model for dynamic simulation of phase changes”. In: *AIChE Journal* 62.9 (2016), pp. 3334–3351.
- [33] W. Wagner, J. Cooper, A. Dittmann, J. Kijima, H.-J. Kretzschmar, A. Kruse, R. Mares, K. Oguchi, H. Sato, I. Stocker, et al. “The IAPWS industrial formulation 1997 for the thermodynamic properties of water and steam”. In: *Journal of Engineering for Gas Turbines and Power* 122.1 (2000), pp. 150–184.

- [34] H. A. Watson, M. Vikse, T. Gundersen, and P. I. Barton. "Reliable Flash Calculations: Part 1. Nonsmooth Inside-Out Algorithms". In: *Industrial & Engineering Chemistry Research* 56.4 (2017), pp. 960–973.
- [35] R. S. Kamath, L. T. Biegler, and I. E. Grossmann. "An equation-oriented approach for handling thermodynamics based on cubic equation of state in process optimization". In: *Computers & Chemical Engineering* 34.12 (2010), pp. 2085–2096.
- [36] H. Cao. "Development of techniques for general purpose simulators". PhD thesis. Stanford University Stanford, CA, 2002.
- [37] D. Collins, L. Nghiem, Y. Li, J. Grabonstotter, et al. "An efficient approach to adaptive-implicit compositional simulation with an equation of state". In: *SPE reservoir engineering* 7.02 (1992), pp. 259–264.
- [38] E. Marchand, T. Müller, and P. Knabner. "Fully coupled generalised hybrid-mixed finite element approximation of two-phase two-component flow in porous media. Part II: numerical scheme and numerical results". In: *Computational Geosciences* 16.3 (2012), pp. 691–708.
- [39] Z. Duan and R. Sun. "An improved model calculating CO₂ solubility in pure water and aqueous NaCl solutions from 273 to 533 K and from 0 to 2000 bar". In: *Chemical geology* 193.3 (2003), pp. 257–271.
- [40] N. Spycher and K. Pruess. "CO₂-H₂O mixtures in the geological sequestration of CO₂. II". In: *Partitioning in chloride brines at* 12.100 (2005), pp. 3309–3320.
- [41] Z. Duan and Z. Zhang. "Equation of state of the H₂O, CO₂, and H₂O-CO₂ systems up to 10 GPa and 2573.15 K: molecular dynamics simulations with ab initio potential surface". In: *Geochimica et Cosmochimica Acta* 70.9 (2006), pp. 2311–2324.
- [42] P. W. Atkins and J. De Paula. *Physikalische chemie*. John Wiley & Sons, 2013.
- [43] A. Fenghour, W. A. Wakeham, and V. Vesovic. "The viscosity of carbon dioxide". In: *Journal of Physical and Chemical Reference Data* 27.1 (1998), pp. 31–44.
- [44] S. Kräutle. "The semismooth Newton method for multicomponent reactive transport with minerals". In: *Advances in Water Resources* 34.1 (2011), pp. 137–151.
- [45] A. Nishida. "Experience in developing an open source scalable software infrastructure in Japan". In: *Computational Science and Its Applications-ICCSA 2010*. Springer, 2010, pp. 448–462.

- [46] P. Bastian. "A fully-coupled discontinuous Galerkin method for two-phase flow in porous media with discontinuous capillary pressure". In: *Computational Geosciences* 18.5 (2014), pp. 779–796.
- [47] Y. Huang, H. Shao, E. Wieland, O. Kolditz, and G. Kosakowski. "A new approach to coupled two-phase reactive transport simulation for long-term degradation of concrete". submitted.
- [48] G. Kosakowski and A. Jakob. *Humidity diffusion through small holes into a waste drum*. Tech. rep. Paul Scherrer Institut (psi), Nov. 2014.
- [49] Q. T. Phung, N. Maes, D. Jacques, G. De Schutter, G. Ye, and J. Perko. "Modelling the carbonation of cement pastes under a CO₂ pressure gradient considering both diffusive and convective transport". In: *Construction and Building Materials* 114 (2016), pp. 333–351.
- [50] L. Nghiem, P. Sammon, J. Grabenstetter, H. Ohkuma, et al. "Modeling CO₂ storage in aquifers with a fully-coupled geochemical EOS compositional simulator". In: *SPE/DOE symposium on improved oil recovery*. Society of Petroleum Engineers. 2004.
- [51] Y. Fan, L. J. Durlofsky, and H. A. Tchelepi. "A fully-coupled flow-reactive-transport formulation based on element conservation, with application to CO₂ storage simulations". In: *Advances in Water Resources* 42 (2012), pp. 47–61.
- [52] C. Lu and P. C. Lichtner. "High resolution numerical investigation on the effect of convective instability on long term CO₂ storage in saline aquifers". In: *Journal of Physics: Conference Series*. Vol. 78. 1. IOP Publishing. 2007, p. 012042.
- [53] M. White and M. Oostrom. *STOMP Subsurface Transport Over Multiple Phases Version 2.0 Theory Guide*. Tech. rep. Pacific Northwest National Laboratory (PNNL), Richland, WA (United States), 2000.
- [54] T. Xu. "TOUGHREACT user's guide: A simulation program for non-isothermal multiphase reactive geochemical transport in variably saturated geologic media, V1. 2.1". In: *Lawrence Berkeley National Laboratory* (2008).
- [55] B. Lothenbach and E. Wieland. "A thermodynamic approach to the hydration of sulphate-resisting Portland cement". In: *Waste Management* 26.7 (2006), pp. 706–719.
- [56] E. Wieland, G. Kosakowski, B. Lothenbach, and D. Kulik. "Preliminary assessment of the temporal evolution of waste packages in the near field of an L/ILW repository". submitted.
- [57] T. Wagner, D. A. Kulik, F. F. Hingerl, and S. V. Dmytrieva. "GEM-Selektor geochemical modeling package: TSolMod library and data interface for multicomponent phase models". In: *The Canadian Mineralogist* 50.5 (2012), pp. 1173–1195.

- [58] D. A. Kulik, T. Wagner, S. V. Dmytrieva, G. Kosakowski, F. F. Hingerl, K. V. Chudnenko, and U. R. Berner. "GEM-Selektor geochemical modeling package: revised algorithm and GEMS3K numerical kernel for coupled simulation codes". In: *Computational Geosciences* 17.1 (2013), pp. 1–24.
- [59] W. Wang, G. Kosakowski, and O. Kolditz. "A parallel finite element scheme for thermo-hydro-mechanical (THM) coupled problems in porous media". In: *Computers & Geosciences* 35.8 (2009), pp. 1631–1641.
- [60] F. Brunner. "Multiphase multicomponent flow in porous media with general reactions: efficient problem formulations, conservative discretizations, and convergence analysis". In: 53.9 (2013), pp. 1689–1699. URL: <https://opus4.kobv.de/opus4-fau/frontdoor/index/index/docId/6858>.
- [61] I. Sin. "Numerical simulation of compressible two-phase flow and reactive transport in porous media-Applications to the study of CO₂ storage and natural gas reservoir." In: *Ecole Nationale Supérieure des Mines de Paris* (2015), pp. 1–265. URL: <https://archives-ouvertes.fr/tel-01306860/document>.
- [62] R. d. Cuveland. "Two-Phase Compositional Flow Simulation with Persistent Variables". PhD thesis. 2015.
- [63] R. Zhao and J. Cheng. "Non-isothermal modeling of CO₂ injection into saline aquifers at a low temperature". In: *Environmental Earth Sciences* 73.9 (2015), p. 5307.
- [64] F. Reif. *Fundamentals of statistical and thermal physics*. Waveland Press, 2009.
- [65] K. Pruess, C. Oldenburg, and G. Moridis. "TOUGH2 user's guide version 2". In: *Lawrence Berkeley National Laboratory* (1999).
- [66] H. Li and J. Yan. "Evaluating cubic equations of state for calculation of vapor–liquid equilibrium of CO₂ and CO₂-mixtures for CO₂ capture and storage processes". In: *Applied Energy* 86.6 (2009), pp. 826–836.
- [67] G. Kosakowski and N. Watanabe. "OpenGeoSys-Gem: a numerical tool for calculating geochemical and porosity changes in saturated and partially saturated media". In: *Physics and Chemistry of the Earth, Parts A/B/C* 70 (2014), pp. 138–149.
- [68] J. C. Walton, S. Bin-Shafique, R. W. Smith, N. Gutierrez, and A. Tarquin. "Role of carbonation in transient leaching of cementitious wasteforms". In: *Environmental science & technology* 31.8 (1997), pp. 2345–2349.

- [69] Y. Huang, T. Nagel, and H. Shao. "Comparing global and local implementations of nonlinear complementary problems for the modeling of multi-component two-phase flow with phase change phenomena". In: *Environmental Earth Sciences* 76.18 (2017), p. 643.
- [70] B. Sleep and J. Sykes. "Modeling the transport of volatile organics in variably saturated media". In: *Water Resources Research* 25.1 (1989), pp. 81–92.
- [71] P. Forsyth. "Three-dimensional modelling of steam flush for DNAPL site remediation". In: *International journal for numerical methods in fluids* 19.12 (1994), pp. 1055–1081.
- [72] J. M. Nordbotten and M. A. Celia. *Geological storage of CO₂: modeling approaches for large-scale simulation*. John Wiley & Sons, 2011.
- [73] T. Xu, R. Senger, and S. Finsterle. "Corrosion-induced gas generation in a nuclear waste repository: Reactive geochemistry and multiphase flow effects". In: *Applied Geochemistry* 23.12 (2008), pp. 3423–3433.
- [74] J. VonNeumann and R. D. Richtmyer. "A method for the numerical calculation of hydrodynamic shocks". In: *Journal of applied physics* 21.3 (1950), pp. 232–237.
- [75] N. C. Marty, C. Tournassat, A. Burnol, E. Giffaut, and E. C. Gaucher. "Influence of reaction kinetics and mesh refinement on the numerical modelling of concrete/clay interactions". In: *Journal of Hydrology* 364.1-2 (2009), pp. 58–72.
- [76] N. Prasianakis, E. Curti, G. Kosakowski, J. Poonoosamy, and S. Churakov. "Deciphering pore-level precipitation mechanisms". In: *Scientific reports* 7.1 (2017), p. 13765.
- [77] Z. Bažant and L. Najjar. "Nonlinear water diffusion in nonsaturated concrete". In: *Matériaux et Construction* 5.1 (1972), pp. 3–20.